NMR, PXRD, AND OPTICAL MICROSCOPY: STUDYING TRANSPORT MECHANISMS IN SPONTANEOUS COCRYSTAL FORMATION

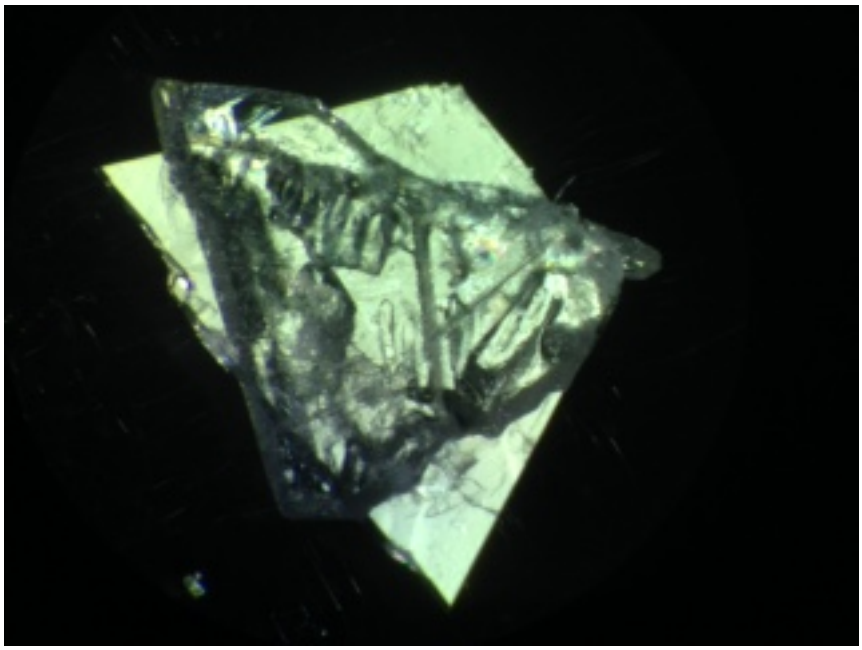

Riley Davies

Advisor: Manish Mehta

2018-2019

Department of Chemistry and Biochemistry

Oberlin College

ABSTRACT

Cocrystals are a class of crystalline materials composed of two or more chemically distinct molecular species joined by non-covalent interactions, often hydrogen- or halogen-bonding. No bonds are broken or formed in the course of generating a cocrystal, but a cocrystal itself possesses a unique set of physical and chemical properties. Cocrystal research focuses primarily on applications in materials science and drug development. The allure of cocrystals within the realm of pharmaceuticals is tied to our ability to "tune" cocrystals to achieve certain properties. By combining an active pharmaceutical ingredient (API) with a viable coformer, the bulk properties of the material, such as solubility and shelf stability, can be altered to improve the utility of the pharmaceutical, but the API will retain its chemical identity within the cocrystal. Cocrystallization methods range from liquid-assisted grinding to spontaneous cocrystallization, and it is this spontaneous reaction that we examine in this thesis.

The transport mechanism (or mechanisms) by which two solid coformers achieve this spontaneous reaction is still unknown, though researchers are exploring several mechanisms, such as amorphous intermediate, low melting point eutectic, and vapor-phase transport. In our lab, we use powder x-ray diffraction (PXRD), solid-state nuclear magnetic resonance (ssNMR), and optical microscopy to elucidate the mechanism by which cocrystals form spontaneously. We explore four interfaces in this thesis: powder-to-powder, vapor-to-powder, powder-to-single crystal, and single crystal-to-single crystal. We report that humidity has a catalytic effect on cocrystallization in 15 cocrystals comprised of small organic molecules, but it is not the key factor in determining cocrystallization kinetics. In studying the vapor-based mechanism, we find no indication of cocrystallization. Our microscopy results demonstrate that coformers have the ability to move at both the molecular and macroscopic level to increase contact with each other.

ACKNOWLEDGEMENTS

The National Science Foundation and Oberlin College for throwing money at our problems.

My parents for throwing moral support at my problems.

Professor Mehta for throwing me at his problems.

TABLE OF CONTENTS

CHAPTER 1: INTRODUCTION

In 1844, German chemist Friedrich Wöhler synthesized a novel material comprised of equal parts quinone and hydroquinone, a material he named quinhydrone. The synthesis of this substance was the first reported instance of a cocrystal in the scientific literature.[1] In the 175 years since Wöhler's discovery, great strides in chemistry have enabled more precise classification of these types of materials. Today, a cocrystal is broadly defined as "a homogeneous crystalline material that is made up of two or more molecules in definite stoichiometric amounts held together by non-covalent forces."[2] These molecular species must be chemically distinct.[3] This definition has caveats to distinguish cocrystals from eutectics, solvates, salts, and other comparable substances. For example, in order to differentiate cocrystals from salts, a substance must possess reduced proton sharing between coformers in order to be considered a cocrystal.[2]

One reason for the utility of cocrystals in applied science, primarily in materials chemistry and pharmaceuticals, is the manner in which the chemical and physical properties of any given cocrystal differ from those of its coformers. Cocrystals retain certain properties from each coformer, leading to the ability to alter bulk properties of one species via cocrystallization with another compound. Recent developments in materials chemistry have demonstrated that cocrystals can influence plastic flexibility and fluorescence of coformers,[4,5] while active pharmaceutical ingredients (APIs) can have altered solubility and bioavailability when paired with a viable coformer.[6-8] This ability to "tune" drugs for desired bulk properties has the potential to expand the number of medications available to the public. Approved pharmaceuticals could be altered for optimized uptake and lengthened shelf life, while promising experimental drugs that would not meet FDA approval could be given an edge through cocrystallization to

form safer, more effective treatment options that have a higher chance of FDA approval. Because cocrystallization occurs without the making or breaking of chemical bonds, these alterations could be performed on species that are already well studied, potentially leading to the discovery of drugs with novel properties, even if using only libraries of established pharmaceuticals for cocrystal APIs.

Before these cocrystals can be created, we must first understand *how* they might be produced from their coformers. The most common methods for cocrystal synthesis are precipitation from solution and liquid-assisted grinding, in which a microdroplet of solvent is used to catalyze a mechanochemical reaction.[2,9-11] While these methods can achieve complete conversion of a reaction mixture to cocrystal on the time scale of minutes to hours, they require solvent or concerted energy input to achieve this result. In a more environmentally friendly and economical method, some coformer mixtures undergo spontaneous rearrangement to form cocrystal.[10,12,13] This method does not require any energy input other than the initial mixing of two powdered coformers, after which the cocrystallization reaction progresses in the solid state. A computational survey of 350 cocrystal systems indicated that cocrystals average an 8 kJ mol^{-1} increase in energetic stability over a mixture of their coformers.[14] Though uncommon, some cocrystal systems were found to be less stable than their coformers, indicating that some reaction mixtures may produce cocrystal under the more energetic conditions of mechanochemistry but show no conversion under spontaneous conditions. In addition to the influence of energetics on the viability of a spontaneous reaction, the rate at which a cocrystal forms is heavily dependent on environmental factors, with humidity being one of the strongest factors in reaction kinetics.[9,15]

Though much research has been focused on the topic of spontaneous cocrystallization, especially in the past decade, the mechanism by which this happens is still unknown. In fact,

there is no guarantee that all cocrystals are formed by the same process. Several mechanisms have been proposed, which include a transient liquid brought about by a eutectic with low melting point; an amorphous solid phase at the interface between coformers; or vapor from a volatile species depositing on the surface of a more stable coformer.[9,16] These mechanisms, however, are not likely to be universal. Similarities in transport mechanism between cocrystals are usually only consistent across species with chemically similar coformers.[17] Other studies have produced mechanistic insights regarding the parameters that influence reaction rate, but do not reveal the means by which material is transported within the solid state reaction mixture.[13]

Because the material transport is occurring at the molecular level, these changes cannot be recorded though unaided observation. In order to learn more about the nature of mass transport within spontaneous cocrystal systems, a multifaceted spectrometric approach must be adopted.[18-20] We primarily used powder x-ray diffraction (PXRD), solid-state nuclear magnetic resonance (ssNMR), and optical microscopy to monitor spontaneous cocrystallization in an attempt to elucidate these transport mechanisms. This set of techniques enabled the cross-referencing of crystal diffraction data with chemical shift data for the same systems,[18] while microscopy provided the opportunity to observe bulk changes, such as color shift or sample movement, that cannot be picked up by the other two techniques.[19,20] PXRD has been a staple of cocrystal characterization due to the unique diffraction patterns of cocrystals when compared to their coformers. NMR is a useful independent complement to PXRD for a few reasons: non-diffracting phases of organic molecules will still be detected by NMR, enabling identification of transient amorphous phases; organic molecules can also be characterized on a carbon-by-carbon level for each chemical species, enabling tracking of change in chemical environment for specific atoms in coformers as cocrystal forms; and, whereas PXRD requires samples to be

restricted to a powdered crystallite form, ssNMR can still be conducted with larger crystals, as long as the crystal can fit inside the sample holder.

We employed these techniques to study four material interfaces: powder-to-powder contact between coformers (Chapter 3), vapor diffusion of a volatile substance onto its powdered coformer (Chapter 4), powdered material in contact with a larger single crystal of its coformer (Chapter 5), and a crystal of each coformer in contact along a shared face. We primarily studied the powder-powder interface for the purpose of producing more kinetics results similar to previous experiments conducted in this lab,[13] while the work with larger crystals aims to simplify the solid-to-solid interface to a single plane of coformer interaction. The vapor diffusion experiments in this report serve to explore the viability of the previously proposed vapor transport model.[10,16]

This thesis focuses primarily on three cocrystal systems for mechanistic insights, and an additional thirteen systems are additionally studied. The primary cocrystal system studied in this project was the caffeine-malonic acid 2:1 cocrystal, which appears in the experiments conducted in Chapters 3, 4, and 5. This cocrystal has received much attention in the literature, is comprised of common materials, and reacts quickly, making it a staple of cocrystal research in our lab.[13,15,21,22] The isoniazid-benzoic acid 1:1 cocrystal was studied for experiments involving the vapor-powder interface (Chapter 4) due to its previously-speculated vapor diffusion mechanism.[10] The theophylline-malonic acid 2:1 cocrystal was selected to study the powder-powder interface (Chapter 3) as well as the single crystal interfaces (Chapters 5 and 6) as a result of previous research and the relative ease with which each coformer grows crystals.[23-26] The other cocrystals were comprised of small diacids and APIs detailed in Chapter 2.2.1.

CHAPTER 2: MATERIALS AND METHODS

2.1. Cocrystal Synthesis

2.1.1. Isoniazid-Benzoic Acid 1:1 Cocrystal

Isoniazid (INA) and benzoic acid (BZE) were purchased from Sigma Aldrich at >99% purity, and 99% ^{13}C carbonyl-enriched benzoic acid was purchased from Cambridge Isotope Labs. These were used without further purification. Ball-milled cocrystal was formed using a procedure published in the literature. A 1:1 stoichiometric ratio of isoniazid and benzoic acid was combined in a Teflon-sealed Retsch 25-mL stainless steel jar with one 7-mm stainless steel shot and milled for 45 minutes at 30 Hz in a Retch MM 400 ball mill. Quantitative conversion to product was confirmed by powder x-ray diffraction (PXRD).

2.1.2. Caffeine-Malonic Acid 2:1 Cocrystal

Caffeine (CA) and malonic acid (MA) were purchased from Sigma Aldrich at >99% purity and were used without further purification. Carbonyl-enriched malonic acid ($^{13}C_1$, 99%) was synthesized in-house in 2017. Ball-milled cocrystal was formed by a procedure similar to the one for the isoniazid-benzoic acid cocrystal. Caffeine and malonic acid were combined in a 2:1 stoichiometric ratio, respectfully, in a Teflon-sealed Retsch 25-mL stainless steel jar with one stainless steel shot and milled for 5 minutes at 30 Hz in a Retsch MM 400 ball mill. Product was confirmed by PXRD. Hand-ground cocrystal was prepared by combining the 2:1 stoichiometric ratio in an agate mortar and pestle and grinding manually for 10-15 minutes.

2.2. Sample Preparation for Powder-Powder Interface Experiments

2.2.1. Preparing Coformers for Spontaneous Cocrystallization

Coformers were prepared by a process similar to the method of preparation of the cocrystals. This series of experiments involved completing a grid (Table 1) of model APIs

(active pharmaceutical ingredients) and some of their known coformers. We tested three APIs—caffeine (CA), theophylline (TH), and nicotinamide (NA)—against each of six small diacids—oxalic acid (OA), malonic acid (MA), maleic acid (ME), fumaric acid (FU), succinic acid (SU), and glutaric acid (GA). Fumaric acid and succinic acid systems do not spontaneously produce cocrystals with caffeine and theophylline, and as such have been excluded from this study.

	Oxalic Acid	Malonic Acid	Maleic Acid	Fumaric Acid	Succinic Acid	Glutaric Acid
Caffeine	2:1	2:1	1:1 2:1	X	X	2:1
Theophylline	2:1	1:1	1:1	X	X	1:1
Nicotinamide	2:1	2:1	2:1	1:1	2:1	1:1

Table 1. Cocrystal systems studied in the powder-powder interface project. Stoichiometric ratios are presented as API:diacid in each cell.

Precise calculation of initial ratio of coformers was not of importance—the powders were mixed later in the procedure, and sample loss leading up to mixture of coformers was not predictable. Each coformer was placed in a separate Teflon-sealed Retsch 25-mL stainless steel jar with one stainless steel shot and milled for 25 minutes at 25 Hz in a Retsch 400 MM ball mill. Each powder was then separately hand-sifted between 45-µm and 90-µm sieves. Sifting was initially performed by a Retsch AS 200 autosifter between 45µm and 75µm sieves, typically at 1.0 mm/"g" for 5 minutes, but following autosifting with hand sifting demonstrated that even at higher intensity and longer sifting duration, autosifting was not as rigorous as hand sifting in achieving desired particle size selection. The 45-90 µm portions of the milled coformers were then stored in separate glass vials.

From the mass of remaining material, powders were combined in stoichiometric ratio (±1 mg) in a third vial. This vial was vortexed for up to 2 minutes before the contents were triple-sifted through a sieve stack consisting of 40- 60- and 80-mesh sieves. The resulting mixture was vortexed for another 2 minutes before ~100-mg aliquots were packed into aluminum PXRD

sample holders. These samples were then placed in glass exposure chambers or under petri dishes depending on the relative humidity (RH) desired. These samples were then periodically removed to collect a PXRD trace for the purpose of tracking cocrystal formation. The typical experiment involved three traces collected in the first 24 hours, followed by one trace collected each day for three days, and three additional traces collected over the next week; however, these time points could not always be maintained. Power outages, seasonal campus closure, conflicting schedules from other labs, and diffractometer malfunctions resulted in some kinetics plots missing desired time points.

2.2.2. Preparing Exposure Chambers

Samples were studied under four conditions: ambient lab environment, 0% RH, 50% RH, and 75% RH. Ambient conditions were met by placing samples in a covered petri dish. The covering dish was raised to permit airflow over the sample. A dry environment (0% RH) was achieved with some success by heating an open glass jar containing a layer of calcium sulfate desiccant in an oven for at least 24 hours before removing from the oven and immediately closing the jar tightly with a screw top lid. The jar was only opened to remove and replace the sample when collecting a PXRD trace, though the sample was at ambient conditions for each 10-minute interval of data collection while inside the diffractometer. The desiccant was reheated when beginning a new experiment. The 50% and 75% RH levels were achieved by using salt solutions to control the environment within an exposure chamber. Saturated calcium nitrate solution was allowed to equilibrate in a glass jar to produce 50% RH, while saturated sodium chloride solution was used to do the same for 75% RH. A small aluminum platform was placed in each solution-based exposure chamber in order to keep the sample holder above the water line.

2.3. Sample Preparation for Vapor-Powder Interface Experiments

2.3.1. Layered Rotor Packing

The layered rotor vapor experiment is an *in situ* nuclear magnetic resonance (NMR) spectroscopy arrangement for testing the viability of a vapor-to-powder interface for cocrystal formation. The objective of this method is to create a closed environment in which the vapor of a volatile solid diffuses through a semi-porous medium, depositing on its coformer, confined to the chamber on the other side of the semi-porous medium. This assembly keeps the solids separate, allowing for only vapor-based transport. The porous medium used in this experiment was crushed glass (44-210 μm), valuable for its traits of being abundant, inexpensive, permeable by vapor, chemically inert, and with no signal in the ^{13}C NMR spectrum. The small glass particle size allows for dense enough packing to keep the two coformers separated. Two cocrystal systems were tested with this method: the INA-BZE 1:1 cocrystal system and the CA-MA 2:1 cocrystal system. For each system, the procedure was identical. First, the powders were lightly ground separately with an agate mortar and pestle. 5-6 mm of crushed glass was packed into a ceramic ssNMR rotor with length 20.96 mm and diameter 4.00 mm (using 7-mm caps). 1-2 mm of one coformer was then packed into the remaining space. The rotor was then sealed and inverted. The bottom cap was removed, and 1-2 mm of crushed glass was scooped out to be replaced by the second coformer (Figure 1). The rotor was then re-sealed and inserted into the NMR probe. Layered rotors were packed in this manner to avoid premature cocrystallization via cross-contamination—residue left on the rotor wall by the first coformer to be packed would come into contact with the other coformer if everything was packed from the same rotor end. This procedure was adapted from an earlier incarnation of the layered rotor experiment in which several layers of each coformer were packed, and shorter caps (3 mm) were employed to

maximize packing volume; however, sample contamination was too common for reliable results. The head of the probe used in these experiments contains a variable temperature control module fitted to a heating coil, permitting sustained high temperatures within the rotor. This temperature controller was used to perform experiments at 60°C and 80°C for both cocrystal systems. The heightened temperature increases volatility of coformers for more rapid vapor saturation of the crushed glass medium.

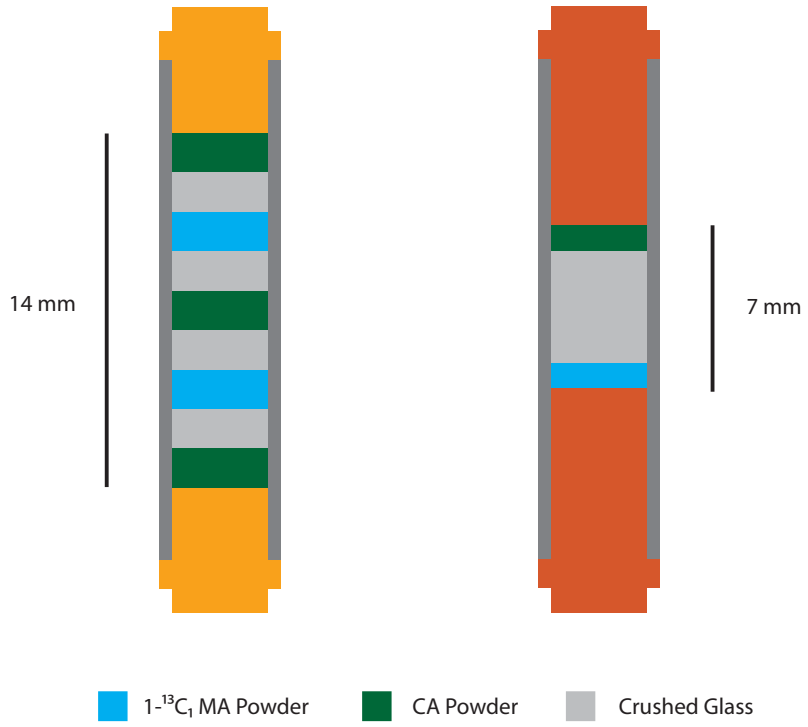

Figure 1. Left: First layered rotor packing arrangement. Right: Current model for packing a layered rotor. CA:$^{13}C_1$ MA 2:1 cocrystal experiment shown as an example.

2.3.2. Two-Chamber Experiment

In this experiment, two open-top chambers, either aluminum PXRD sample holders or glass vials, are each filled with one coformer. The two-chamber experiment is studied by NMR, but is more easily supported by PXRD analysis. This method was used to study the vapor-powder interface *ex situ*. These chambers are placed in a petri dish that is then wrapped in

aluminum foil and placed under the aluminum block of a temperature-controlled heating block (VWR) (Figure 2). This placement minimizes temperature gradient within the petri dish by providing heating from the temperature source below and the aluminum block above. An initial experiment in which the petri dish was simply placed on the aluminum block created such a large temperature gradient that volatile coformer crystals began to form on the aluminum foil. With more uniform heating, the coformer did not deposit directly onto the foil, enabling greater saturation of the petri dish environment with coformer vapor. After 1-2 weeks, the chamber containing the less volatile coformer was then checked by PXRD and NMR for any deposited residue from the other coformer or for cocrystal.

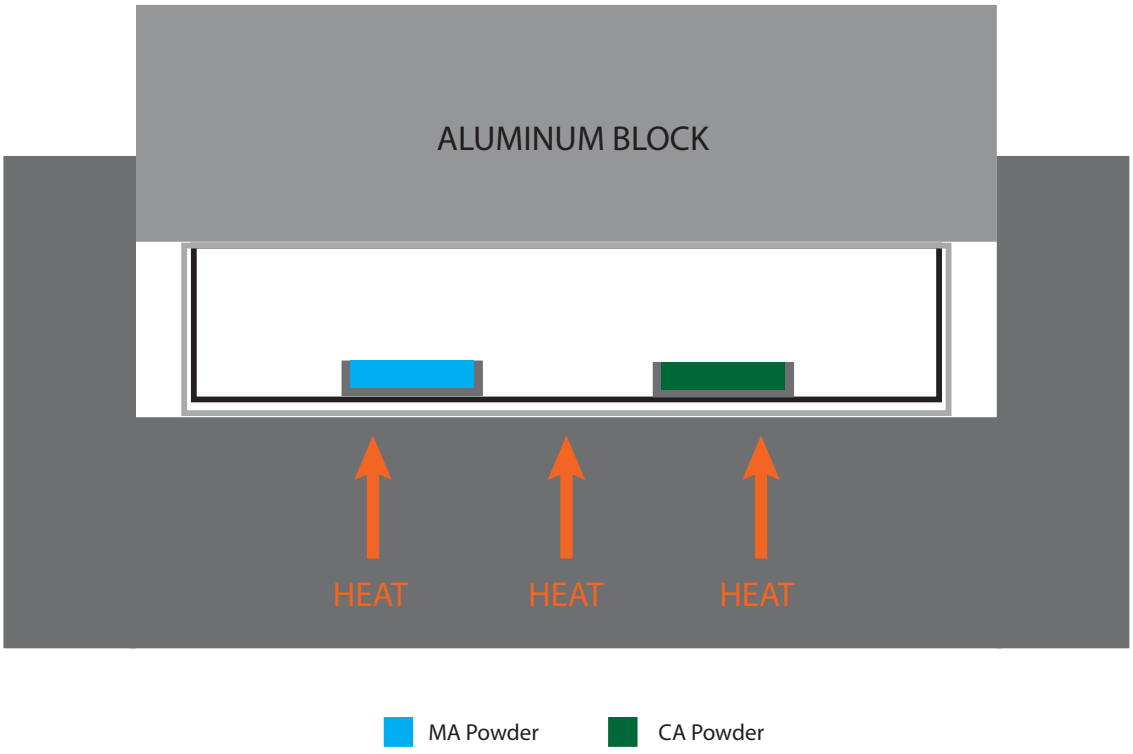

Figure 2. *Ex situ* two-chamber experimental apparatus. Powders are contained in aluminum PXRD sample holders. CA:MA 2:1 cocrystal experiment shown as an example.

2.4. Sample Preparation for Powder-Single Crystal Interface Experiments

2.4.1. Growing Coformer Crystals

Needle-shaped malonic acid crystals were grown by precipitation from a 1:30 methanol:chloroform mixture at 40°C. Plate-like malonic acid crystals were grown by precipitation from water at 50°C (Figure 3). Theophylline crystals were grown from ethanol at room temperature in a 10-mL glass vial. Carbonyl ^{13}C-enriched malonic acid crystals were precipitated from acetone at room temperature. All crystallizations were performed in 10-mL glass sample vials.

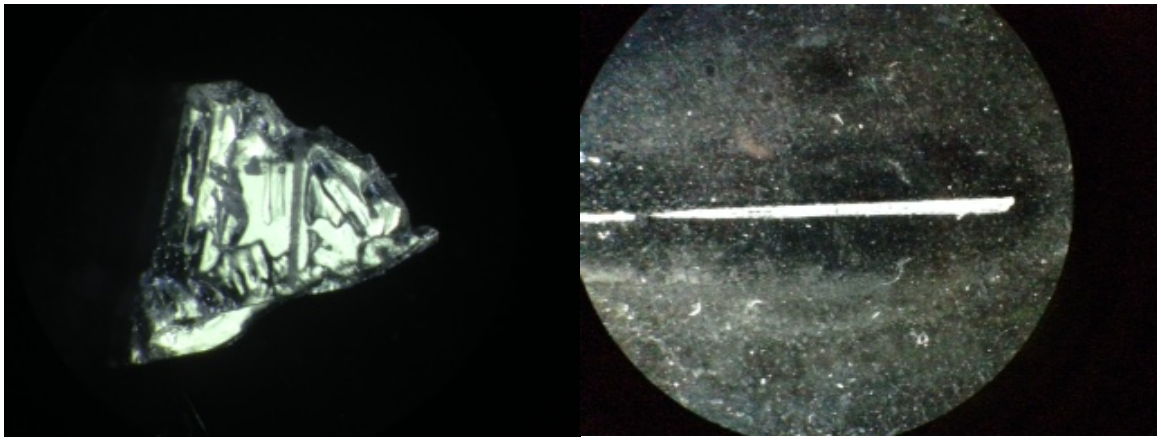

Figure 3. Plate crystal (left) and needle crystal (right) of malonic acid.

2.4.2. Optical Microscopy Studies

Microscopy experiments for the powder-single crystal interface were performed through application of powder to the surface of a needle-like crystal. These experiments were performed at ambient conditions on microscope slides. Crystals grown in the lab were first placed on the microscope slide, followed by addition of powder to the slide such that the coformers were in contact with one another. These experiments were then monitored using polarized light time lapse video capture over the course of days or weeks to study the extent and nature of interaction between powder and crystal.

2.4.3. *In Situ* Solid-State NMR Experiments

Two procedures were followed for the powder-single crystal experiment. In the first experiment, a ^{13}C-enriched malonic acid plate crystal was placed in a thin-walled ceramic rotor and partially covered in caffeine that was lightly ground with an agate mortar and pestle. The contents of the rotor were then monitored in 128-scan frames for 72 frames, yielding approximately 1 week of interaction between powder and crystal. In the second experiment, caffeine powder was added to the same rotor until the malonic acid crystal was completely covered. The powder was then compressed with an aluminum tamper until the malonic acid crystal fragmented under pressure (Figure 4). The contents of the rotor were then monitored in 80 128-scan frames over a week.

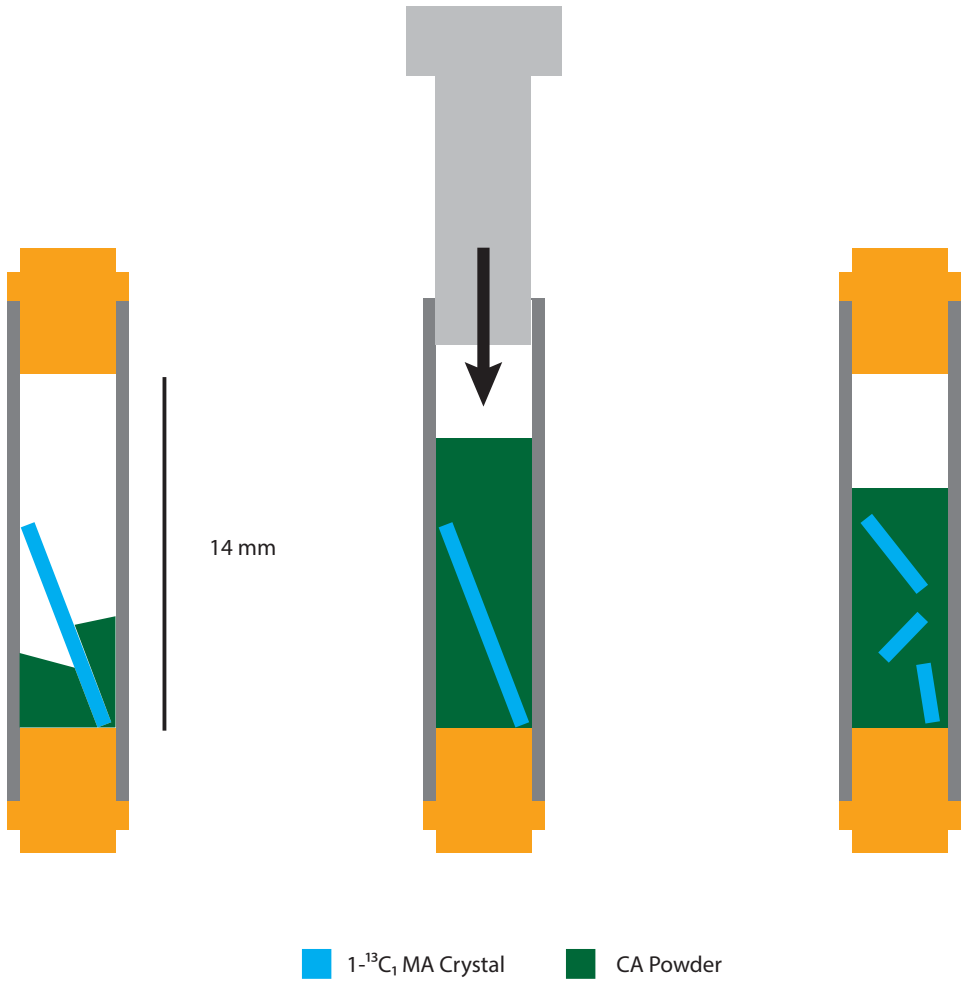

Figure 4. Powder-Single Crystal *in situ* NMR arrangement. Left: Single crystal (cyan) in contact with coformer powder (green). Middle: Single crystal covered in coformer powder and lightly crushed. Right: Crystal shards embedded in coformer powder to increase surface area for cocrystallization. CA:MA 2:1 cocrystal experiment shown as an example.

2.5. Sample Preparation for Single Crystal-Single Crystal Interface Experiments

Plate-like malonic acid crystals and theophylline crystals from 2.4.1 were used in these experiments. A theophylline crystal was placed on top of a malonic acid crystal such that contact between the broad flat surfaces of each coformer was maximized. This arrangement was then monitored using polarized light in either still images or time lapse video capture over the course of days or weeks. The crystals were then examined for any changes to structure.

2.6. Experimental Parameters for PXRD Analysis

Powder samples were packed into aluminum sample holders machined in-house to match the dimensions of a Rigaku Ultima IV multipurpose x-ray diffractometer, which was used to collect data. The surface of a sample was flattened with a microscope slide into a wafer of ~1 mm depth. The sample was then analyzed with 1.541-Å X-rays (Cu K-α) at a rate of 4 degrees 2θ per minute, with a range from 5 degrees to 40 degrees 2θ, and a sampling width of 0.02 degrees.

Raw data files (.raw) were first processed using Rigaku's Peak Search program to eliminate baseline counts and reduce noise through a smoothing function. A processed .raw file was then converted into a plaintext (.txt) format using Rigaku's Binary-to-ASCII program. This text file of processed data was then imported into custom *MatLab* code to plot the PXRD trace in number of counts over 2θ in degrees. A second custom program was written in order to track kinetics for the powder-powder interface experiments. This program takes two predefined 2θ values of one coformer resonance and one cocrystal resonance. To account for angle measurement error, the program shifts this 2θ value by a maximum of 0.06 degrees (3 data points) in either direction to find an x-ray count maximum. The trace is then integrated over each of these 2θ values in a range ± 0.6 degrees from the new maximum, and these integrals are normalized.

Imported text files at each time point were then run through the code to acquire cocrystal and coformer signal intensities, which are plotted as a normalized ratio of cocrystal signal over combined coformer and cocrystal signal over all collected time points. The diffraction resonances selected for each system were chosen in order to minimize overlap between coformer and cocrystal in PXRD traces (Table 2). Multiple kinetics curves can be plotted on the same axes for comparative study.

Cocrystal System	Coformer Peak (° 2θ)	Cocrystal Peak (° 2θ)
CA:OA 2:1	26.42	24.82
CA:MA 2:1	27.06	22.46
CA:ME 1:1	11.98	13.24
CA:ME 2:1	11.98	13.58
CA:GA 2:1	11.98	10.36
TH:OA 2:1	12.72	17.30
TH:MA 1:1	7.26	14.72
TH:ME 1:1	12.72	27.30
TH:SU 2:1	20.04	24.40
TH:GA 1:1	12.72	23.36
NA:OA 2:1	14.74	18.08
NA:MA 2:1	14.74	15.24
NA:ME 2:1	28.06	26.32
NA:FU 1:1	14.74	17.88
NA:SU 2:1	25.80	17.86
NA:GA 1:1	14.76	16.94

Table 2. Cocrystal systems and associated peaks selected for data analysis in kinetics plots.

2.7. Experimental Parameters for NMR Analysis

NMR samples were analyzed using a 600 MHz spectrometer (14.1 Tesla magnet; Magnex) with a Discovery console (Tecmag) equipped with a 4 mm magic angle spinning probe (Doty Scientific Inc.). Most MAS experiments were conducted at a spin speed of 9 kHz ± 2 Hz. Spin speed and temperature were regulated by a custom-built controller. Experiments involving interface with single crystals were conducted without spinning. All data were collected with a sweep width of ±33333 Hz, and spectral frequencies of 600.381 MHz (^{1}H channel) and 150.986 MHz (^{13}C channel) were used in acquisition. CA:MA 2:1 data were collected with 4096 acquisition points, INA:BZE 1:1 with 1024 acquisition points, and single crystal experimental data with 512 acquisition points. Acquisition time was 15 μs per point. Parameters for data collection were programmed via Tecmag TNMR software.

TNMR was also used to begin data processing. In performing Fourier transform (FT) without apodization on the free induction decay (FID) for each experiment, zero fills were applied in order to achieve a resolution of 0.054 ppm per acquisition point (8k points total). Adamantane was used as a secondary chemical shift reference to orient all spectra at 38.484 ppm. TNMR files (.tnmr) were exported from the software as plaintext (.txt) and plotted using *MatLab*.

2.8. Experimental Parameters for Optical Microscopy Analysis

Optical microscopy was performed on a Zeiss Discovery V.20 SteREO microscope with an attached light polarizer. All results were obtained either as single frame captures of a defined time points in an experiment or as time-lapse recordings of a powder-crystal system. Time-lapse experiments were conducted at one frame per hour. The level of magnification varied between 9.4x and 83.0x for experiments. All reaction systems were illuminated by both a backlight and two LED lamps placed above the microscope stage adjacent to the microscope lens.

Microscopy images were labeled with time, date, and scale using Zeiss proprietary software. Snapshots and time-lapse recordings were exported as images (.png) and videos (.avi) using the same software package. Additional markers were added to exported images using Adobe *Illustrator*.

CHAPTER 3: POWDER-POWDER INTERFACE EXPERIMENTS

This chapter contains the results of experiments on the powder-powder interface for spontaneous cocrystal formation, using the sample preparation method explained in Section 2.2. These experiments were completed as part of an umbrella project to investigate the kinetics of spontaneous cocrystal formation when exposed to a selection of solvent vapors such as water, ethanol, and acetone. In this chapter we report the effect of variation in humidity on rate of cocrystallization. Comparative experiments such as these provide information that frames the larger picture of coformer transport mechanisms by demonstrating the efficacy of environmental manipulation on reaction rate. This chapter is organized by active pharmaceutical ingredient. All kinetics plots are included in Appendix A.

3.1. Caffeine Cocrystals

Caffeine spontaneously forms cocrystals with four of the diacids addressed in this thesis: oxalic acid, malonic acid, maleic acid, and glutaric acid. Caffeine cocrystallizes with maleic acid in both 1:1 and 2:1 stoichiometric ratios. Fumaric acid and succinic acid do not form cocrystals with caffeine. The rate and extent of cocrystallization varied significantly across the five caffeine cocrystals studied. Of these systems, the CA:MA 2:1 system was the only one to achieve complete conversion to cocrystal at 75% RH, and it did so more rapidly than any of the 15 other cocrystals formed in this project (Figure 5). This cocrystal system has made for a reliable standard when conducting most other experiments in the lab due to the short time scale on which CA:MA 2:1 forms compared to other API-diacid cocrystals.

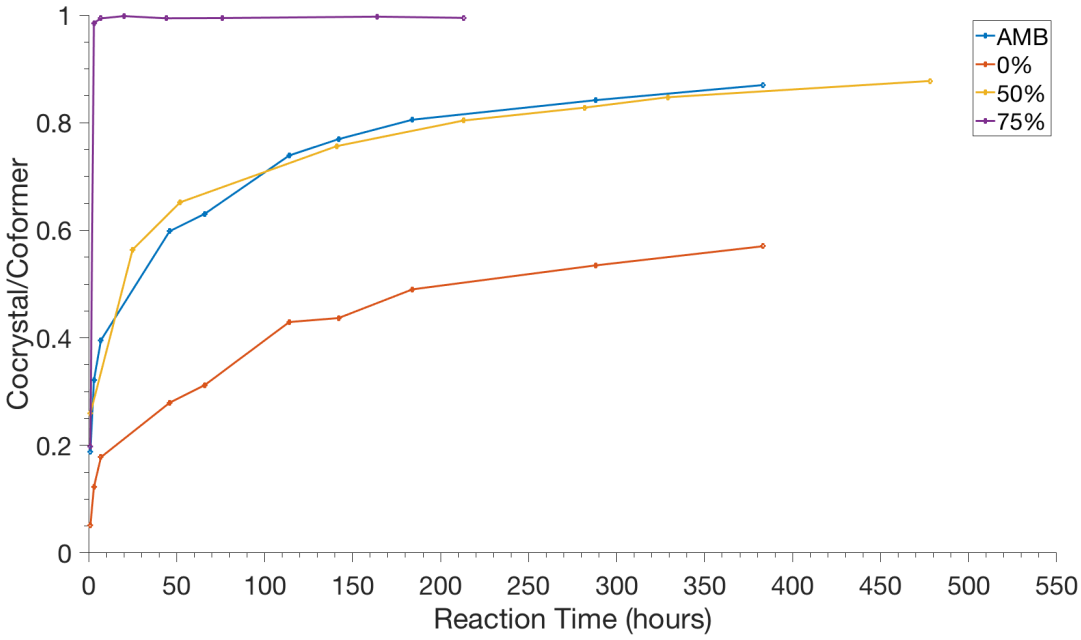

Figure 5. Caffeine-malonic acid 2:1 cocrystal kinetics plots at ambient conditions, 0% RH, 50% RH, and 75% RH.

The CA:OA 2:1 system achieved 75% conversion at 75% RH, 50% RH and ambient bore similar kinetic profiles, and the sample exposed to 0% RH was significantly less effective at cocrystallizing (Figure B2). This pattern of the influence of humidity on kinetics is also observed in Figure 5, and this phenomenon holds constant for most cocrystal systems in this study. The two CA:ME systems (1:1 and 2:1) both demonstrate an odd phenomenon whereby the samples at 75% RH cocrystallize at a rate that far exceeds that of the CA:ME samples at other humidity levels (Figures B6, B8). Though the 75% RH samples always have the highest rate of conversion throughout this project, no others show a gap in conversion so drastic as the threefold difference between CA:ME 1:1 conversion rates and the eightfold difference between CA:ME 2:1. Also of note is the shape of the CA:ME 2:1 75% kinetics curve, which suggests that the rate of reaction appears to increase over the first 150 hours of exposure. The 2:1 system also progresses much more slowly than the 1:1 system, only having achieved 20% conversion in 250 hours while the

1:1 system surpassed 50% conversion at its first time point. After this initial rapid conversion, the 1:1 system appears to halt all progress. The system with glutaric acid, the largest diacid, 2:1 CA:GA, converts to cocrystal at approximately the same rate as the CA:ME 2:1 system at 75% RH, though the samples at lower humidity levels demonstrate more success in conversion to CA:GA 2:1 (Figure B10).

3.2. Theophylline Cocrystals

Theophylline forms the fewest number of cocrystals, seeing only TH:OA 2:1, TH:MA 1:1, TH:GA 1:1, and TH:ME 1:1 as experiments with any conversion to cocrystal. The fumaric acid and succinic acid systems showed no signs of cocrystal formation. Cocrystal systems containing theophylline demonstrated the greatest ratio of cocrystal signal to coformer signal by the end of the exposure period, with the TH:MA 1:1 system reaching complete conversion at 75% RH on approximately the same time scale as the 2:1 CA:MA system (Figure 6).

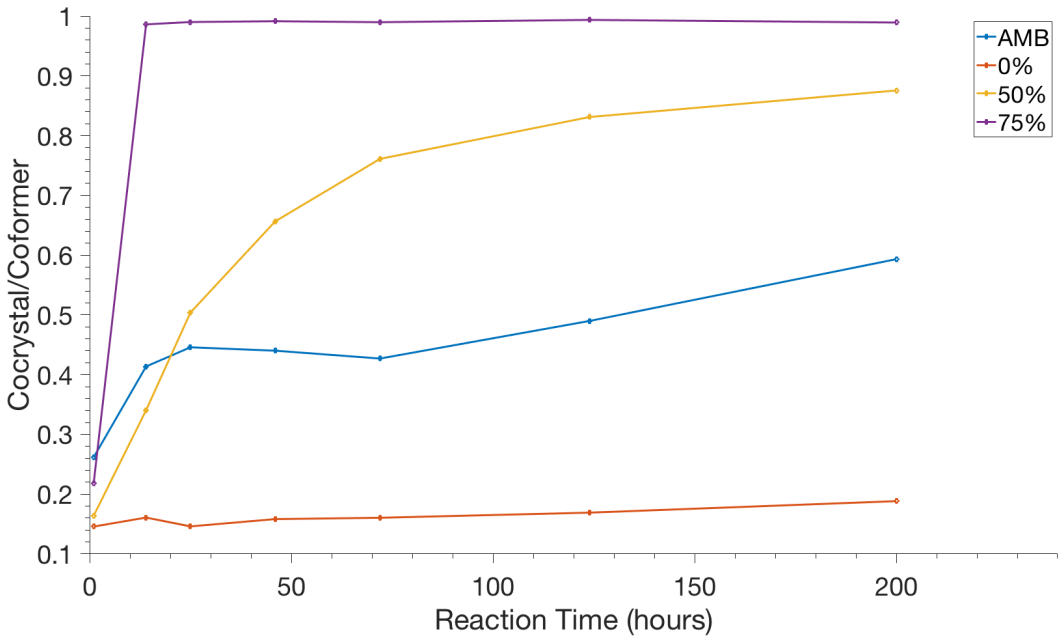

Figure 6. Theophylline-malonic acid 1:1 cocrystal kinetics plots at ambient conditions, 0% RH, 50% RH, and 75% RH.

THOA 2:1 was significantly slower to cocrystallize, even in comparison to CA:OA 2:1, though it still achieved >50% conversion to cocrystal in under two weeks (Figure B12). The TH:ME 1:1 system, while not having a comparable rate of reaction to TH:MA 1:1, was also able to achieve complete conversion after approximately two weeks (Figure B16). The TH:GA 1:1 system, like the CA:ME systems, appears to have a discrepancy between 75% RH conversion and other humidity levels (Figure B18). The 75% RH sample achieved 90% conversion after 200 hours, while the samples at other humidity levels stagnated at no more than 20% conversion. Though there is little increase in cocrystal signal intensity for these lower humidity levels, the samples at ambient conditions and 50% RH are closely grouped and have made twice as much progress toward cocrystallization as has the 0% RH sample. That these samples were already in this order when data collection began suggests that most of the cocrystallization occurred during the coformer mixing procedure, before the first PXRD trace was collected.

3.3. Nicotinamide Cocrystals

The nicotinamide systems were less successful in spontaneously forming cocrystals than both the caffeine and theophylline systems in terms of maximum conversion over each experiment's time frame—no systems reached complete conversion to cocrystal at 75% RH. Unlike caffeine and theophylline, nicotinamide is able to spontaneously form cocrystal with both fumaric acid (1:1) and succinic acid (2:1). The system containing malonic acid, NA:MA 2:1, converted to cocrystal most rapidly; however, the reaction slowed to a before reaching 80% conversion to cocrystal at 75% RH (Figure 7).

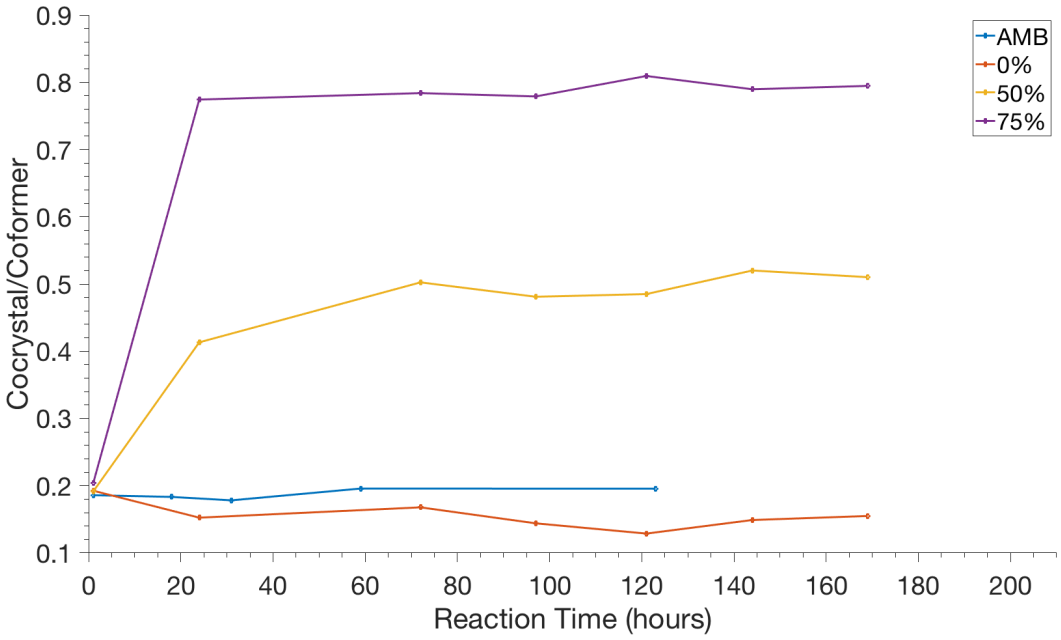

Figure 7. Nicotinamide-malonic acid 2:1 cocrystal kinetics plots at ambient conditions, 0% RH, 50% RH, and 75% RH.

The NA:OA 2:1 system was slower to cocrystallize than the NA:MA 2:1 system, though it still reached almost 50% conversion after 250 hours (Figure B20). The NA:ME 2:1 system achieved conversion to an extent comparable to the CA:MA 2:1 system at 75% RH, but unlike the caffeine system, this nicotinamide system demonstrated noticeable conversion in the lower-humidity samples (Figure B24). Because neither caffeine nor theophylline could produce a cocrystal with fumaric acid, NA:FU 2:1 conversion rate has no other experiment for direct comparison. This experiment was unremarkable, with 50% conversion after two weeks at 75% RH and reaction rates at lower humidity that matched the shape of the 75% RH curve (Figure B26). The NA:SU 2:1 system was much slower than the fumaric acid system, only achieving 25% conversion over a similar two-week period (Figure B28). The NA:GA 1:1 system was the second most reactive system after NA:MA 2:1, achieving 70% conversion at 75% RH after two weeks (Figure B30).

3.4. Considerations in Kinetics Experiments

In the course of conducting these experiments, a few problems arose beyond the logistical issues mentioned at the end of Section 2.2.1. The physical properties of the samples often changed over the course of the reaction. The most common change was observed when washing powders out of their aluminum sample holders at the end of an experiment. The coformers, which were all instantly soluble loose powders at the time of packing, turned into a single cohesive chip of material that lasted as long as 20 seconds under a steady stream of water after two weeks in an exposure chamber. This wafer of material often broke into shards rather than crumble into the cocrystal powder that is formed when performing a cocrystal synthesis by grinding. While this change alone was not a problem, this rearrangement of material sometimes caused warping and buckling of the powder within the sample holder. This phenomenon made analysis by x-ray diffraction difficult, because warping and stiffening of the powder happened concurrently. Thus, powders could not be re-packed without crushing and grinding the sample, ruining the experiment by imparting mechanical energy into the system. This problem sometimes arose more than a week into experiments, which then required 1-2 days of sample preparation and 2 more weeks of data collection to repeat. Due to the limitations that these interruptions posed on the project, time and resources for repeat trials could only be expended for reexamining data sets that were either too small for proper kinetics analysis or for PXRD traces that had been compromised by physical displacement of powder on a sample holder by buckling.

Though less common, sample was sometimes lost in the course of an experiment as a result of high humidity. Deliquescence was not an issue with the coformer mixtures in the project, but a there were a few instances of lost sample in 75% RH conditions causing a drop in signal-to-noise ratio in the course of an experiment. Higher humidities were likely responsible

for minor dissolution of sample without noticeable water condensation in these cases. This issue was fixable by a repeat trial.

A third issue occurred in sample preparation, and that issue was the matter of static charge generated by the grinding of powders. Whether by ball mill or mortar and pestle, some coformers consistently generated such high charge density that they were propelled in distances exceeding one foot simply by scraping powder from the inside of a milling jar. These powders stuck to paper, jumped out of glass vials, and clung to the underside of sieves, making size selection almost impossible. Because the project involved the effect of humidity on cocrystallization and called for freshly ground coformers, leaving a coformer in a humidity chamber prior to mixing may induce the formation of a solvate—an unacceptable possibility when tracking cocrystal reaction kinetics; however, letting a ground coformer sit at lower humidity in the hope of sufficient charge dissipation without the assistance of water vapor took several days, once again rendering the powder unusable. Attempting to salvage as much powder as possible in these conditions could take up to 6 hours of sample transfer prior to setting up an experiment. Yields lower than 0.1% were possible depending on the day of milling, as was the case in a NA:GA 1:1 sample preparation, leading to sample preparation needing to be restarted another day for lack of material.

While these problems had the immediate effect of significant increase in project inefficiency, they also present some potential issues in the way that the reactions progressed. The hardening of the samples may lock particles in place at the crystallite level, preventing islands of coformer from dissipating (spontaneous powder movement is discussed in Section 5.1.1). The ease with which some materials, primarily caffeine, nicotinamide, and glutaric acid, pick up static charge during grinding may also play a role in how readily coformers will cocrystallize.

Though experiments with sample loss were repeated when identified, the presence of sample loss as a factor in humidity chambers is another potential roadblock in achieving 100% conversion to cocrystal, because sample is not likely to be in the desired stoichiometric ratio, resulting in an imbalance in coformer availability that is only exacerbated as time progresses.

CHAPTER 4. VAPOR-POWDER INTERFACE EXPERIMENTS

This chapter details the viability of the vapor-powder interface as a mechanism for cocrystal formation. Five years ago, we conducted a single trial in the layered rotor experiment (Section 2.3.1) in a less refined rotor packing method. This *in situ* NMR technique was revisited and improved in order guard against cross-contamination of coformers inside the NMR rotor during packing (Figure 1). These experiments focused on the CA:MA 2:1 system, and have since been extended to the INA:BZE 1:1 system. An *ex situ* method (Section 2.3.2) was also developed to perform side-by-side study by PXRD for both the CA:MA 2:1 and INA:BZE 1:1 systems.

4.1. Isoniazid-Benzoic Acid 1:1 Cocrystal

We began testing the vapor-based mechanism of cocrystallization using the INA:BZE 1:1 system. We chose this cocrystal for two reasons: Sarceviča, et al. report that this cocrystal forms spontaneously at ambient conditions, and benzoic acid possesses several desirable qualities for conducting the layered rotor experiment: it is a small organic molecule (similar to other substances that we study); it has high volatility for vapor generation; it's high melting point (>100°C) means that it can withstand variable-temperature experiments; and it is relatively inexpensive for ^{13}C labeled material.[10]

Experiments in the vapor-powder interface began with the INA:BZE 1:1 system at 80°C (referred to as the "high-temperature" experiment). We first conducted the layered rotor experiment outlined in Section 2.3.1 but found that isoniazid and benzoic acid undergo no conversion to cocrystal (Figure 8). We then tested the INA:BZE 1:1 system using the *ex situ* method described in Chapter 2.3.2, but no cocrystal signal was identified for this experiment either (Figure 9). These initial results suggested that the INA:BZE 1:1 does not form via a vapor-based mechanism.

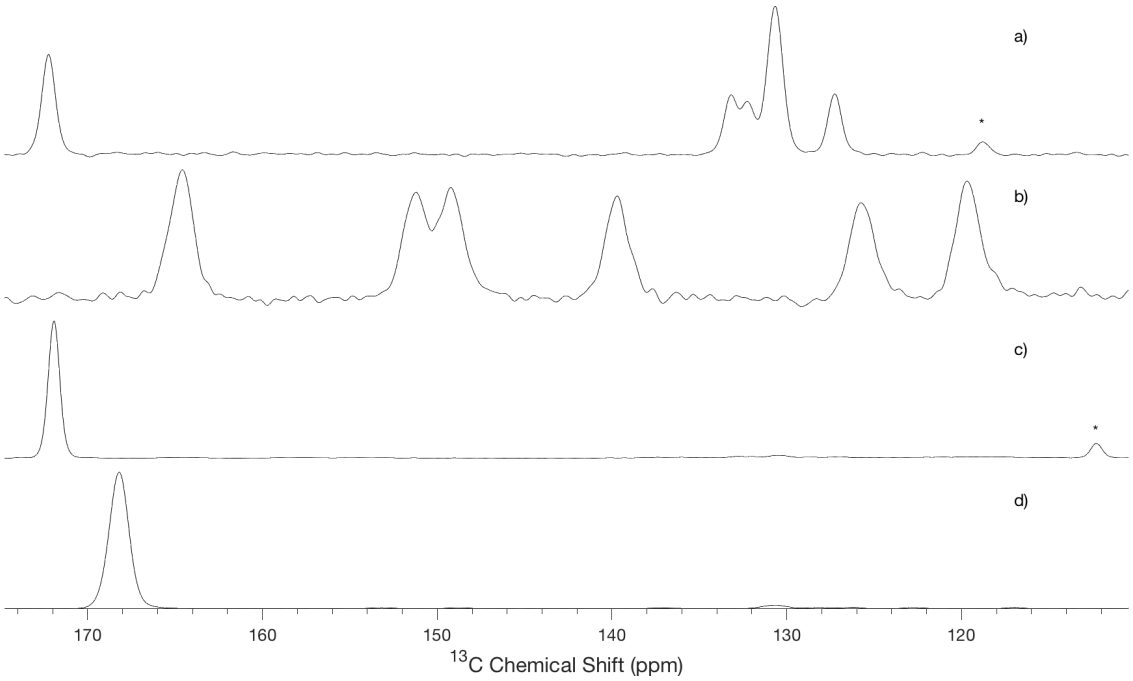

Figure 8. ^{13}C-NMR. Singly-layered INA:BZE rotor experiment at 80°C. a) BZE; b) INA; c) Layered rotor with carbonyl-labeled BZE after heating the rotor for 24 hours inside the spectrometer; d) INA:BZE 1:1 cocrystal. Spinning side bands are marked with an asterisk.

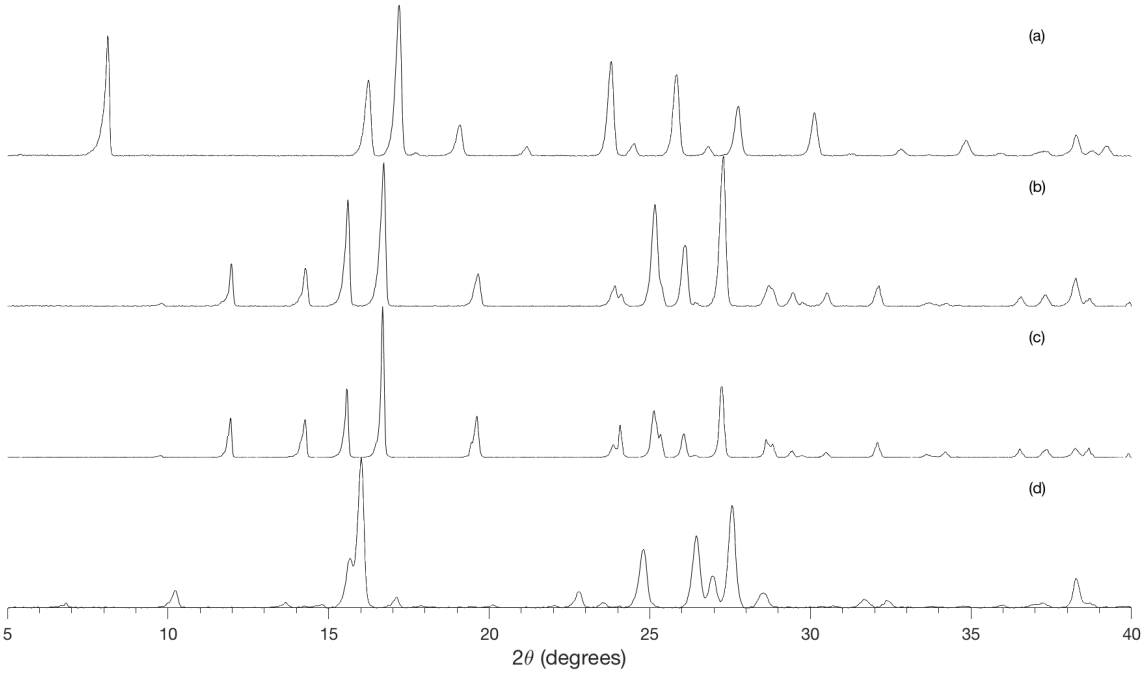

Figure 9. PXRD. Two-chamber vapor experiment with INA and BZE in separate PXRD sample holders in an aluminum foil-covered petri dish at 80°C. a) INA; b) BZE; c) INA sample holder after 7 days; d) INA:BZE 1:1 cocrystal.

The high-temperature experiment was then conducted in reverse by heating milled INA:BZE 1:1 cocrystal in an open 10-mL vial at 80°C on a heating block, following the first iteration of the procedure mentioned in Chapter 2.3.2. This experiment was conducted to test the thermodynamic stability of the cocrystal at 80°C—if the system was incapable of maintaining its composition at high temperatures, then we would not expect volatile benzoic acid vapor to spontaneously form the cocrystal with isoniazid at under the same conditions. The PXRD trace of the sample after several days of heating indicated decomposition of the cocrystal (Figure 10). While isoniazid signal increased, no benzoic acid signal was observed, suggesting that benzoic acid sample was escaping as vapor. In a repeat trial, the same experiment was conducted in a closed container in order to recrystallize vapor near the cap of the vial, the part of the closed system furthest from the heat source. Needle-like crystals matching the diffraction pattern of benzoic acid began to form along the rim of the container after a few days. These results indicate that 80°C was not only too high of a temperature for cocrystallization to occur, but that the isoniazid powder was not a favorable location for benzoic acid vapor to settle. These findings explain the lack of cocrystal signal in both *in situ* and *ex situ* high-temperature experiments as well as the absence of unreacted benzoic acid on the *ex situ* isoniazid sample.

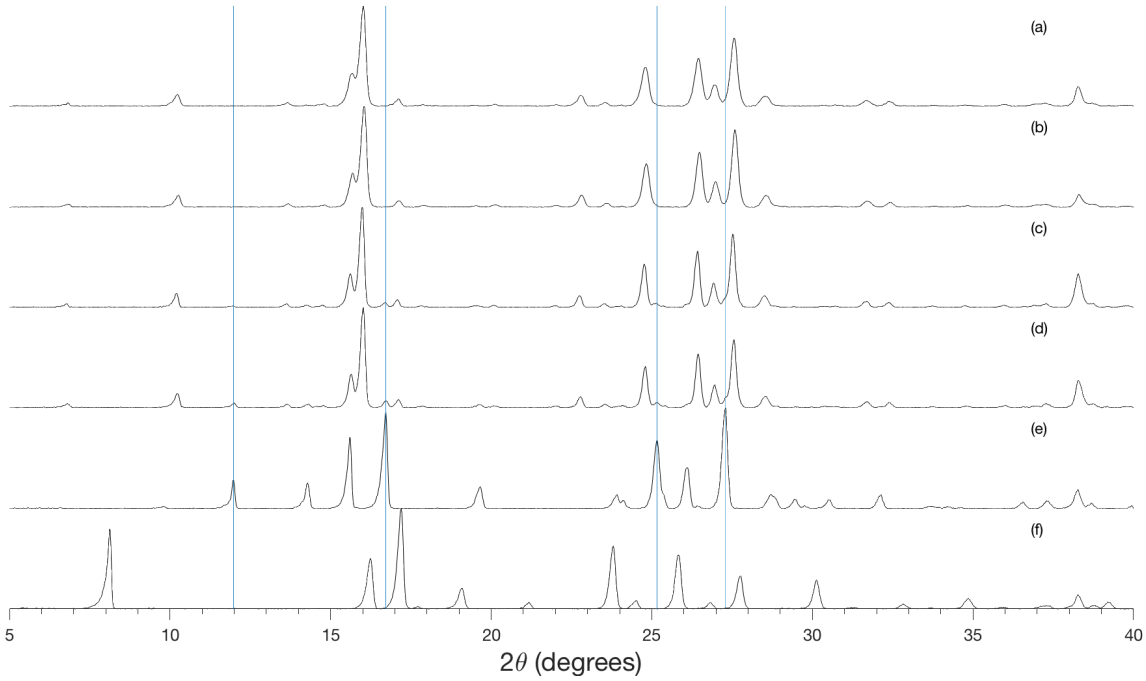

Figure 10. PXRD. Decomposition experiment for INA:BZE 1:1 at 80°C. a) INA:BZE 1:1 cocrystal; Milled cocrystal before heating; c) Milled cocrystal after 24 hours; d) Milled cocrystal after 40 hours; e) INA; f) BZE. INA begins to appear in significant quantity as indicated by change at angles marked by blue vertical lines.

Because the decomposition experiment had demonstrated that an 80°C environment was unstable to cocrystal formation, the next step in studying the vapor-powder interface was to reduce the temperature of the reaction environment. We repeated the layered rotor and two-chamber experiments at 35°C to determine if INA:BZE 1:1 cocrystal was a more favorable state than benzoic acid vapor at lower temperatures. Both *in situ* (Figure 11) and *ex situ* (Figure 12) experiments showed no change in sample chemistry. The *ex situ* experiment once again showed no evidence of benzoic acid deposit on isoniazid. Between high- and low-temperature experiments, both *in situ* and *ex situ*, no evidence was found for a vapor-based mechanism of transport for the spontaneous formation of the INA:BZE 1:1 cocrystal.

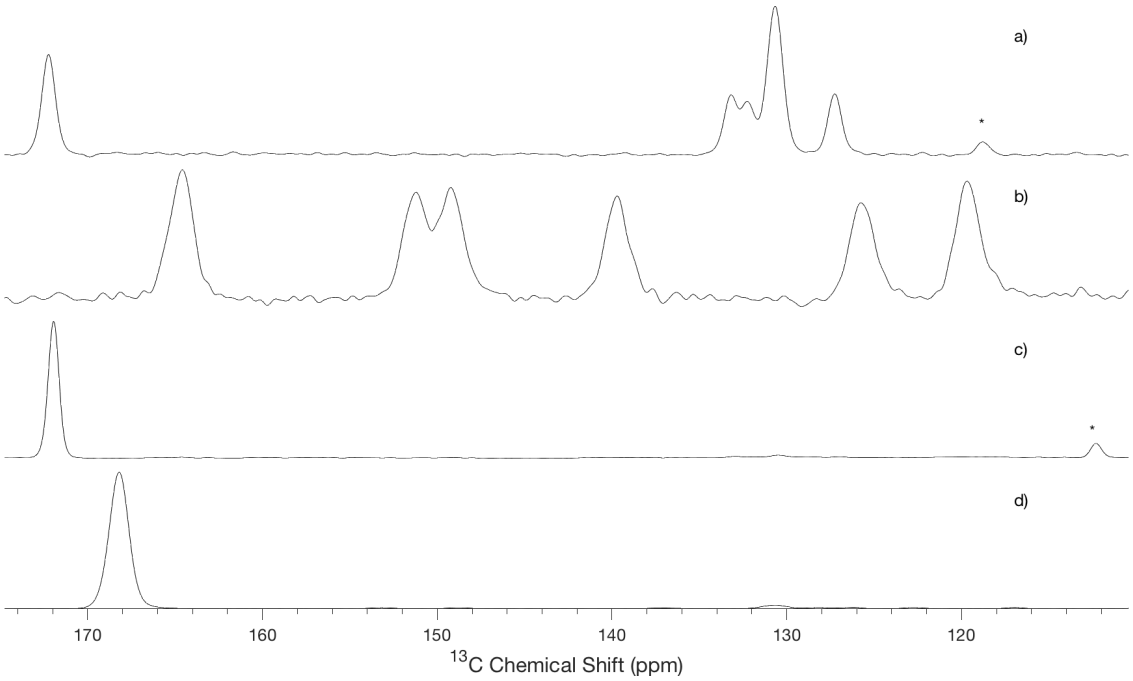

Figure 11. ^{13}C-NMR. Singly-layered INA:BZE rotor experiment at 35°C. a) BZE; b) INA; c) Layered rotor with carbonyl-labeled BZE after heating the rotor for 24 hours inside the spectrometer; d) 1:1 INA:BZE cocrystal.

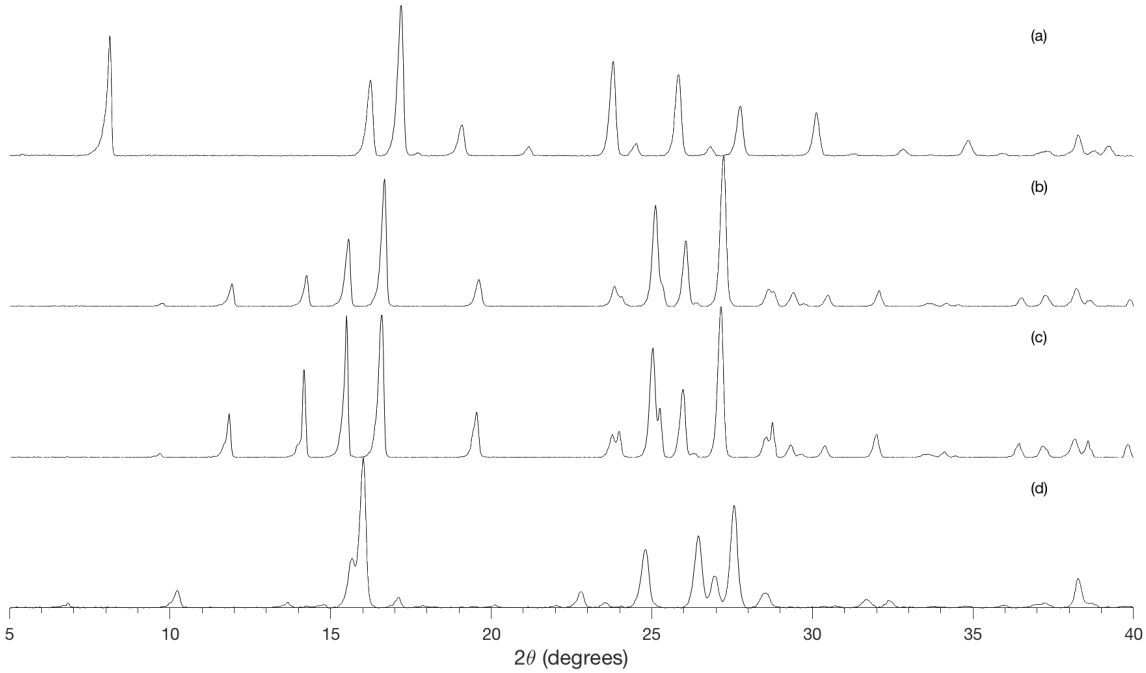

Figure 12. PXRD. Two-chamber vapor experiment with INA and BZE in separate PXRD sample holders in an aluminum foil-covered petri dish at 35°C. a) INA; b) BZE; c) INA sample holder after 8 days; d) INA:BZE 1:1 cocrystal.

4.2.Caffeine-Malonic Acid 2:1 Cocrystal

In order to add another dimension to the exploration of the vapor-powder interface, the CA:MA 2:1 system, which had been used initially to implement the *in situ* NMR experiment, was studied alongside the INA:BZE 1:1 system. Once again we used *in situ* and *ex situ* methods at 80°C. Just as we found for INA:BZE 1:1, these high temperature experiments also yielded negative results, as indicated by the lack of change in the NMR spectrum and absence of malonic acid signal and cocrystal signal in the caffeine PXRD trace (Figures 13 and 14).

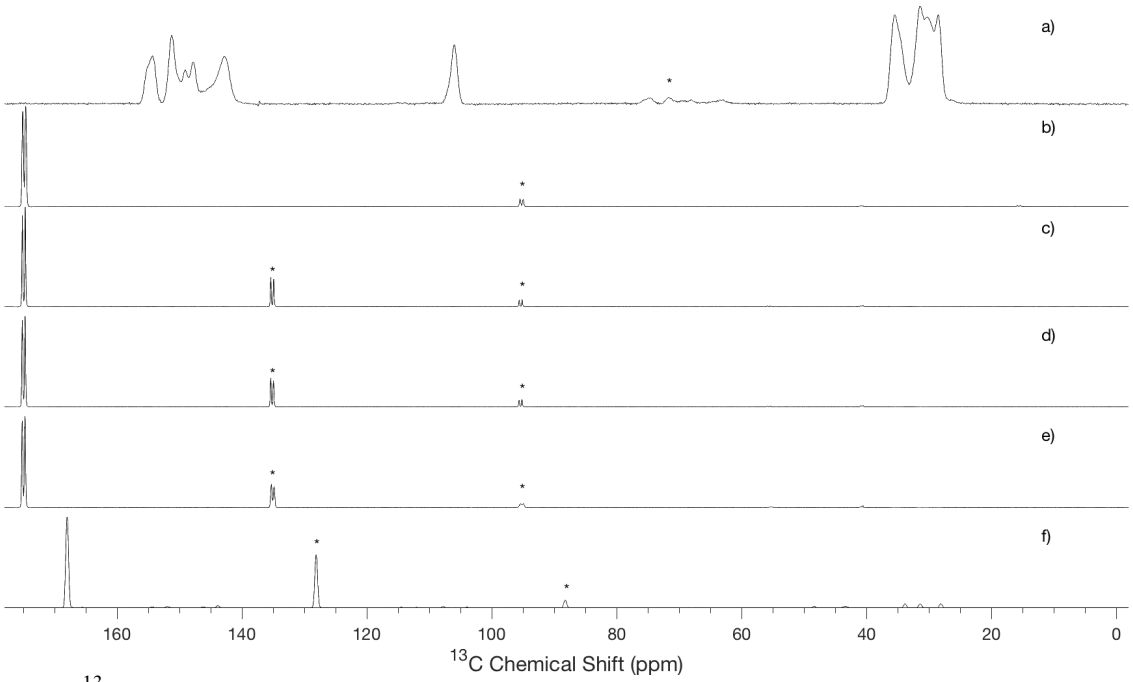

Figure 13. ^{13}C-NMR. Time-sampled spectra from the singly-layered CA:MA rotor experiment at 80°C. a) CA; b) 1-$^{13}C_1$ MA; c) Layered rotor after initial packing; d) Layered rotor after 2 days; e) Layered rotor after 18 days; f) 2:1 CA:1-$^{13}C_1$ MA cocrystal. Spinning side bands are marked with an asterisk.

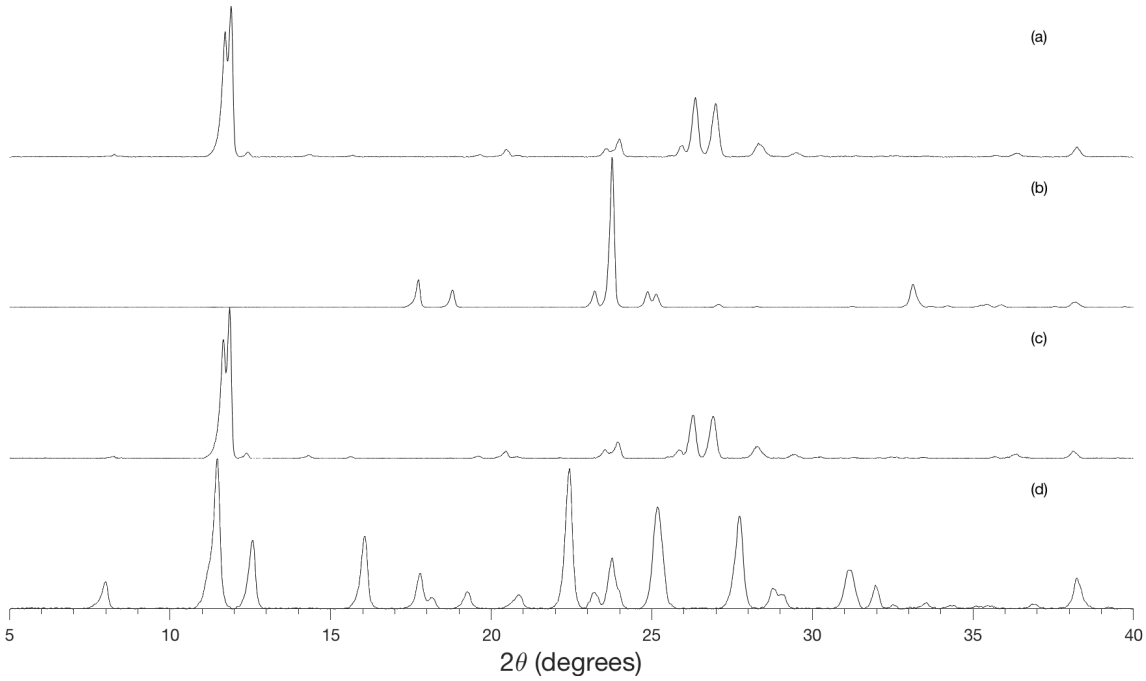

Figure 14. PXRD. Two-chamber vapor experiment with CA and MA in separate PXRD sample holders in an aluminum foil-covered petri dish at 80°C. a) CA; b) MA; c) CA sample after 8 days; d) CA:MA 2:1 cocrystal.

After the absence of positive results in the high temperature experiments for the 2:1 CA:MA system, the same question was posed regarding the stability of the cocrystal at 80°C, and so a sample of cocrystal was subjected to the same conditions as described in Chapter 4.2.3. Though not as rapid a decomposition, decrease in cocrystal signal and increase in caffeine signal was observed in a matter of days (Figure 15). The more volatile malonic acid did not appear in the PXRD trace. The consistency of the results across the 1:1 INA:BZE and 2:1 CA:MA systems indicate that at temperatures high enough to impel significant sublimation of coformer, cocrystallization may be thermodynamically unfavorable.

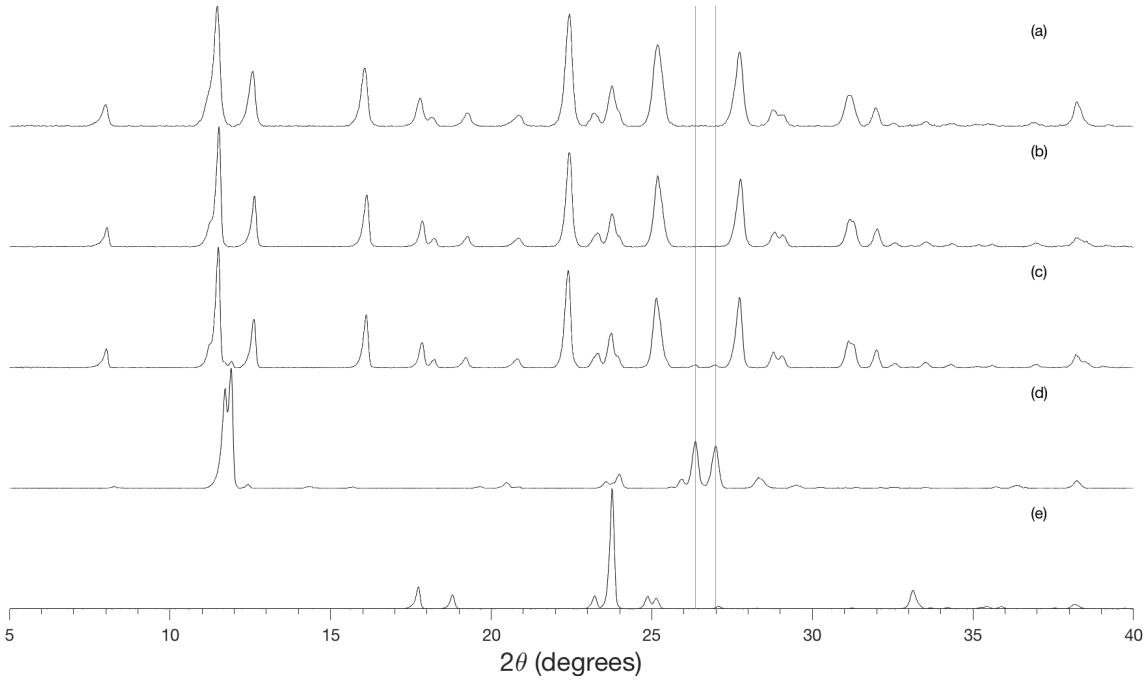

Figure 15. PXRD. Decomposition experiment for CA:MA at 80°C. a) 2:1 CA:MA cocrystal; b) Milled cocrystal before heating; c) Milled cocrystal after 35 days; d) CA; e) MA. Vertical lines indicate increase in CA signal in c).

The CA:MA 2:1 system was also studied at 35°C to match the INA:BZE 1:1 data set, and the *in situ* (Figure 17) and *ex situ* (Figure 18) experiments indicated no cocrystallization. The results for the CA:MA 2:1 vapor-powder interface experiments point toward the same conclusion as was found for the INA:BZE 1:1 system, namely that a vapor-based mechanism is unlikely.

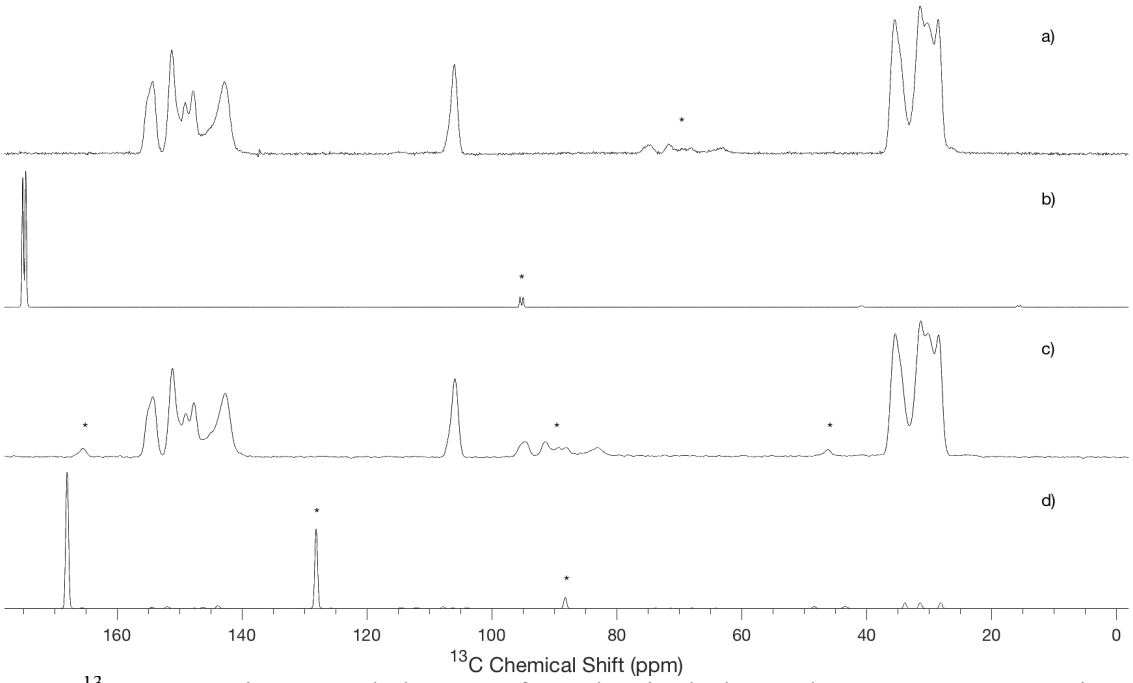

Figure 16. ^{13}C-NMR. Time-sampled spectra from the singly-layered CA:MA rotor experiment at 35°C. a) CA; b) 1-$^{13}C_1$ MA; c) CA sample after 1 day; d) 2:1 CA:MA cocrystal. Spinning side bands are marked with an asterisk.

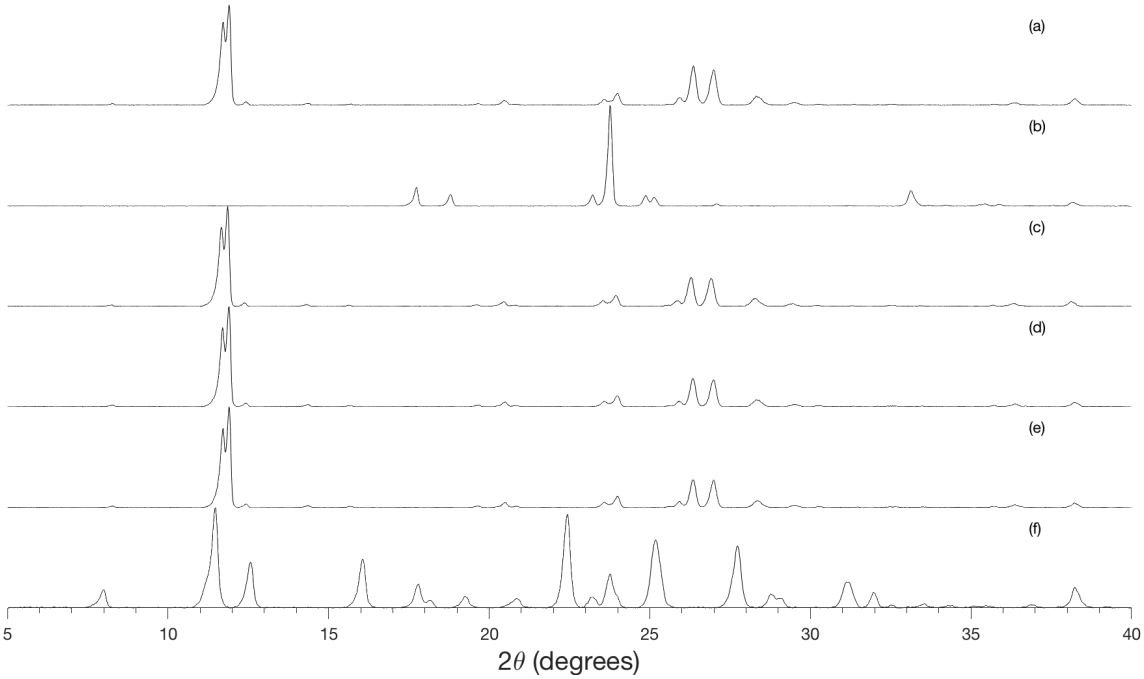

Figure 17. PXRD. Two-chamber vapor experiment with CA and MA in separate PXRD sample holders in an aluminum foil-covered petri dish at 35 C. a) CA; b) MA; c) CA sample holder at initial state; d) CA sample holder after 7 days; e) CA sample holder after 31 days; f) 2:1 CA:MA cocrystal.

CHAPTER 5: POWDER-SINGLE CRYSTAL INTERFACE EXPERIMENTS

In addition to the powder-powder and vapor-powder interfaces, we tested the interface between a powdered species and a larger crystal (millimeter-to-centimeter in size) of its coformer. This interface served as a transition from the well-studied powder-powder interface—which is a mixture of an indeterminate number of crystallite interfaces—to the single crystal-single crystal interface. One advantage of this system when compared to the single crystal-single crystal interface is that only one coformer needs to be capable of forming large crystals. Despite caffeine's inability to form large crystals, we can conduct experiments with the CA:MA 2:1 system due to the ease with which we can grow malonic acid crystals.

5.1. 2:1 Caffeine-Malonic Acid System

5.1.1. Microscopy Results

Malonic acid crystals can be being grown as both plates and needles, making this system ideal for studying the powder-single crystal interface. The microscopy experiments were performed using the procedure outlined in Chapter 2.4.2. The first experiment, involving an aliquot of caffeine powder in contact with the tapered end of a malonic acid crystal, displayed two significant changes over the course of a week. The first noticeable change was the alteration of the shape and color of the malonic acid crystal. As time passed, the tip of the malonic acid crystal receded, and the color of the crystal at points of contact with caffeine powder began to change. We also noticed that caffeine powder had moved spontaneously. As time passed, caffeine that had been placed in the area surrounding the crystal began to "hug" the malonic acid, crowding the crystal's surface (Figure 18).

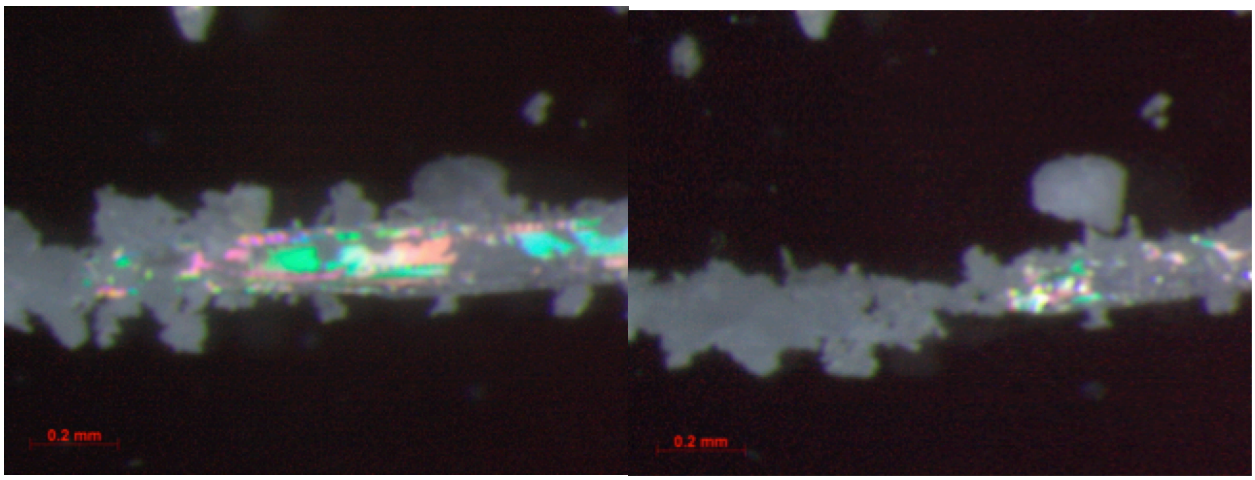

Figure 18. Malonic acid crystal in contact with caffeine powder at initial time point (left) and after 275 hours (right).

This movement appears to have limited range, as powder at the edge of the image does not undergo any movement relative to the crystal. While the nanometer-thin tip of the crystal was expected to change, whether by reaction with caffeine or atmospheric moisture, we did not anticipate the spontaneous bulk movement of caffeine powder. In order to perform a more rigorous analysis of this phenomenon, the procedure was repeated alongside an uncaffeinated malonic acid crystal that served as a control for environmental effects. Though the results were replicable, the control crystal also underwent color change and size reduction (Figure 19). The spontaneous movement of caffeine had not been observed before, but the crystal changes in the control demanded that a second technique be used to determine what was occurring to the malonic acid at the molecular level.

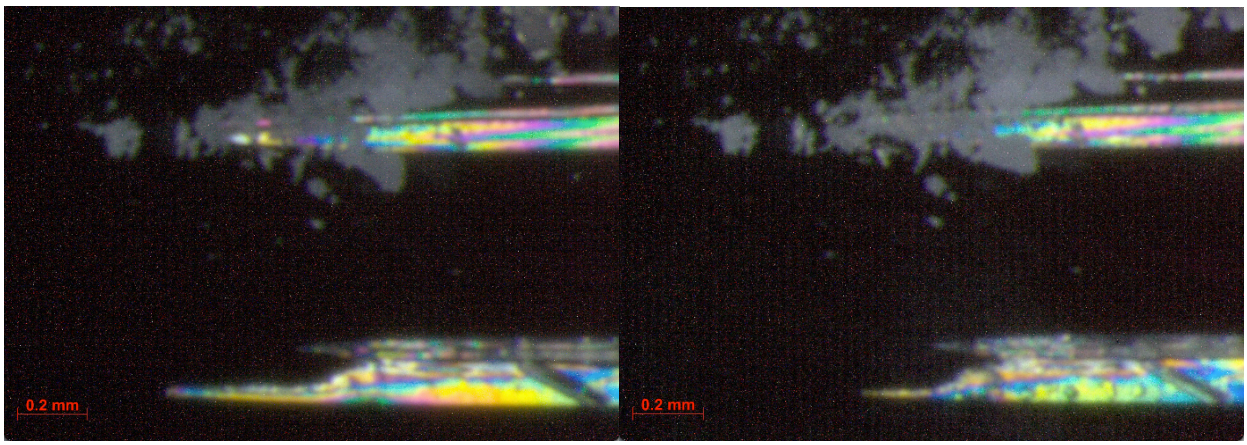

Figure 19. Malonic acid crystal in contact with caffeine powder at initial time point (left) and after 100 hours (right). Control malonic acid crystal not in contact with caffeine powder is present in the bottom half of each figure.

5.2.1. NMR Results

After examining the powder-single crystal interface with microscopy, *in situ* NMR experiments were conducted to take a more precise approach to the system. NMR spectroscopy of a plate crystal of ^{13}C single carbonyl-enriched malonic acid and caffeine powder combined in a thin-walled NMR rotor showed no signs of conversion after one week of study (Figure 20). Caffeine and malonic were demonstrated to form a significant amount of cocrystal in a matter of hours at ambient conditions when comprised of a thoroughly mixed sample of powders, so the presence of the crystal is the most likely explanation for the lack of conversion to cocrystal. In the follow-up experiment where the crystal was completely covered by caffeine powder and lightly crushed, no change was observed after a week (Figure 21). The goal of this experiment was to minimize the risk of conversion by mechanochemistry while opening up more surfaces on the crystal for reaction with caffeine, but the increased surface area did not appear to encourage any cocrystallization. These findings suggest that cocrystallization does not occur by spontaneous invasion of crystallites of one species by molecules of its coformer.

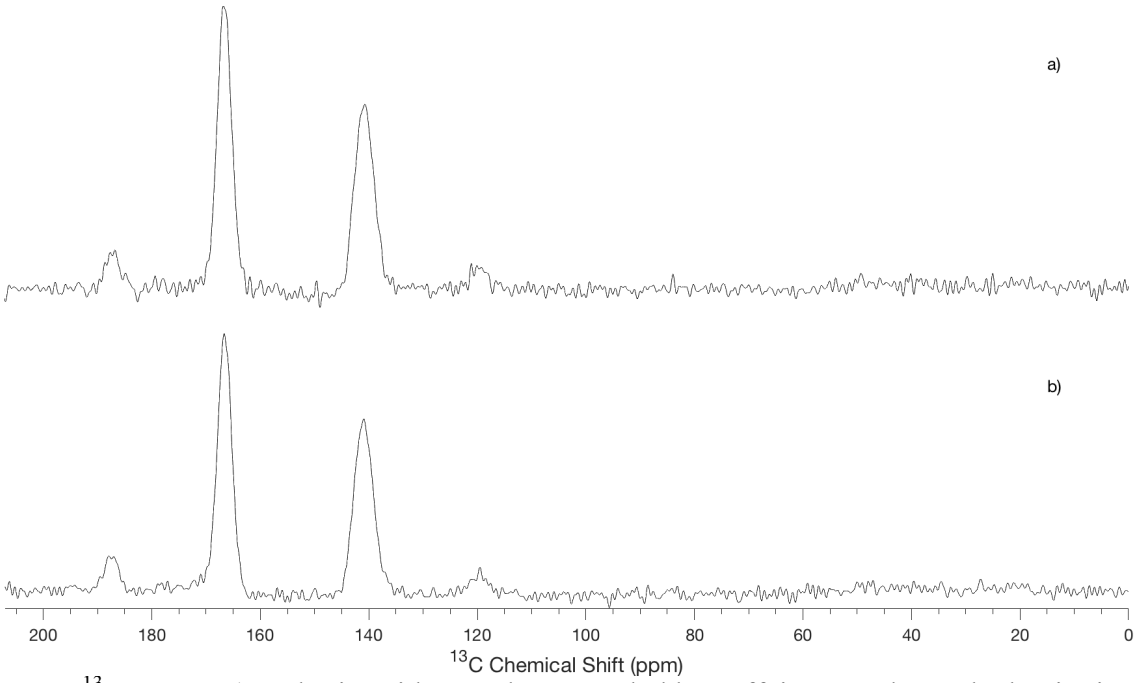

Figure 20. ^{13}C-NMR. a) malonic acid crystal surrounded by caffeine powder at the beginning of the experiment *in situ* powder-single crystal CA:MA 2:1 experiment; b) powder-crystal arrangement after 6 days.

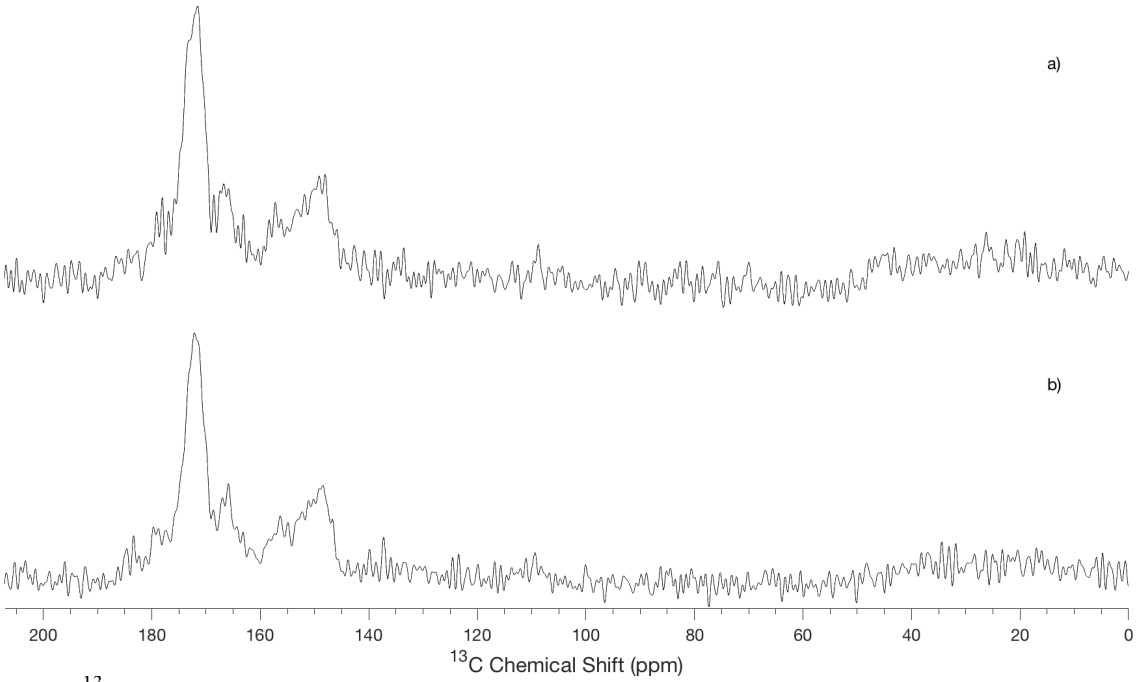

Figure 21. ^{13}C-NMR. a) fragmented malonic acid crystal surrounded by caffeine powder immediately after recording Figure 20b; b) powder-crystal arrangement after 7 days (approximately two weeks from first contact between caffeine and malonic acid).

5.2. 2:1 Theophylline-Malonic Acid System

We began study of the TH:MA 1:1 cocrystal alongside the CA:MA 2:1 cocrystal for the powder-single crystal interface. Unlike, caffeine, theophylline is capable of growing macroscopic crystals(Section 2.4.1), giving the TH:MA 1:1 system the advantage of being able to undergo powder-single crystal experiments with either coformer as the crystal. Unfortunately, due to a hard disk crash while gathering time lapse footage, much of the data from these experiments have been lost. Furthermore, no NMR data has yet been acquired. One photograph taken through the eyepiece of the microscope at 96.0x magnification shows some cracking of the theophylline crystal at contact sites with malonic acid powder (Figure 22).

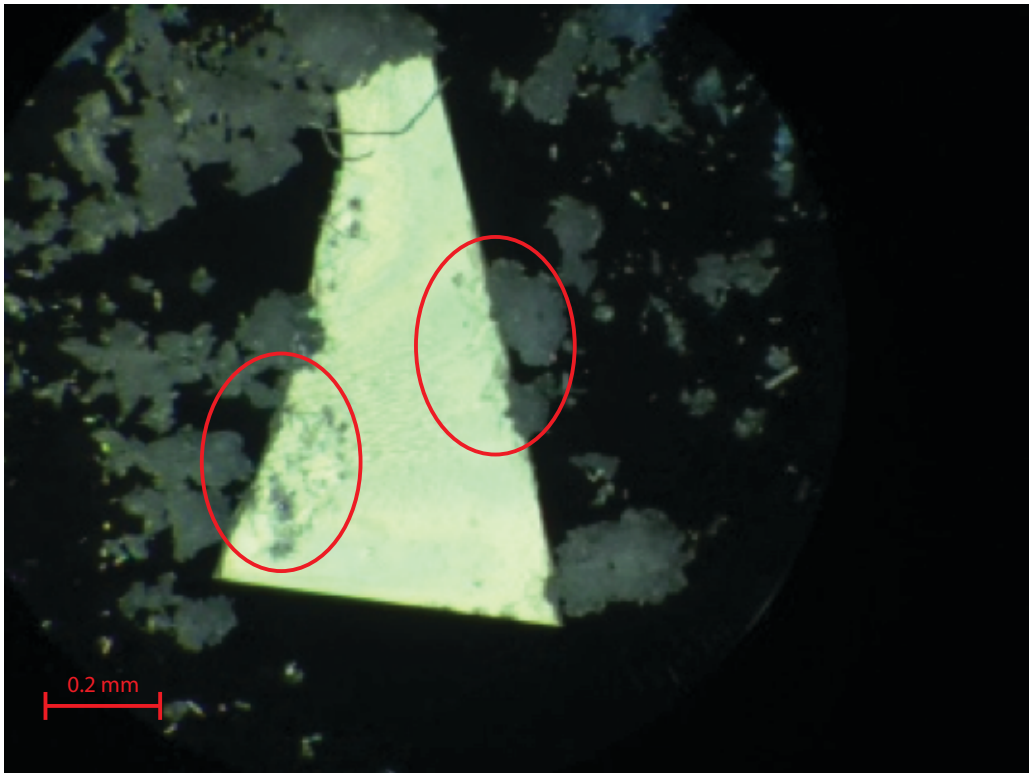

Figure 22. Theophylline crystal in contact with malonic acid powder after 6 days at ambient conditions. Signs of cracking along the edge of the crystal are highlighted with red circles. Scale bar is approximate.

CHAPTER 6: SINGLE CRYSTAL-SINGLE CRYSTAL INTERFACE EXPERIMENTS

We finish the research presented in this thesis with some early results in studying the interface between two large crystals (millimeter to centimeter size). Due to caffeine's inability to grow large crystals, we had to abandon the CA:MA 2:1 cocrystal for these experiments. The TH:MA 1:1 system was used instead of CA:MA 2:1 to conduct preliminary experiments in the single crystal-single crystal interface. Theophylline is capable of growing broad, razor-thin crystals that interface well with malonic acid's plate crystals. These experiments, like the TH:MA 1:1 experiments in Chapter 5, were also lost. We took more pictures through the microscope eyepiece in order to produce some results.

The microscopy experiment detailed in Chapter 2.5 yielded no visible change after 200 hours of monitoring, but after removing the theophylline crystal from the malonic acid crystal a hole in the theophylline crystal at the point of contact with malonic acid became visible. (Figure 23). This experiment was repeated, and a hole of similar shape was once again produced after waiting 200 hours. No NMR experiments have been conducted yet.

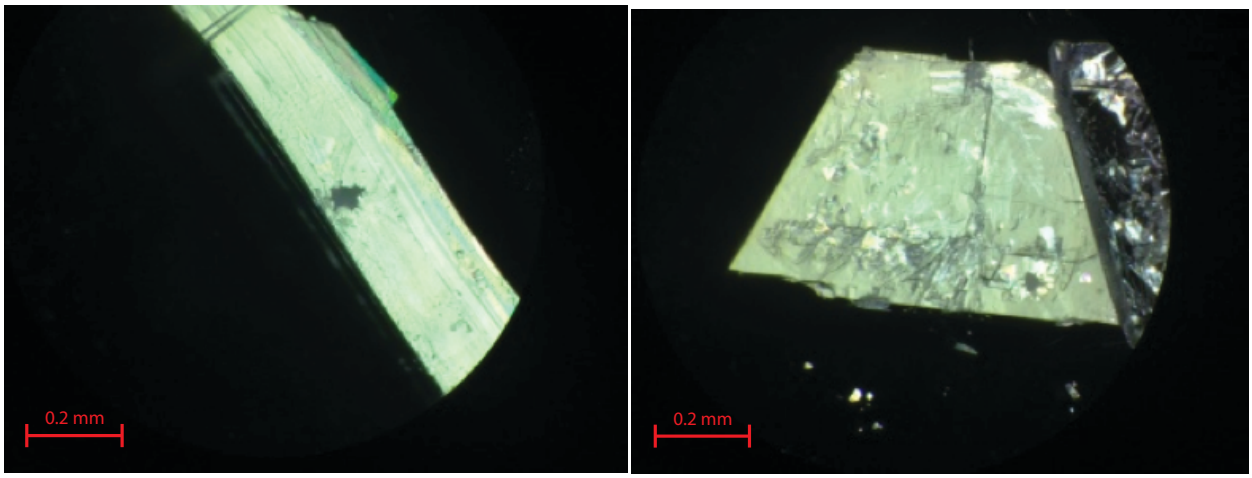

Figure 23. Left: First theophylline crystal after removal from malonic acid plate crystal. Hole present in center of crystal. Right: Second theophylline crystal after removal from the same malonic acid plate crystal, edge of malonic acid crystal present to the right of theophylline. Hole present in lower right of crystal. Scale bars are approximate.

The presence of this hole in the theophylline crystals indicates that despite the initial powder-single crystal NMR results for the CA:MA 2:1 system (Section 5.2.1), large crystals are capable of reacting with their coformers. The shape of the hole, when compared to the cracks on the theophylline crystal in Figure 22, suggests that the cocrystallization is initiated by physical contact between coformers, but once this contact has been established, spontaneous cocrystallization can occur deeper than at the surface level of the crystal.

CHAPTER 7: CONCLUSIONS AND FUTURE WORK

Humidity has consistent and measurable influence on the rate of spontaneous cocrystallization. Cocrystallization experiments in the powder-powder interface demonstrated that higher levels of humidity correspond to increased rate of spontaneous cocrystallization and lead to a greater percent conversion to cocrystal. These effects are consistent across APIs and diacids. Though some cocrystal systems display negligible reactivity under dry conditions, others, such as CA:OA 2:1, still manage to achieve a significant amount of conversion in the same environment. These findings suggest that water vapor has a catalytic effect on cocrystallization, but is not necessary for the reaction to progress.

Complete conversion to cocrystal is possible at particle size 45-90 microns. The experiments in spontaneous cocrystallization of CA:MA 2:1 and TH:MA 1:1 from mixed powder demonstrate that the transport mechanism for these two systems facilitates quantitative conversion at high humidity and small crystallite size. These results must mean that the molecules near the core of each crystallite, up to 90 microns in size, come into contact with molecules of the other coformer in the mixture. The transport mechanism necessitates a means by which molecules of one coformer can penetrate crystals of the other coformer, or else the crystallites are eroded or cracked in some way that leaves the inside of each crystallite open to cocrystallization. The results from Chapters 5 and 6 illustrate this phenomenon by showing the localized disruption of crystal structure at points of contact with known coformers.

Larger crystals appear to be more resistant to cocrystallization. This finding indicates that there is a limit to the extent of transport presented in the previous paragraph, evidenced by the lack of new signals appearing in the spectra of the powder-single crystal NMR experiments. Despite this dearth of evidence for cocrystallization supplied by the NMR spectra, the results of

the microscopy experiments suggest that coformers still interact spontaneously at larger crystal sizes. In addition to repeating the experiments from the lost data, we will conduct the powder-single crystal TH:MA 1:1 experiments by NMR. The powder used in the powder-single crystal experiments may also undergo chemical change, so scaling up these experiments to generate enough powder for PXRD analysis is another crucial step to understanding material transport.

The vapor-based mechanism of transport is unlikely for both caffeine-malonic acid 2:1 and isoniazid-benzoic acid 1:1 cocrystallization. The *in situ* and *ex situ* experiments for studying the vapor-based mode of transport both yielded no cocrystal. The volatile substance, whether benzoic acid or malonic acid, may not be forming cocrystal because the entire environment in which the experiment is occurring is uniformly heated. In the future, setting up experiments so that the more stable coformer is at a lower temperature, through use of a cold finger coated in coformer, will provide a favorable environment for the volatile vapor to deposit on its coformer.

Powder moves spontaneously when in contact with a crystal of its coformer. This discovery from the interaction between caffeine powder and malonic acid crystal illustrates that the interaction between coformers is not just a molecular-level interaction. We can deduce that the cocrystallization mechanism involves coformers rearranging themselves at both the molecular level to form hydrogen bonds and in bulk to maximize contact between coformers. This interaction is difficult to study by PXRD and NMR, because it involves movement of sample over space, but we will pursue this phenomenon with microscopy: we will study the relative favorability of cocrystallization, placing one substance alongside two coformers. We have already begun this work by grinding three substances together (e.g. CA, OA, and MA) to determine which cocrystal (CA:MA 2:1 or CA: OA 2:1) is more favorable. Studying spontaneous bulk movement under a microscopy will provide a parallel line of inquiry.

APPENDIX A: MOLECULAR AND CRYSTAL STRUCTURES

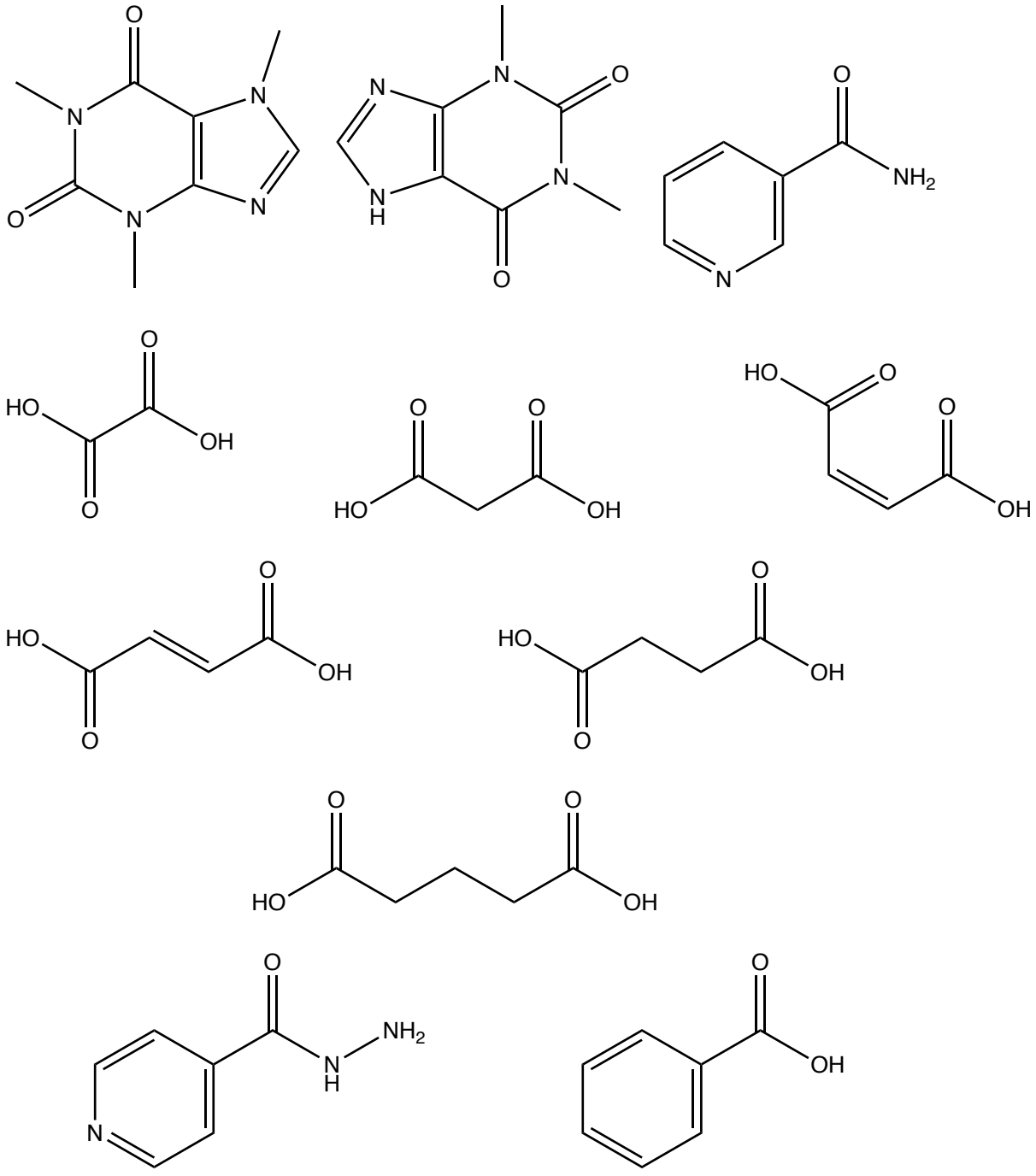

Figure A1. Molecular diagrams of species used in cocrystallization reactions. First row: caffeine, theophylline, nicotinamide. Second row: oxalic acid, malonic acid, maleic acid.
Third row: fumaric acid, succinic acid. Fourth row: glutaric acid. Fifth row: isoniazid, benzoic acid.

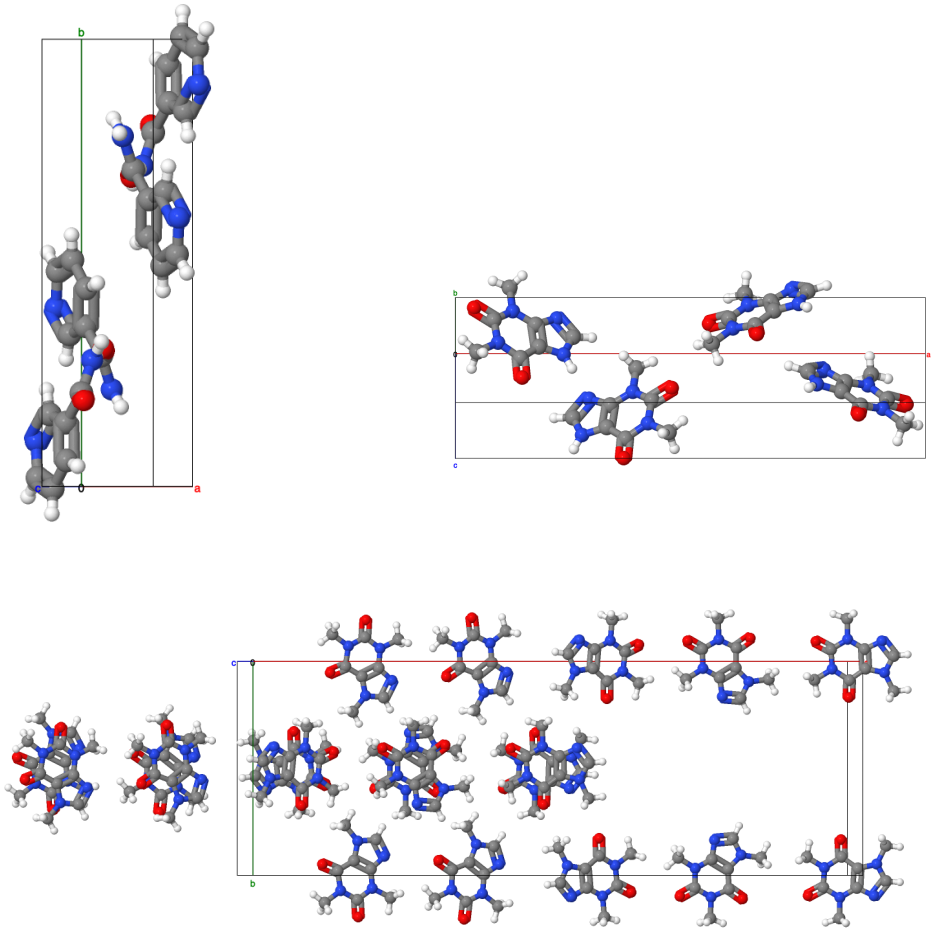

Figure A2. Crystal structures, clockwise from upper left: nicotinamide,[27] theophylline,[28] and caffeine.[29]

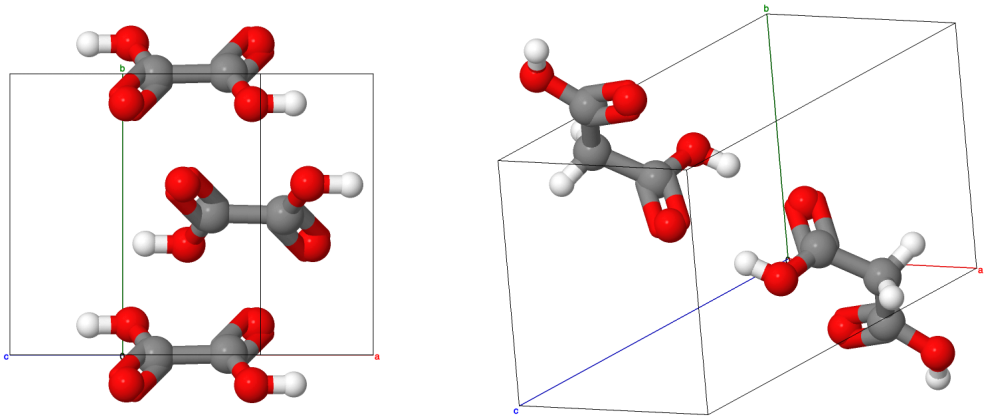

Figure A3. Crystal structures of oxalic acid (left)[30] and malonic acid (right).[28]

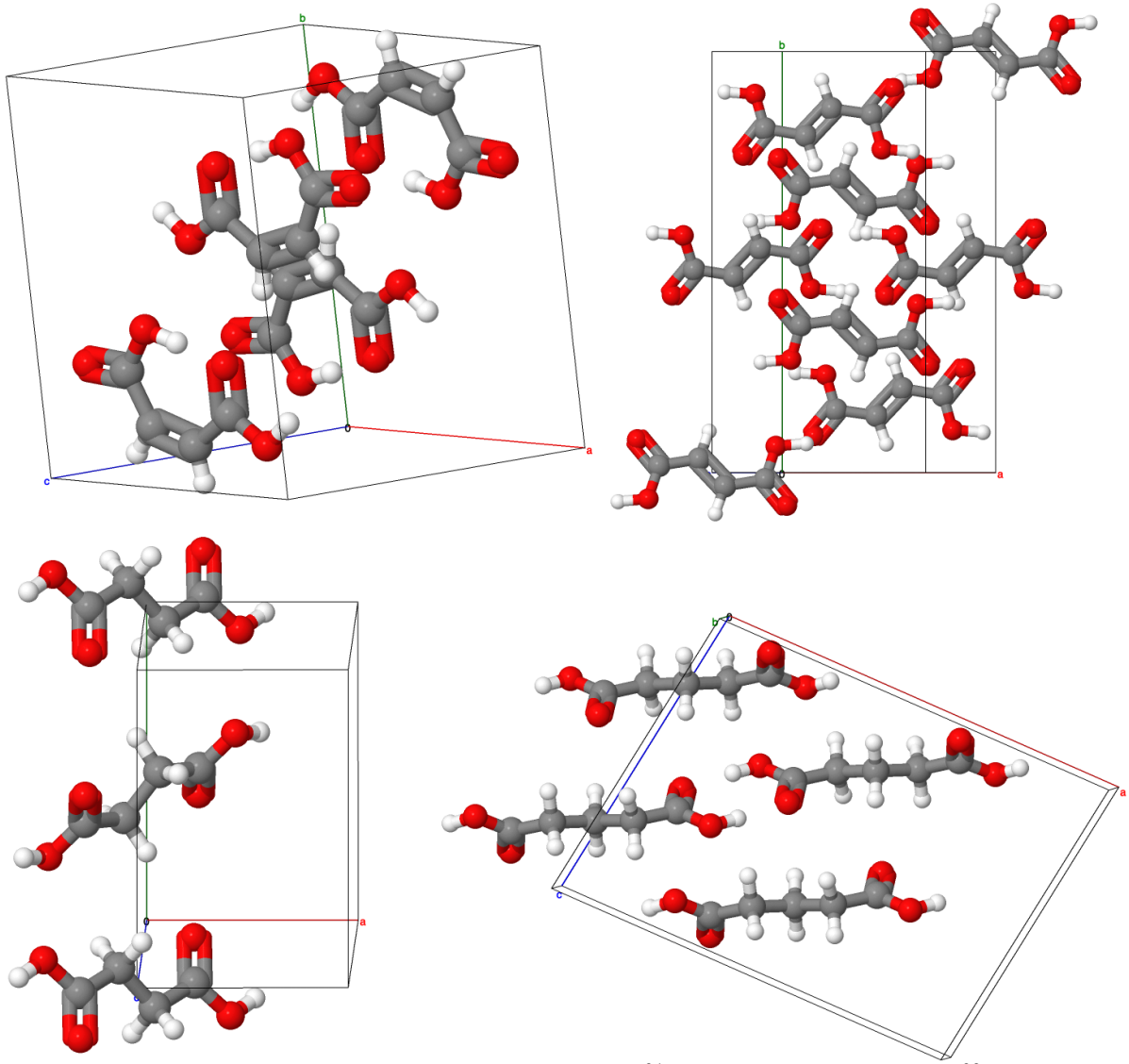

Figure A4. Crystal structures of maleic acid (top left),[31] fumaric acid (top right),[32] succinic acid (bottom left),[33] and glutaric acid (bottom right).[33]

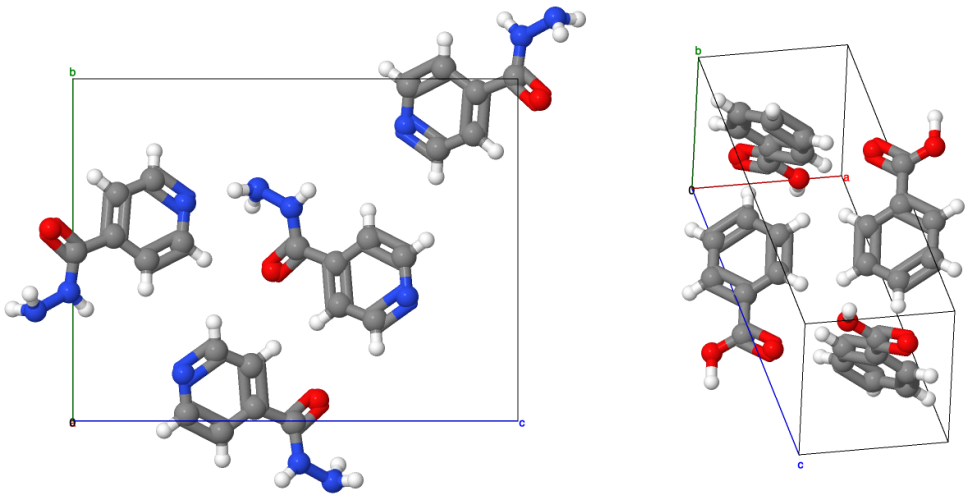

Figure A5. Crystal structures of isoniazid (left)[34] and benzoic acid (right).[35]

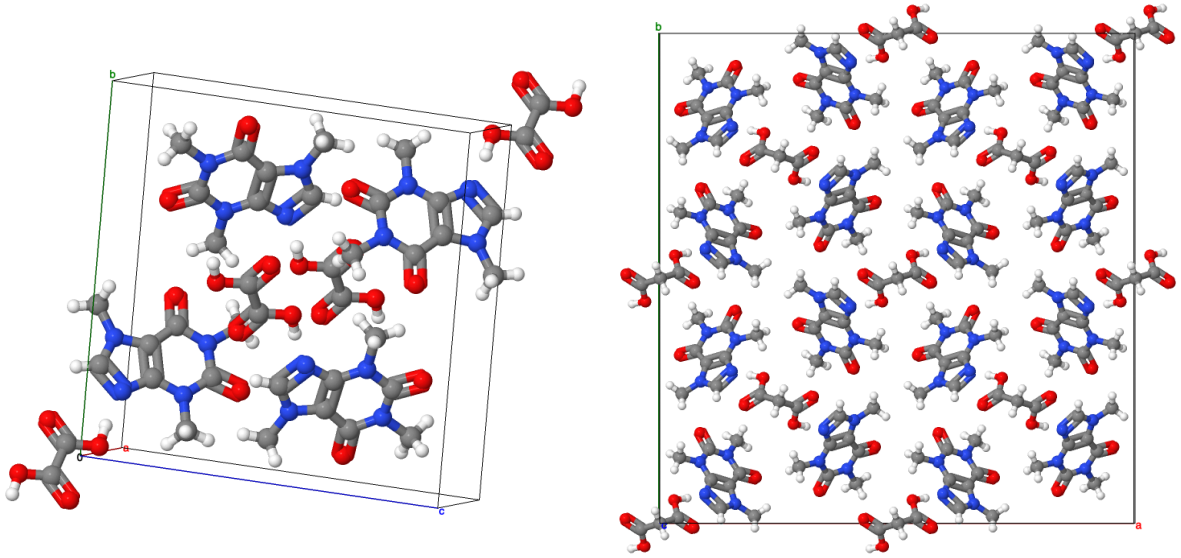

Figure A6. Crystal structures of caffeine-oxalic acid 2:1 cocrystal (left) and caffeine-malonic acid 2:1 cocrystal (right).[36]

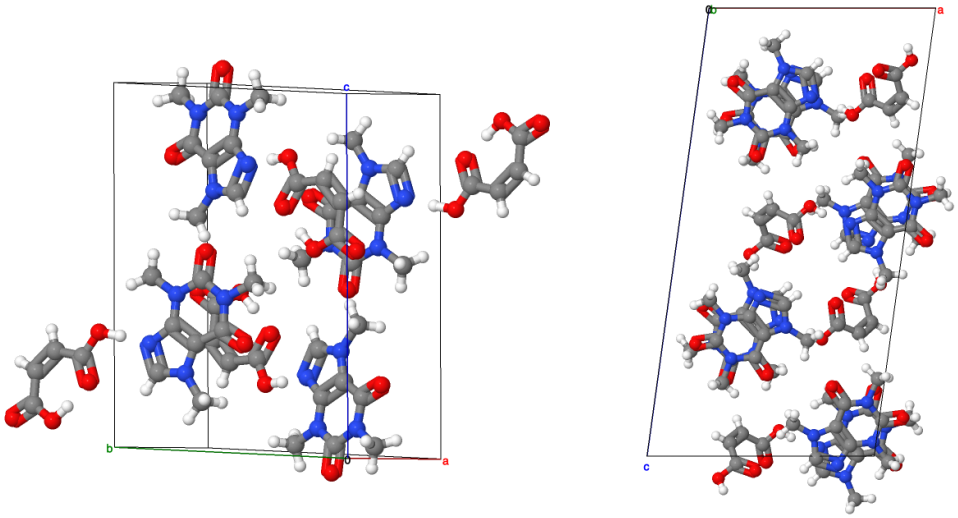

Figure A7. Crystal structures of caffeine-maleic acid 2:1 (left)[37] and 1:1 (right) cocrystal.[36]

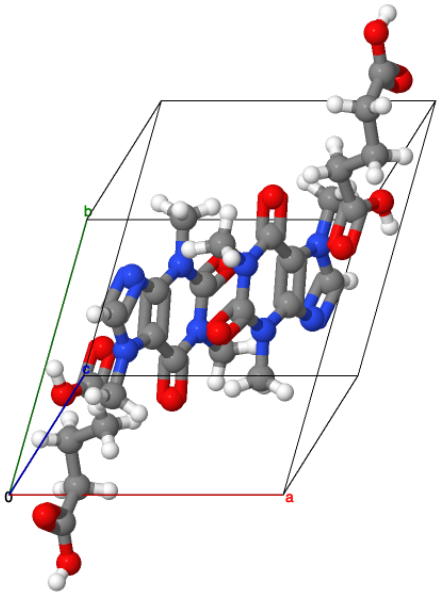

Figure A8. Crystal structure of caffeine-glutaric acid 1:1 cocrystal.[36] The caffeine-glutaric acid 2:1 crystal structure was not available via the Cambridge Structural Database.

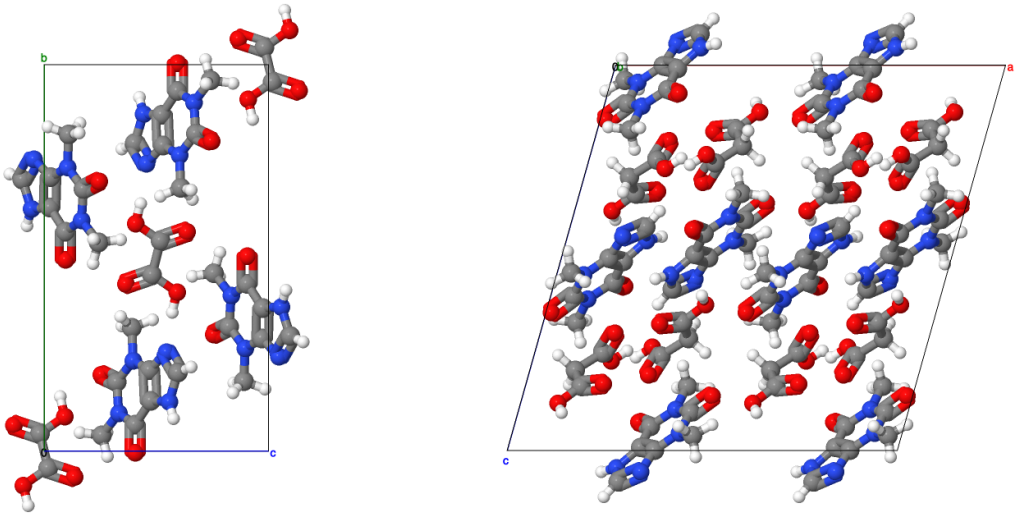

Figure A9. Crystal structures of theophylline-oxalic acid 2:1 cocrystal (left) and theophylline-malonic acid 1:1 cocrystal (right).[38]

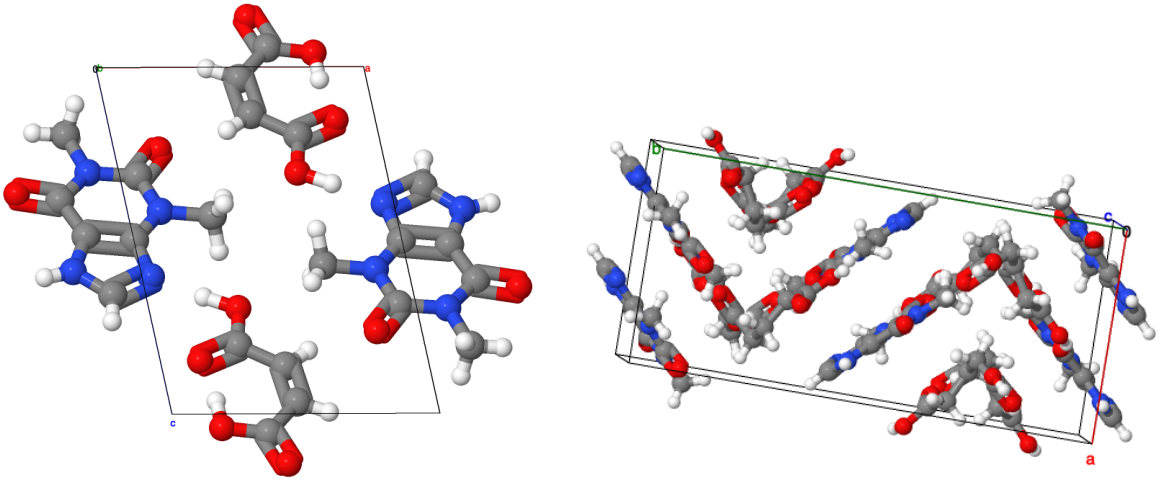

Figure A10. Crystal structures of theophylline-maleic acid 1:1 cocrystal (left) and theophylline-glutaric acid 1:1 cocrystal (right).[38]

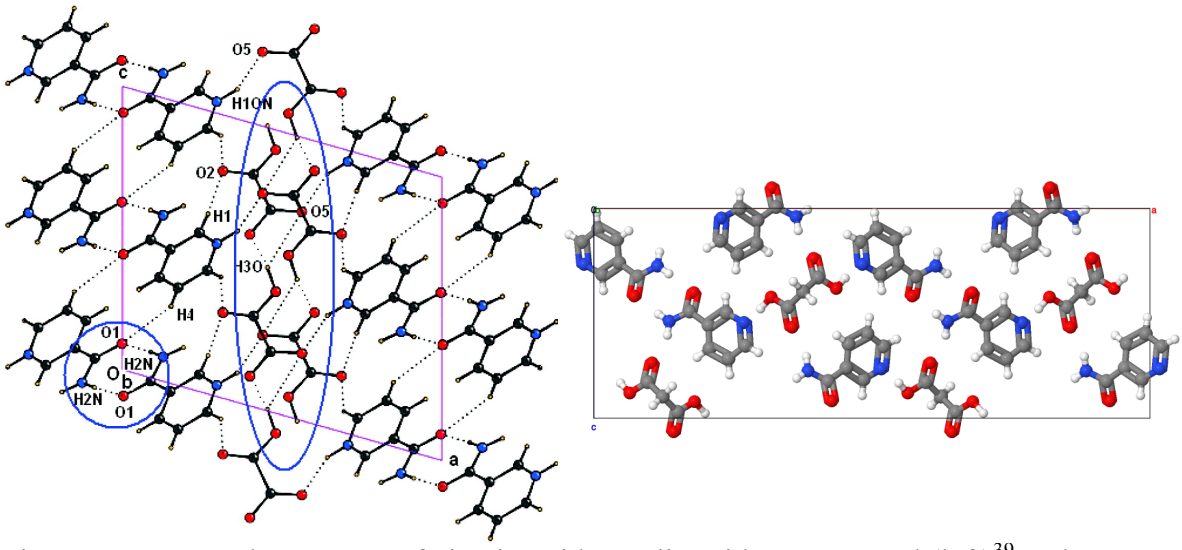

Figure A11. Crystal structures of nicotinamide-oxalic acid 2:1 cocrystal (left)[39] and nicotinamide-malonic acid 2:1 cocrystal (right).[40] The nicotinamide-oxalic acid 2:1 crystal was not available via the Cambridge Structural Database.

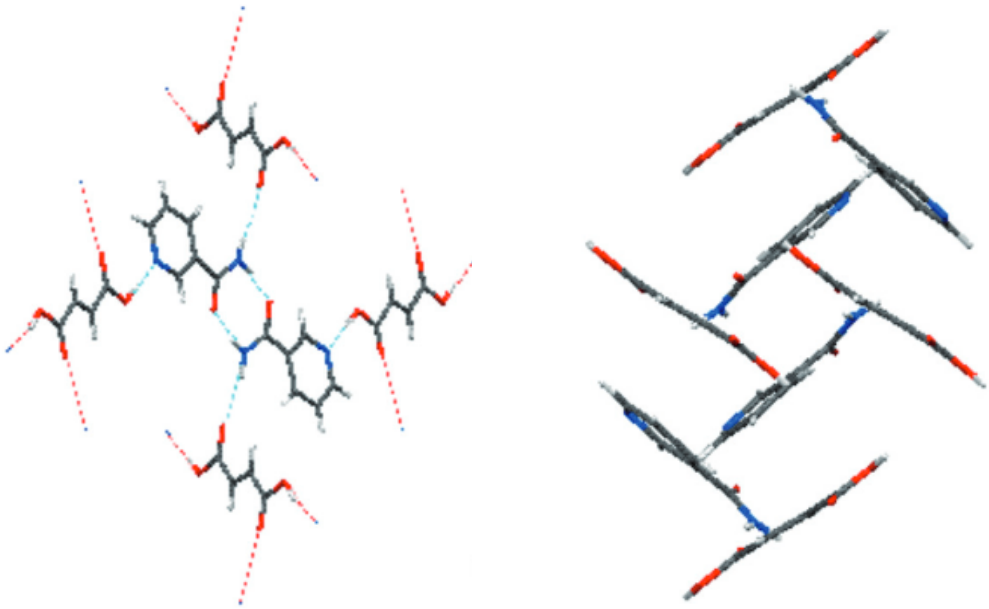

Figure A12. Crystal structure of nicotinamide-fumaric acid 1:1 cocrystal.[41] The structure for this crystal was not available via the Cambridge Structural Database. The nicotinamide-maleic acid 2:1 cocrystal was not available in any format.

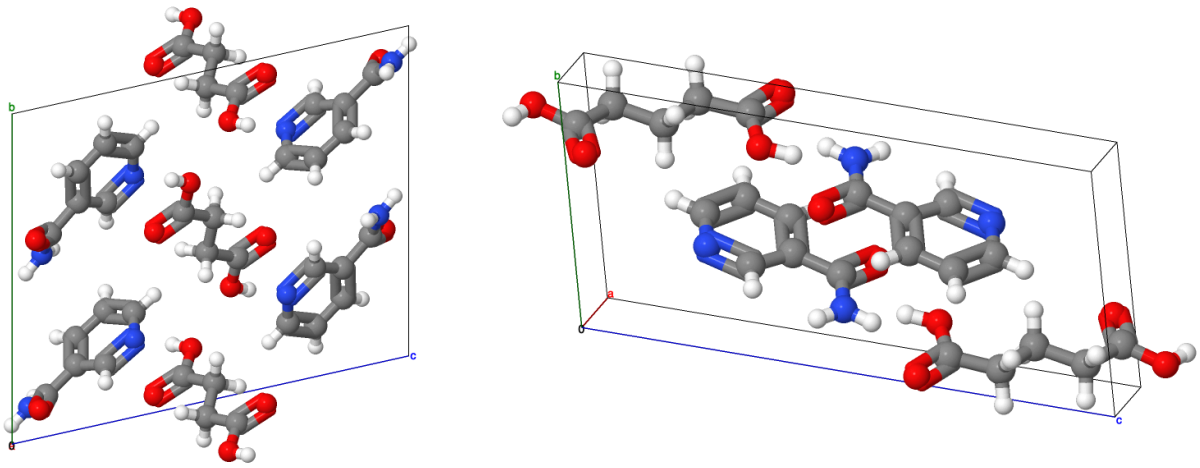

Figure A13. Crystal structures of nicotinamide-succinic acid 2:1 cocrystal (left)[42] and nicotinamide-glutaric acid 1:1 cocrystal (right).[40]

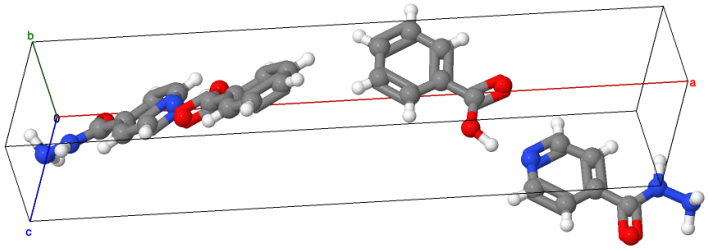

Figure A14. Crystal structure of isoniazid-benzoic acid 1:1 cocrystal.[43]

APPENDIX B: PXRD TRACES AND POWDER KINETICS PLOTS

This appendix contains PXRD traces for all cocrystals and coformers studied in Chapter 3. Vertical blue lines in the odd numbered figures indicate the value of 2θ used to track cocrystallization. Each set of PXRD traces is also accompanied by kinetics plots for the formation of the associated cocrystal at ambient conditions, 0% RH, 50% RH, and 75% RH.

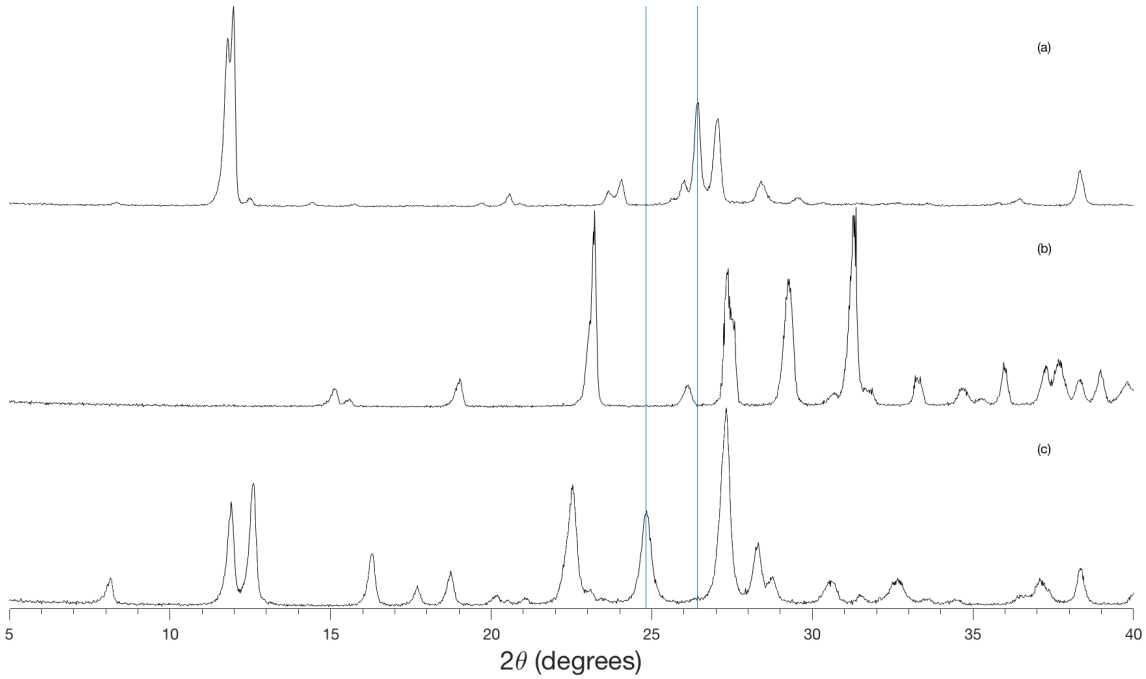

Figure B1. PXRD traces of a) caffeine, b) oxalic acid, and c) caffeine-oxalic acid 2:1 cocrystal.

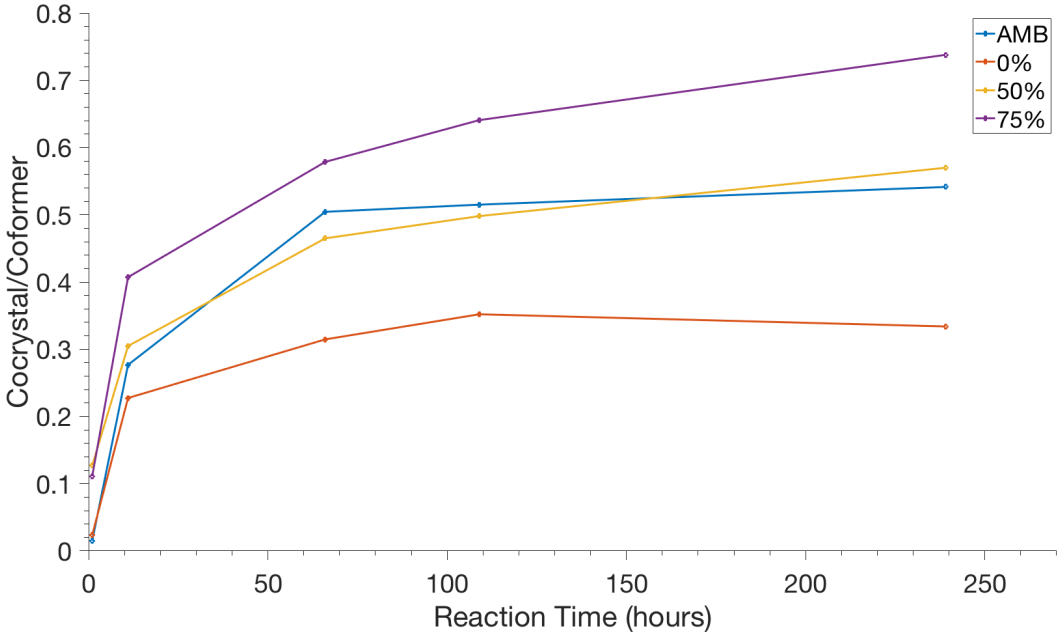

Figure B2. Powder-powder kinetics plots of caffeine-oxalic acid 2:1.

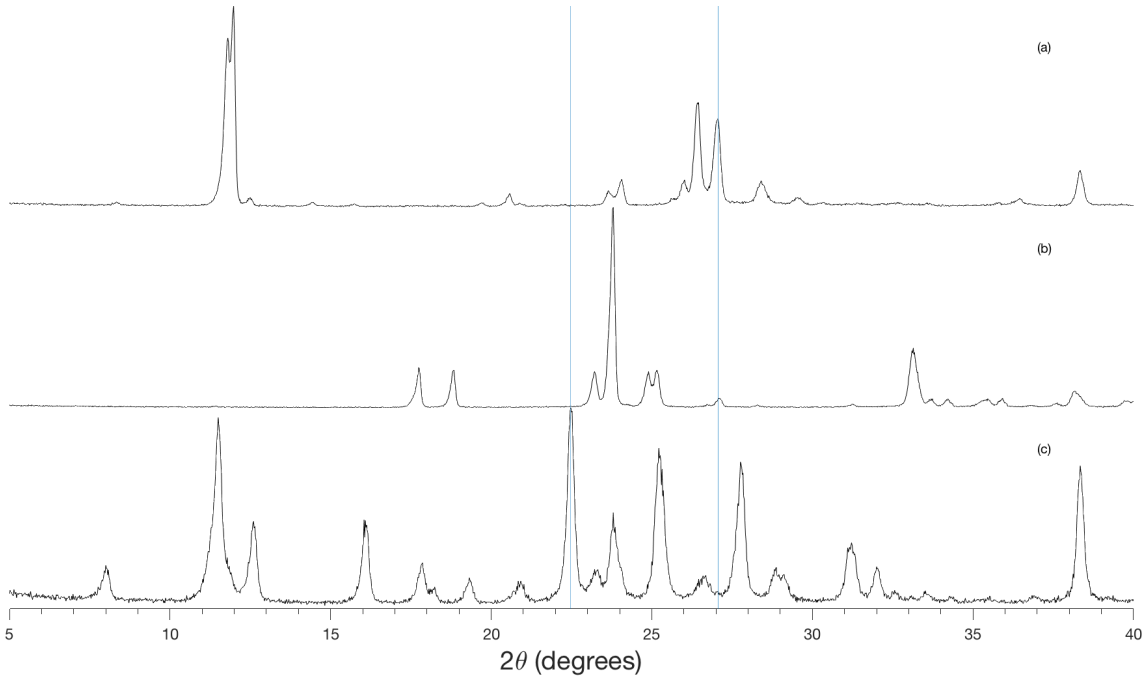

Figure B3. PXRD traces of a) caffeine, b) malonic acid, and c) caffeine-malonic acid 2:1 cocrystal.

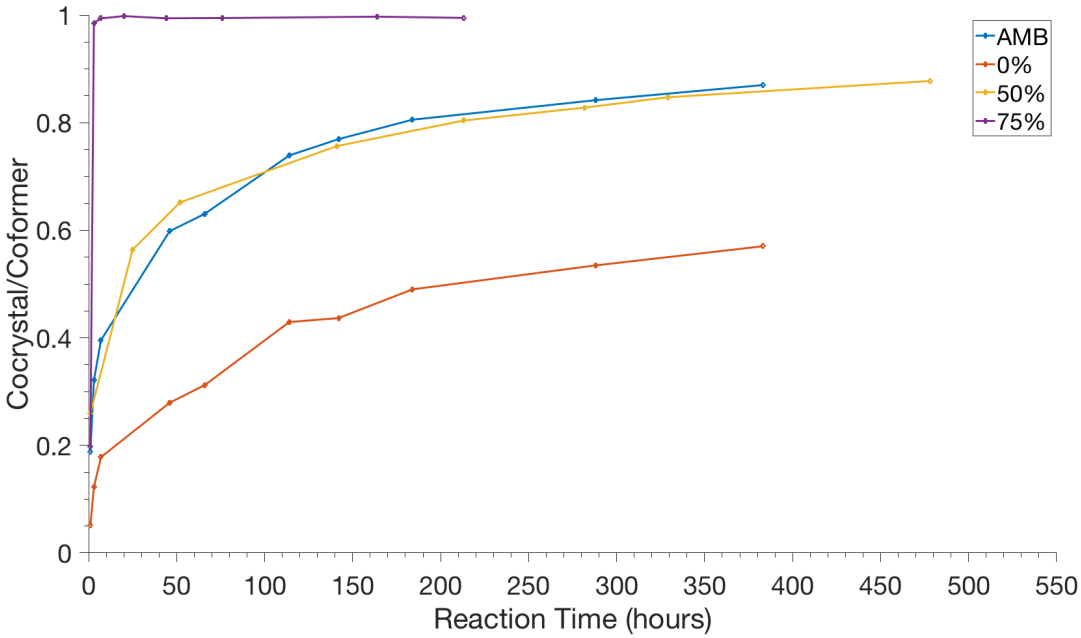

Figure B4. Powder-powder kinetics plots of caffeine-malonic acid 2:1.

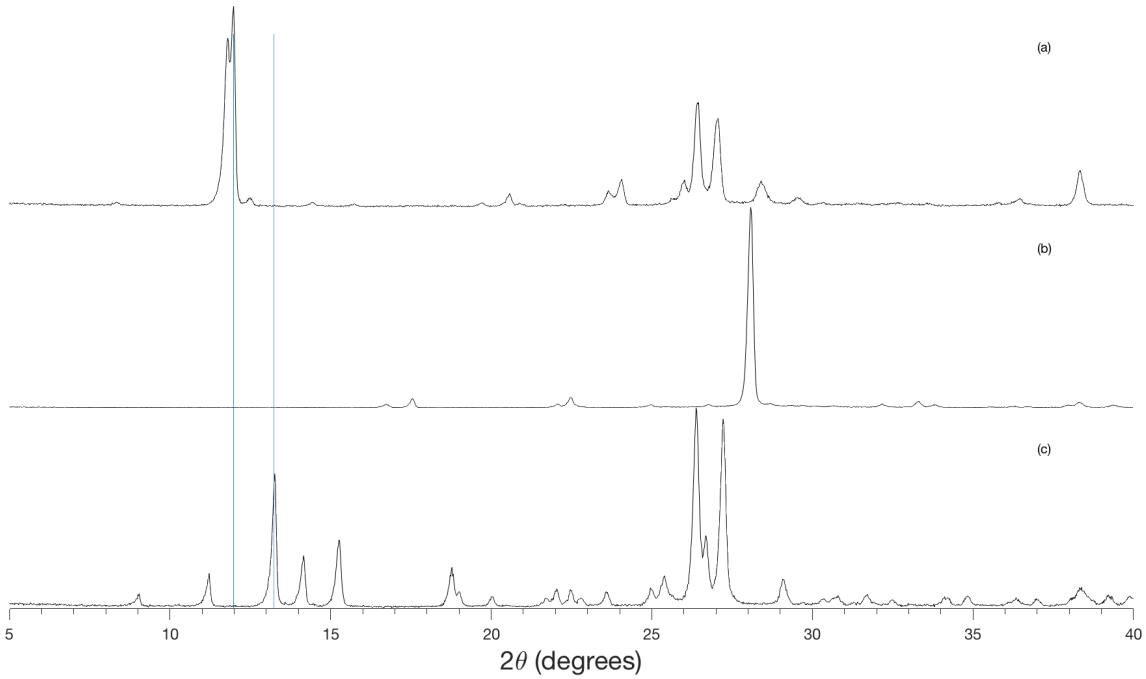

Figure B5. PXRD traces of a) caffeine, b) maleic acid, and c) caffeine-maleic acid 1:1 cocrystal.

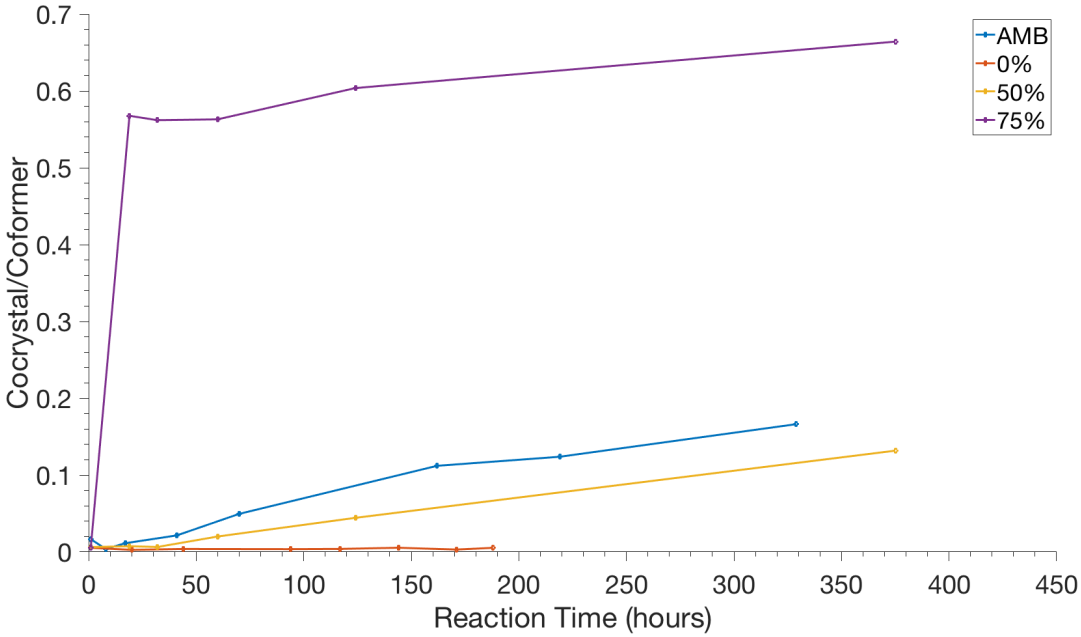

Figure B6. Powder-powder kinetics plots of caffeine-maleic acid 1:1

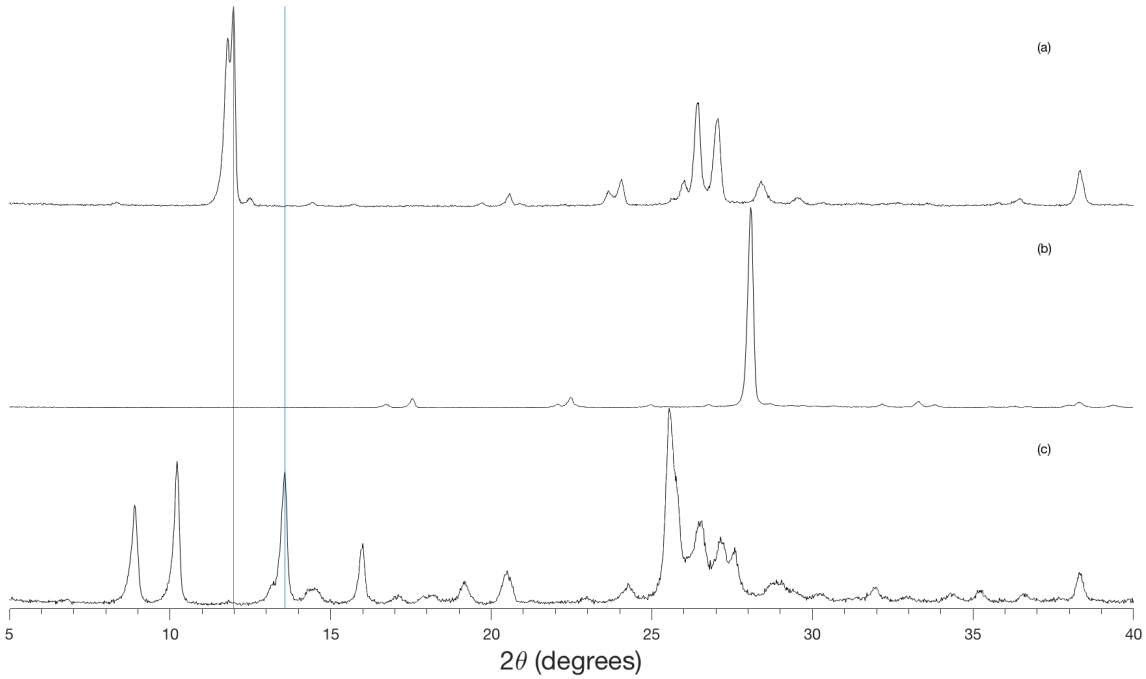

Figure B7. PXRD traces of a) caffeine, b) maleic acid, and c) caffeine-maleic acid 2:1 cocrystal.

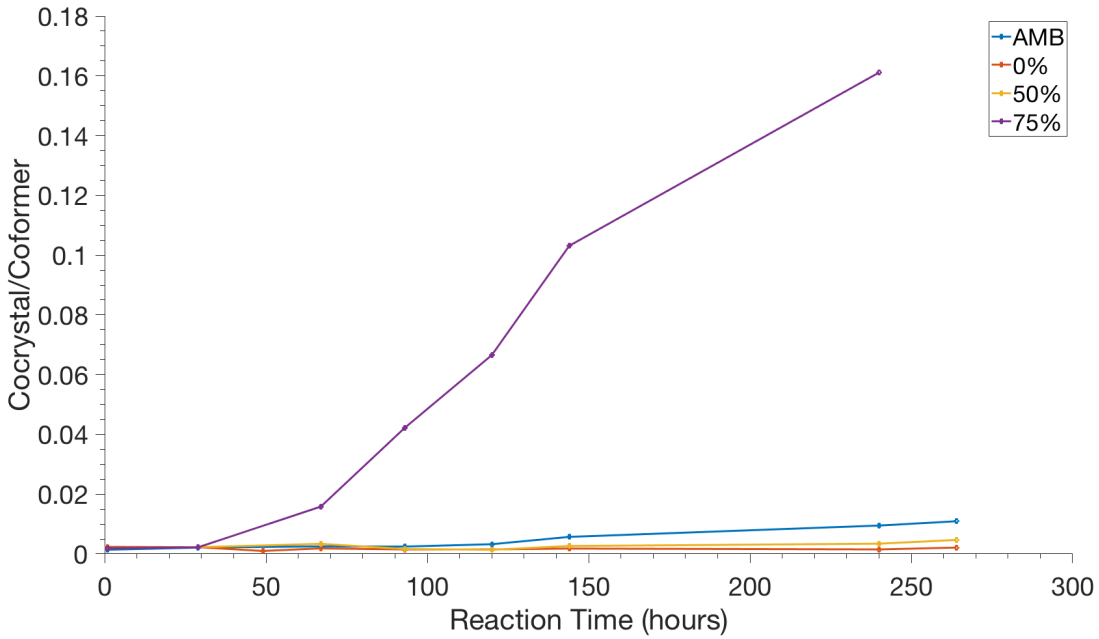

Figure B8. Powder-powder kinetics plots of caffeine-maleic acid 2:1

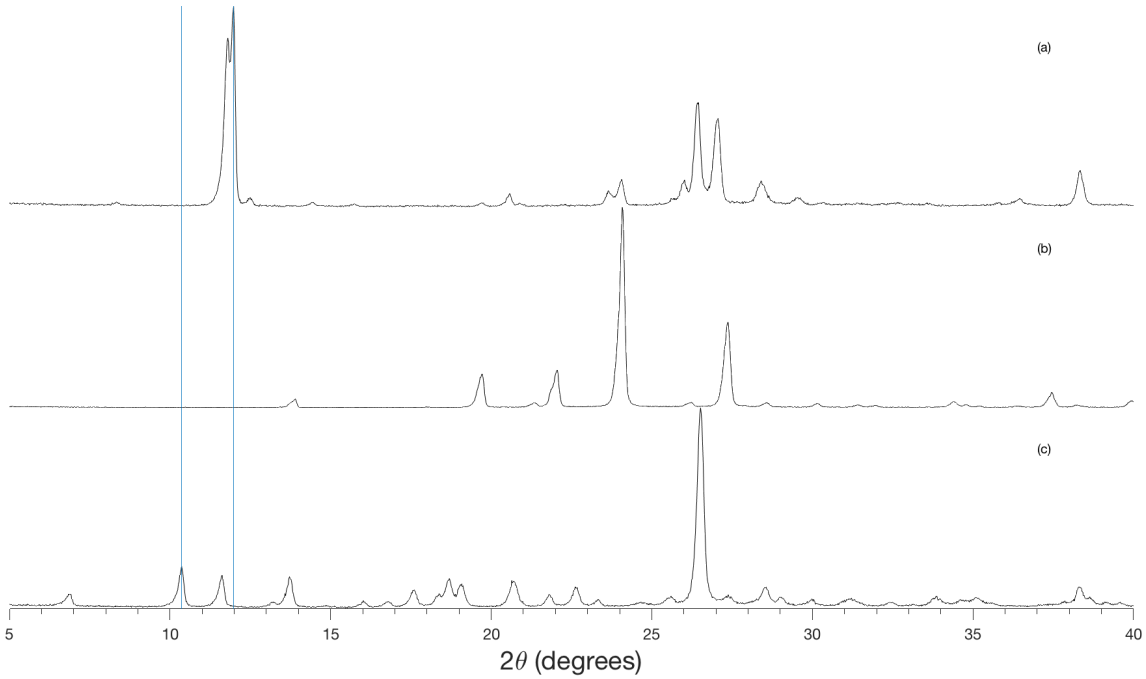

Figure B9. PXRD traces of a) caffeine, b) glutaric acid, and c) caffeine-glutaric acid 2:1 cocrystal.

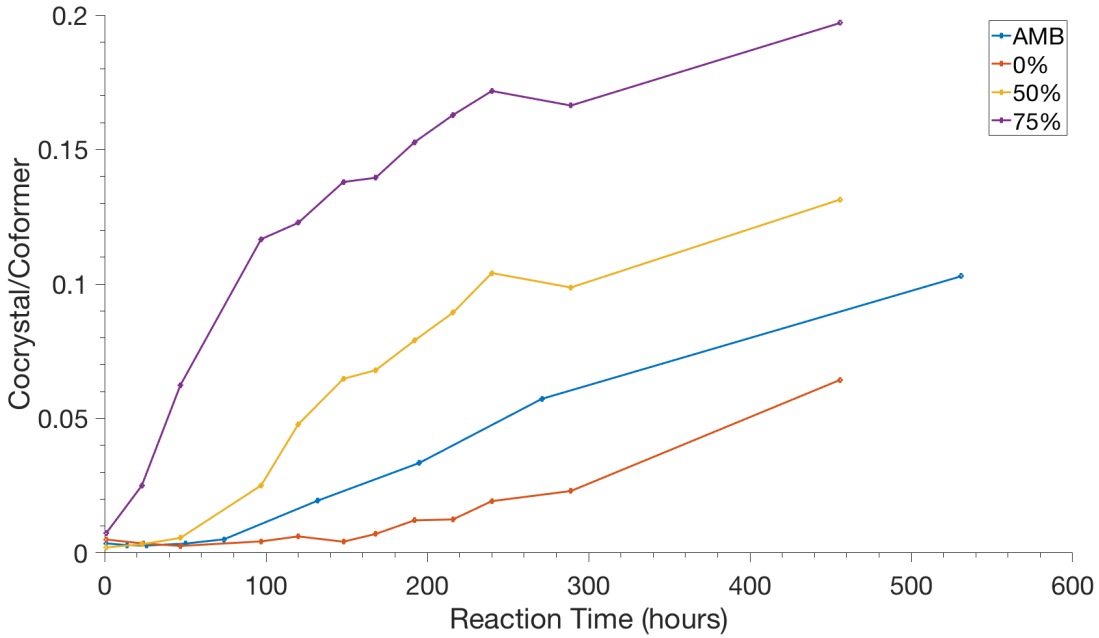

Figure B10. Powder-powder kinetics plots of caffeine-glutaric acid 2:1

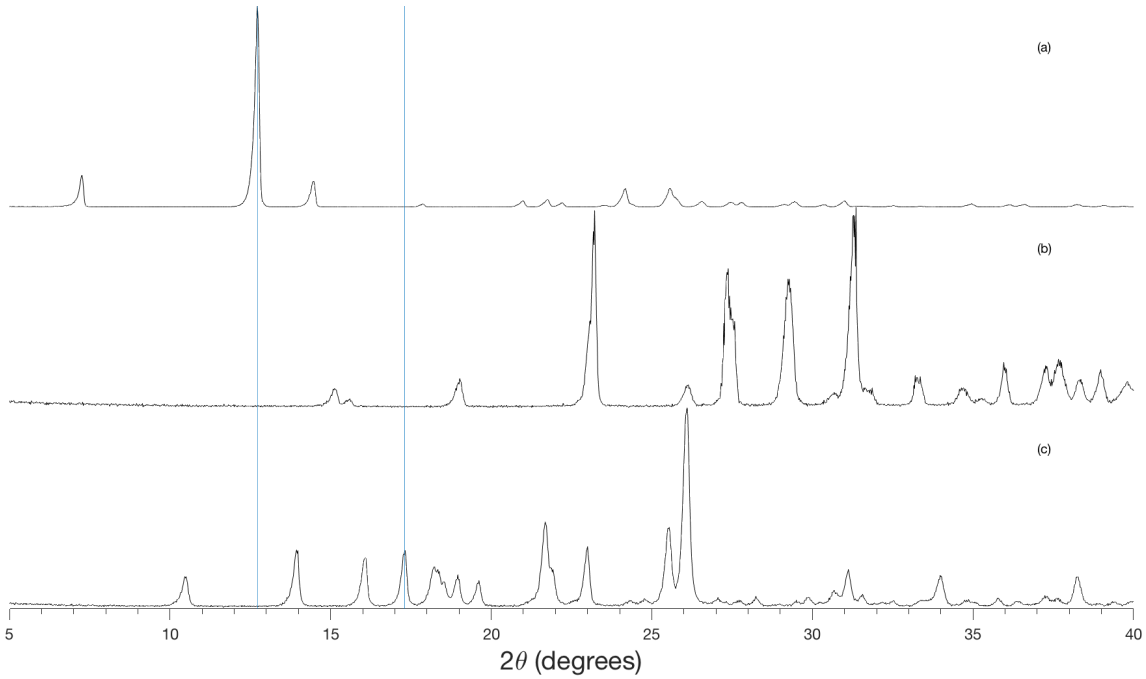

Figure B11. PXRD traces of a) theophylline, b) oxalic acid, and c) theophylline-oxalic acid 2:1 cocrystal.

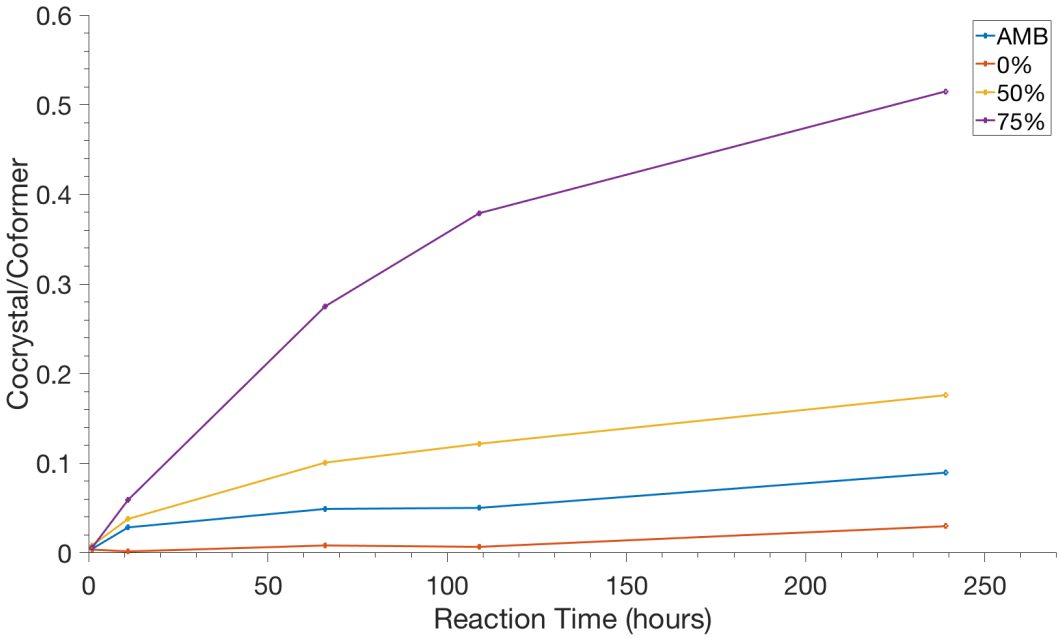

Figure B12. Powder-powder kinetics plots of theophylline-oxalic acid 2:1.

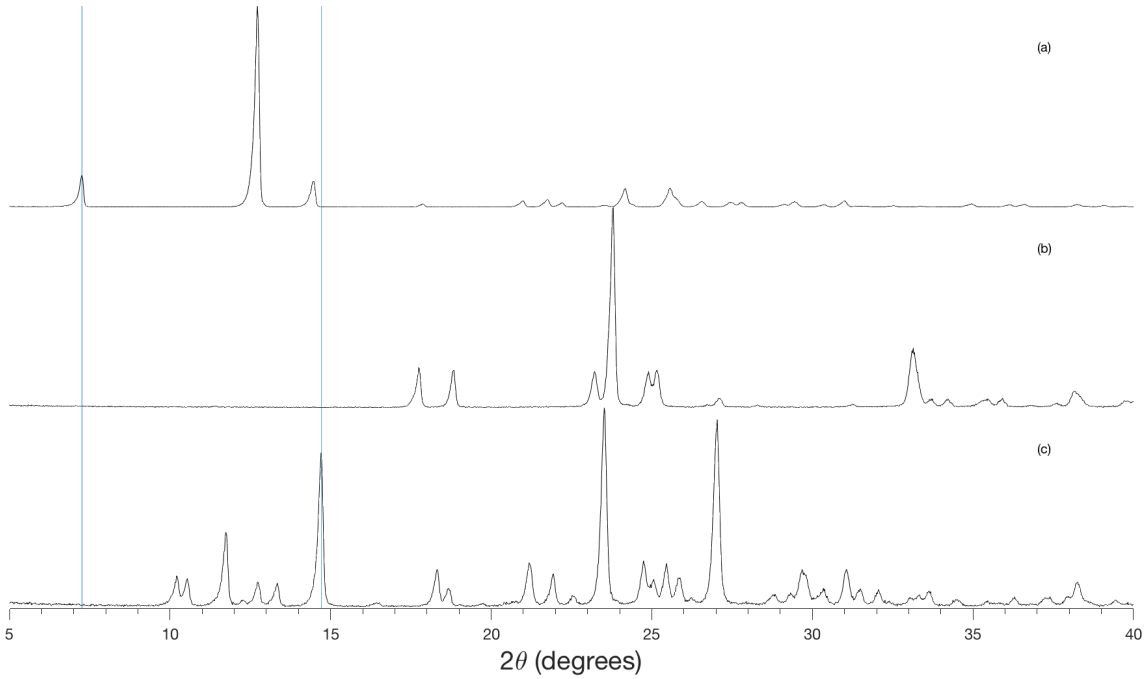

Figure B13. PXRD traces of a) theophylline, b) malonic acid, and c) theophylline-malonic acid 1:1 cocrystal.

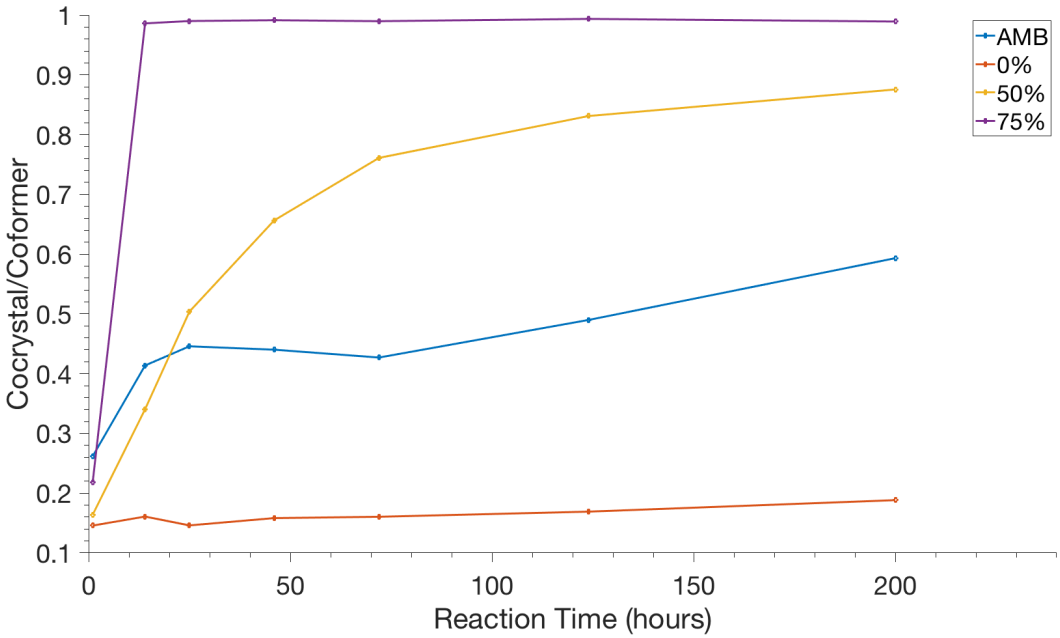

Figure B14. Powder-powder kinetics plots of theophylline-malonic acid 1:1.

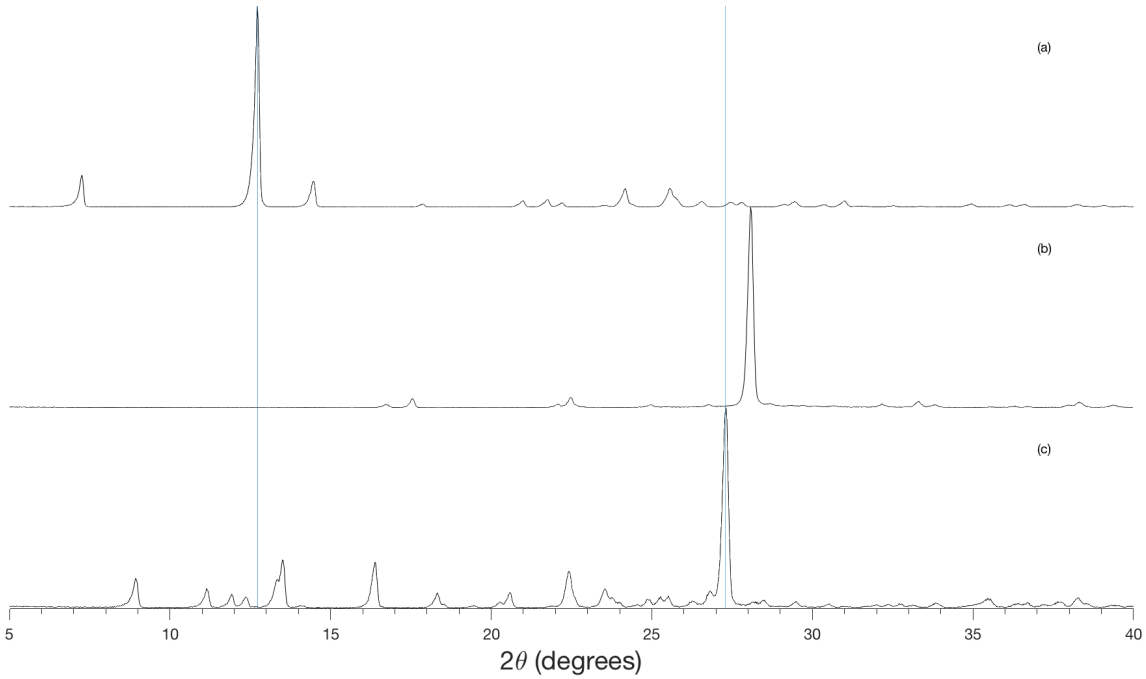

Figure B15. PXRD traces of a) theophylline, b) maleic acid, and c) theophylline-maleic acid 1:1 cocrystal.

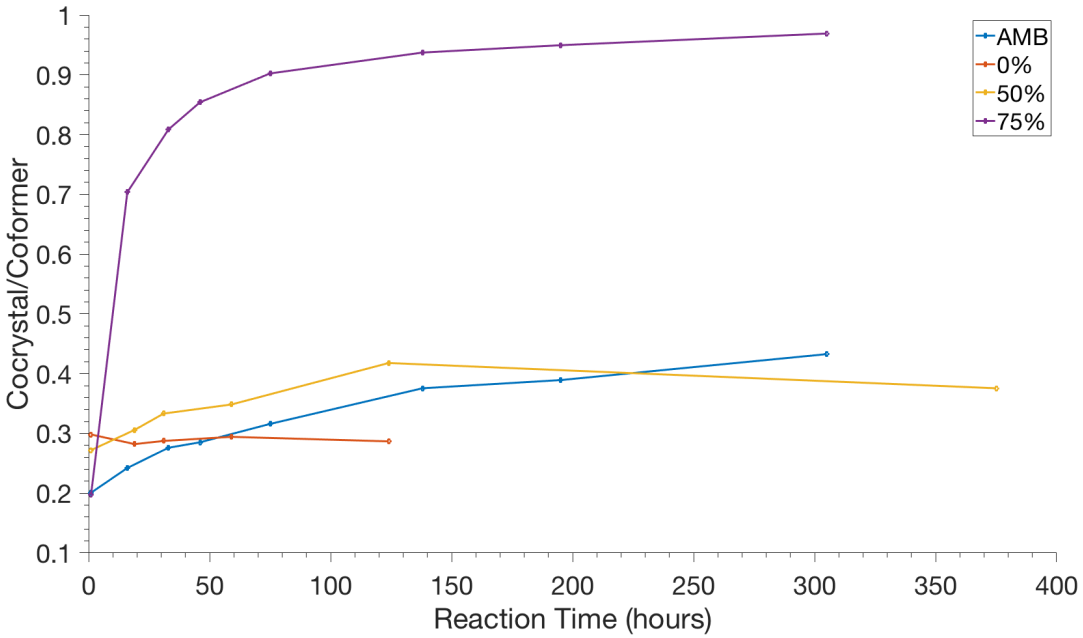

Figure B16. Powder-powder kinetics plots of theophylline-maleic acid 1:1.

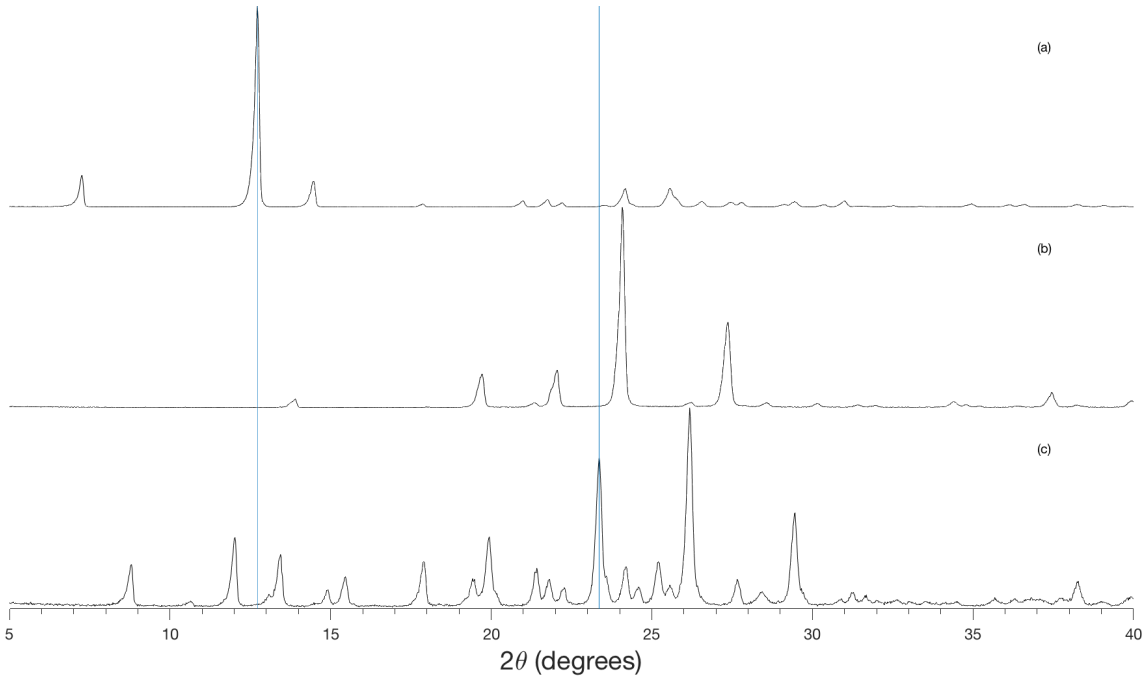

Figure B17. PXRD traces of a) theophylline, b) glutaric acid, and c) theophylline-glutaric acid 1:1 cocrystal.

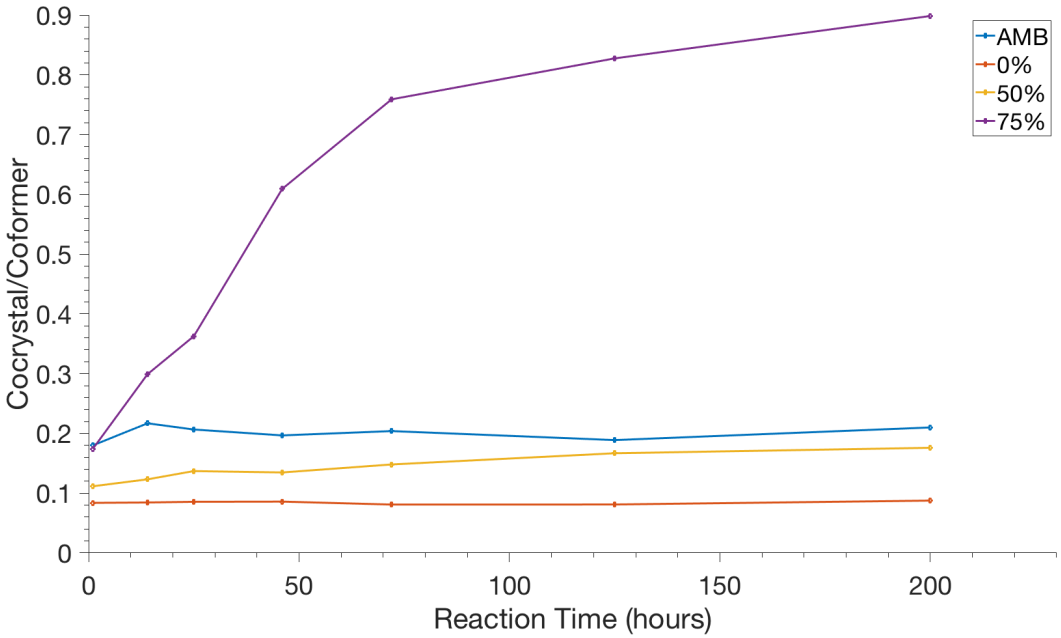

Figure B18. Powder-powder kinetics plots of theophylline-glutaric acid 1:1.

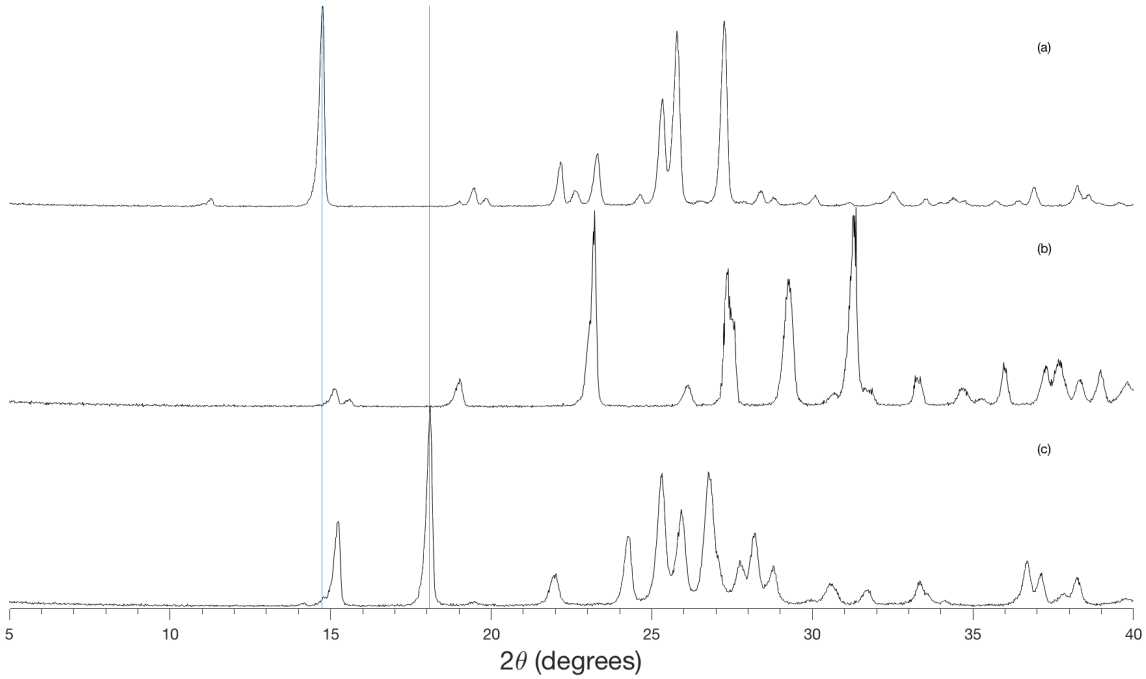

Figure B19. PXRD traces of a) nicotinamide, b) oxalic acid, and c) nicotinamide-oxalic acid 2:1 cocrystal.

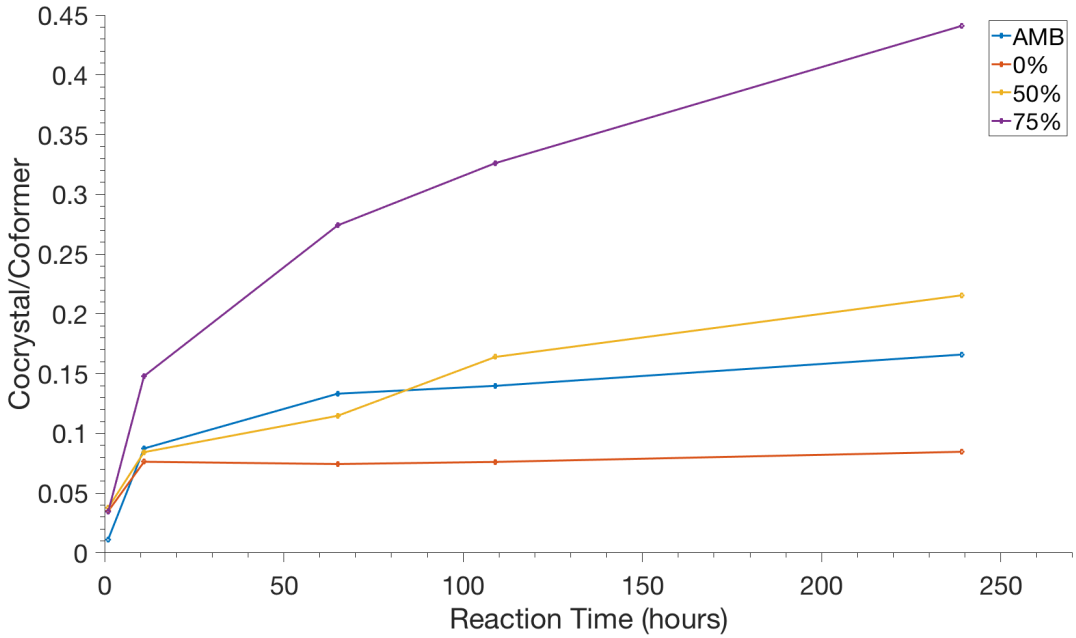

Figure B20. Powder-powder kinetics plots of nicotinamide-oxalic acid 2:1.

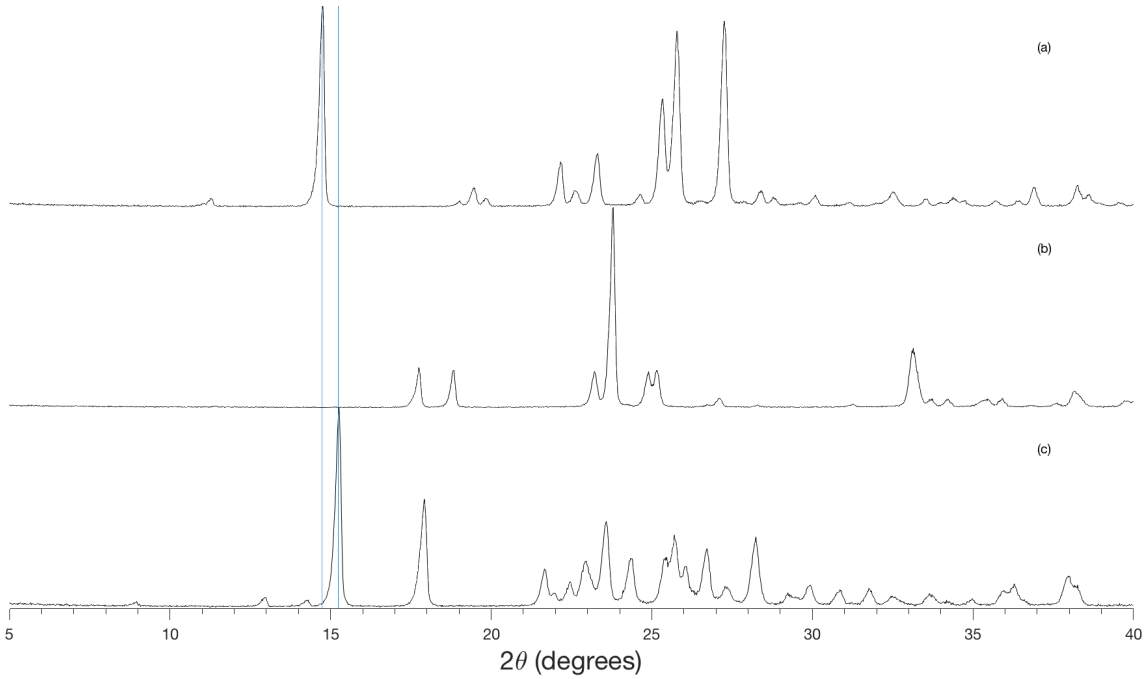

Figure B21. PXRD traces of a) nicotinamide, b) malonic acid, and c) nicotinamide-malonic acid 2:1 cocrystal.

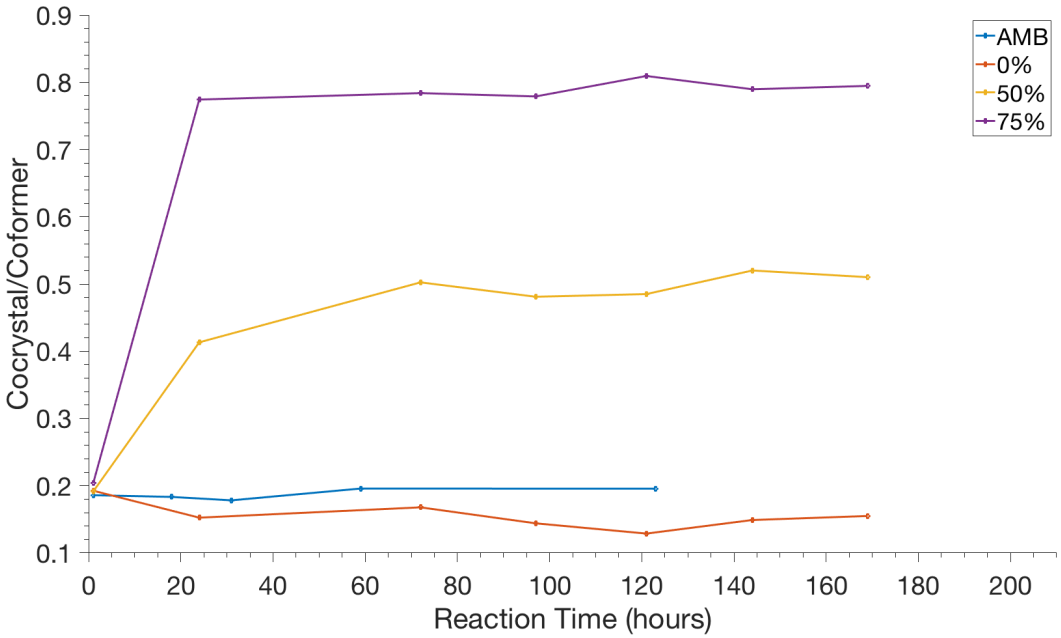

Figure B22. Powder-powder kinetics plots of nicotinamide-malonic acid 2:1.

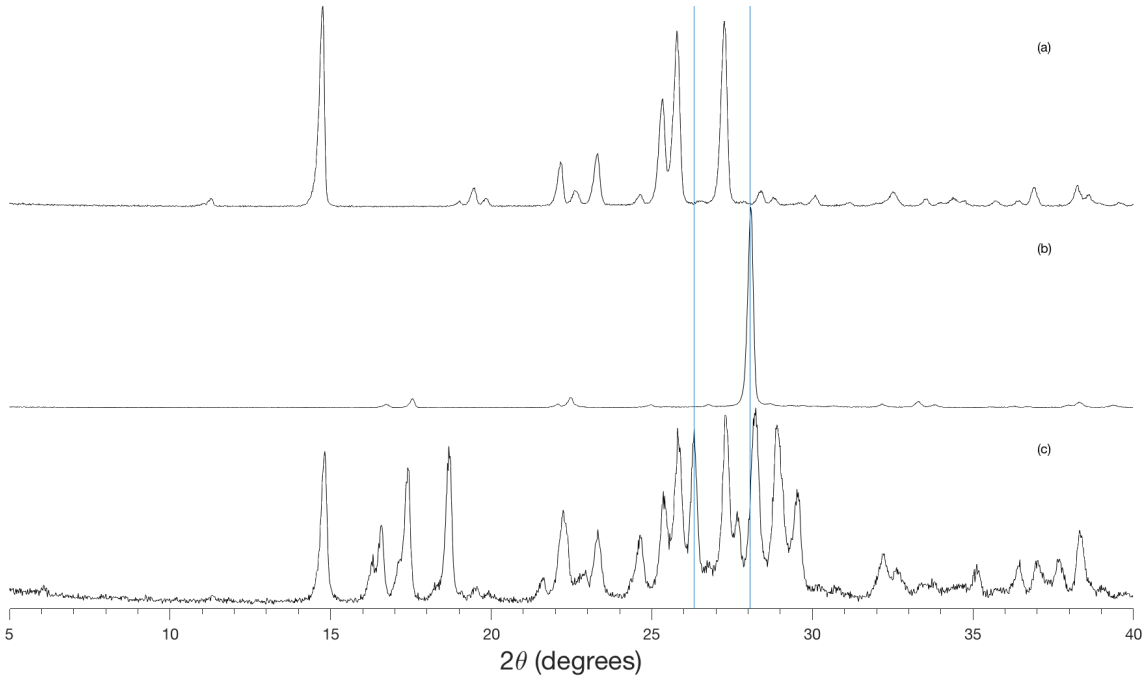

Figure B23. PXRD traces of a) nicotinamide, b) maleic acid, and c) nicotinamide-maleic acid 2:1 cocrystal.

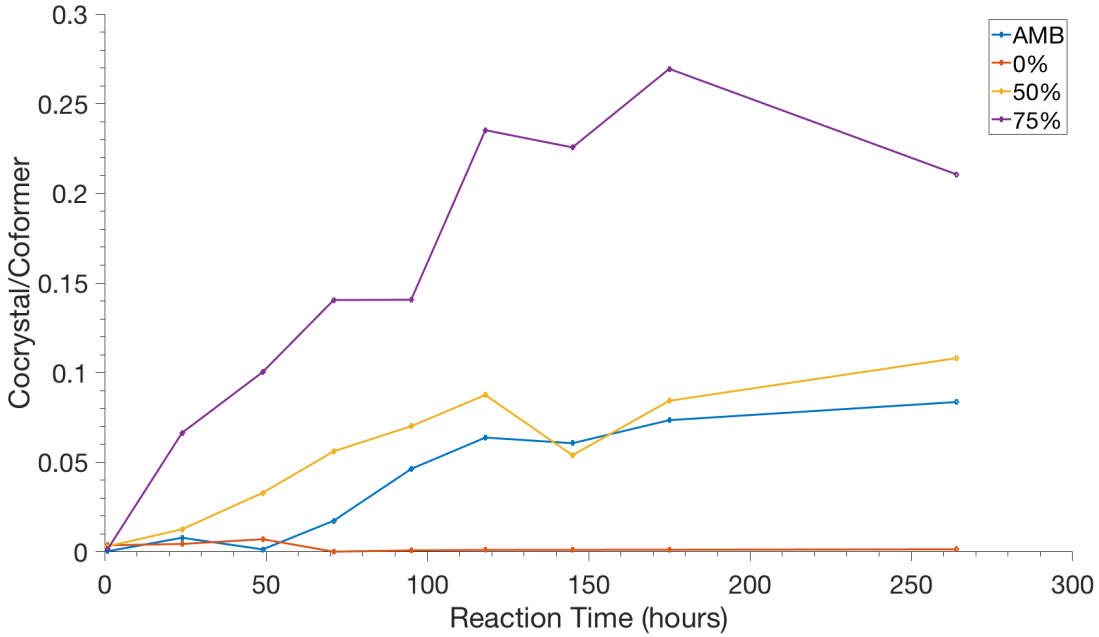

Figure B24. Powder-powder kinetics plots of nicotinamide-maleic acid 2:1.

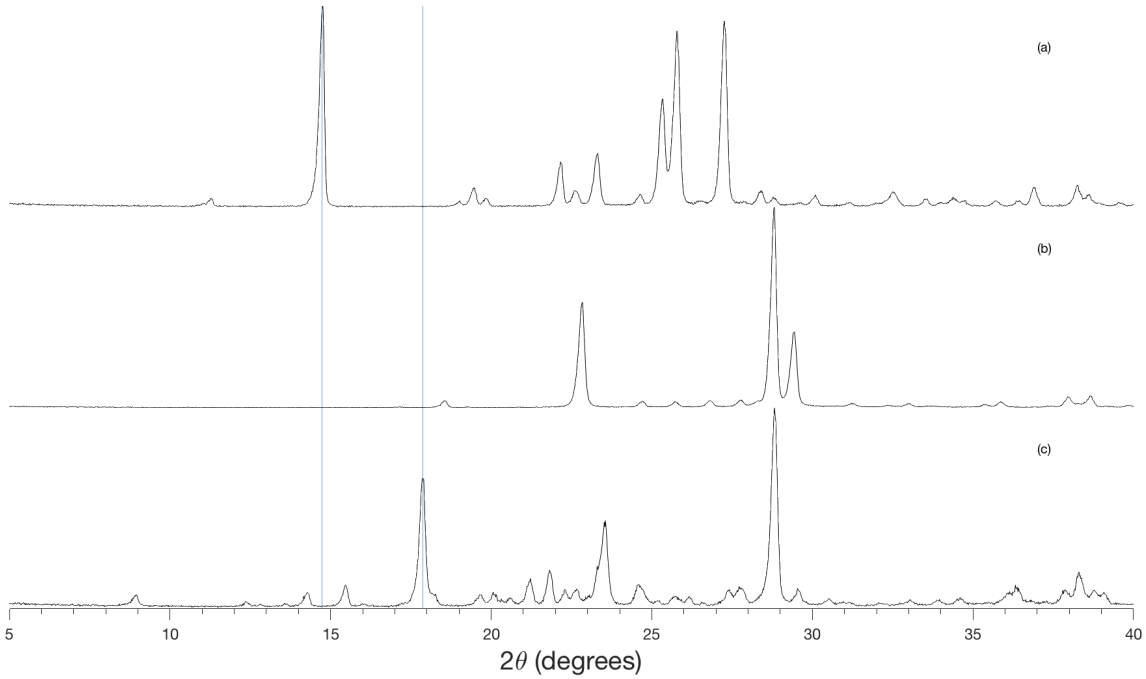

Figure B25. PXRD traces of a) nicotinamide, b) fumaric acid, and c) nicotinamide-fumaric acid 1:1 cocrystal.

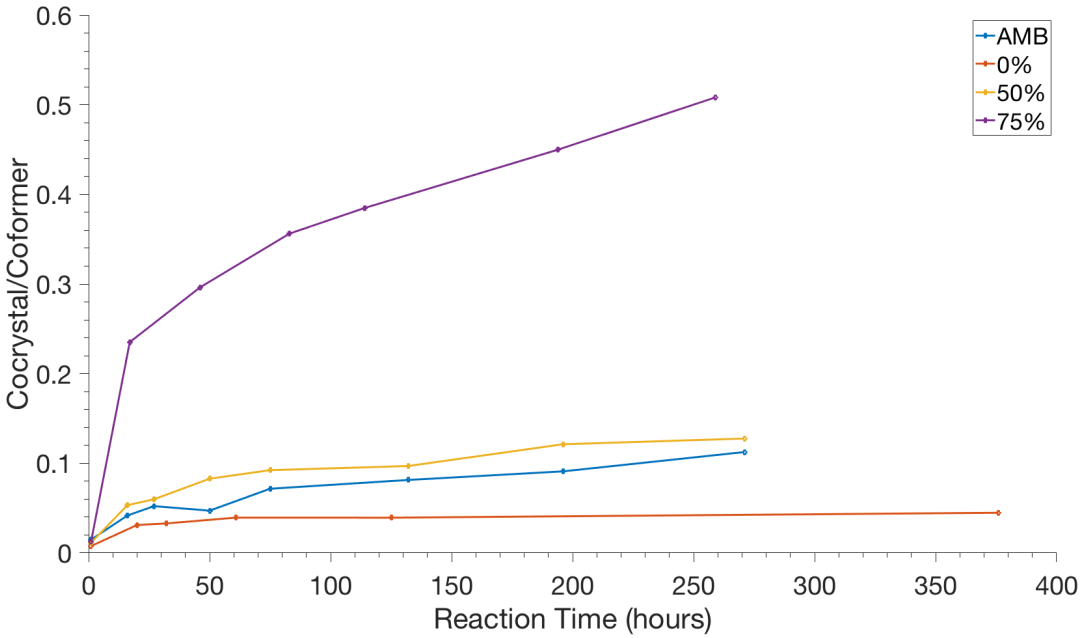

Figure B26. Powder-powder kinetics plots of nicotinamide-fumaric acid 1:1.

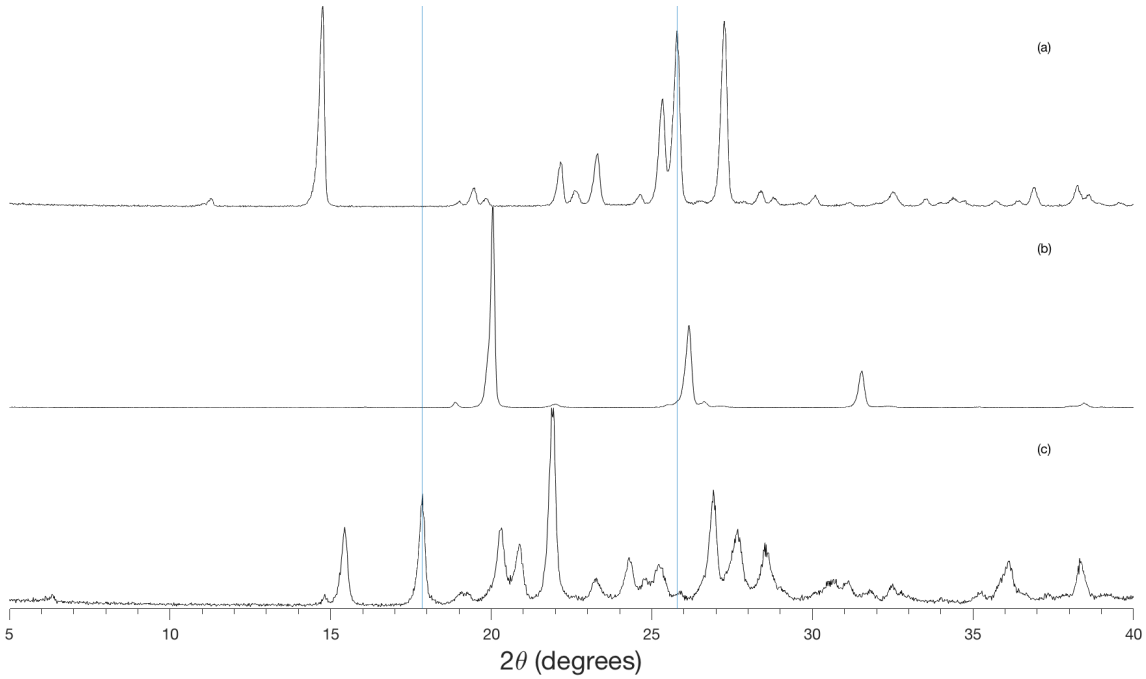

Figure B27. PXRD traces of a) nicotinamide, b) succinic acid, and c) nicotinamide-succinic acid 2:1 cocrystal.

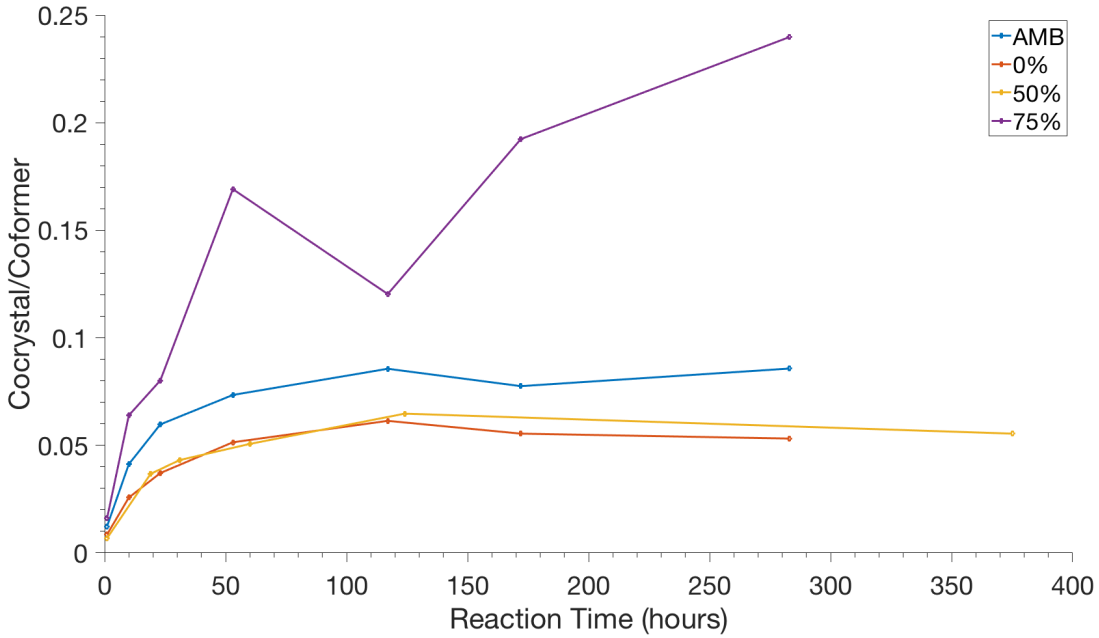

Figure B28. Powder-powder kinetics plots of nicotinamide-succinic acid 2:1.

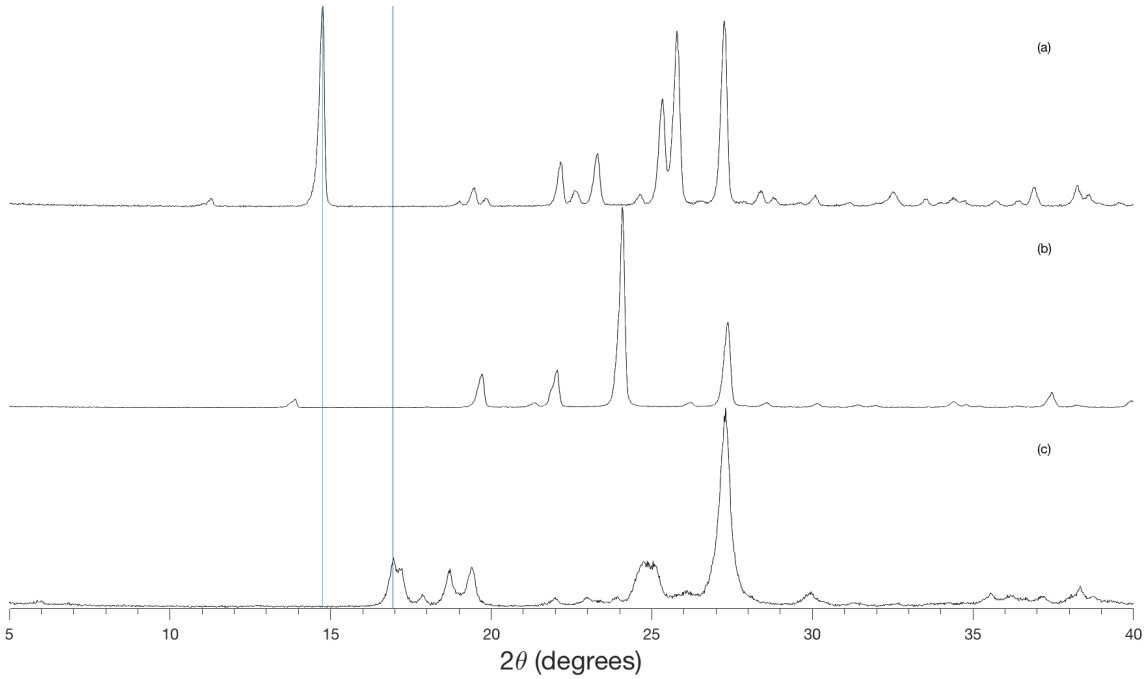

Figure B29. PXRD traces of a) nicotinamide, b) glutaric acid, and c) nicotinamide-glutaric acid 1:1 cocrystal.

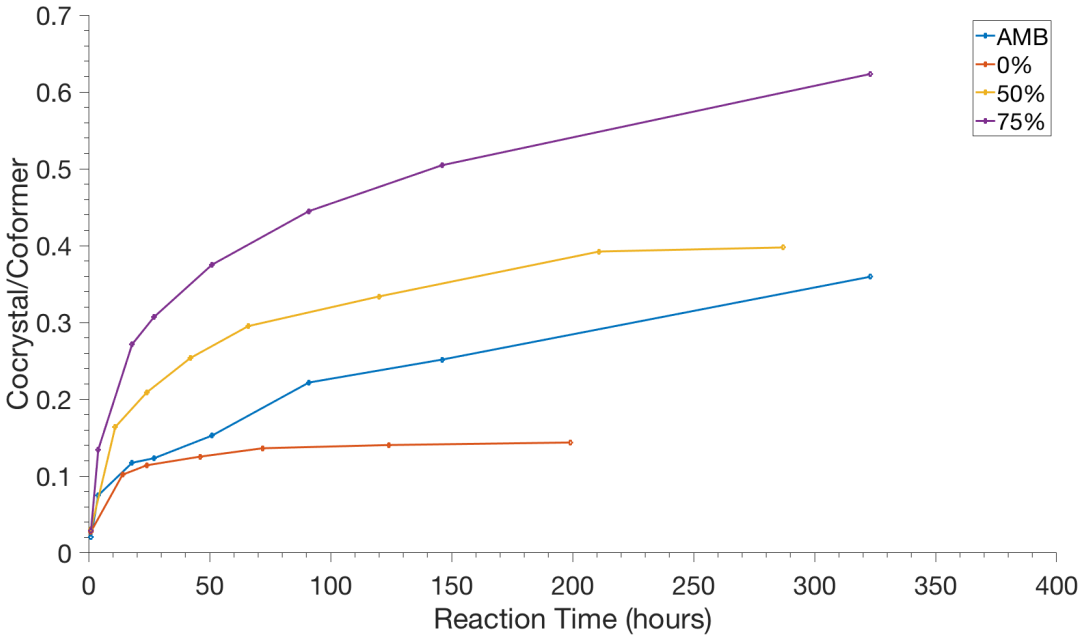

Figure B30. Powder-powder kinetics plots of nicotinamide-glutaric acid 1:1.

REFERENCES

1. Wöhler, F. Untersuchungen Über das Chinon. *Annalen der Chem. Und Pharm.* **1844**, *51*, 145-163.
2. Stoler, E.; Warner, J. C. Non-Covalent Derivatives: Cocrystals and Eutectics. *Molecules* **2015**, *20*, 14833-14848.
3. Steed, J. W. The Role of Co-Crystals in Pharmaceutical Design. *Trends Pharmacol. Sci.* **2013**, *34*, 185-193.
4. Nath, N. K.; Hazarika, M.; Gupta, P.; Ray, N. R.; Paul, A. K.; Nauha, E. Plastically Bendable Crystals of Probenecid Acid and Its Cocrystal with 4,4'-Bipyridine. *J. Mol. Str.* **2018**, *1160*, 20-25.
5. Christopherson, J.-C.; Topić, F.; Barrett, C. J.; Friščić, T. Halogen-Bonded Cocrystals as Optical Materials: Next-Generation Control over Light-Matter Interactions. *Cryst. Growth Des.* **2018**, *18*, 1245-1259.
6. Schultheiss, N.; Newman, A. Pharmaceutical Cocrystals and Their Physicochemical Properties. *Crys. Growth Des.* **2009**, *9*, 2950-2967.
7. Bak, A.; Gore, A.; Yanez, E.; Stanton, M.; Tuufekcic, S.; Syed, R.; Akrami, A.; Rose, M.; Supraneni, S.; Bostick, T.; King, A.; Neervannan, S.; Otovic, D.; Koparkar, A. The Co-Crystal Apprach to Improve the Exposure of a Water-Insoluble Compound: AMG 517 Sorbic Acid Co-Crystal Characterization and Pharmacokinetics. *J. Pharm. Sci.* **2008**, *97*, 3942-3956.
8. Trask, A. V.; Motherwell, W. D. S.; Jones, W. Pharmaceutical Cocrystallization: Engineering a Remedy for Caffeine Hydration. *Cryst. Growth Des.* **2005**, *5*, 1013-2021.
9. Fernandes, J.; Sardo, M.; Mafra, L.; Choquesillo-Lazarte, D.; Massiocchi, N. X-Ray and NMR Crystallography Studies of Novel Theophylline Cocrystals Prepared by Liquid Assisted Grinding. *Cryst. Growth Des.* **2015**, *15*, 2674-2683.
10. Sarceviča, I.; Orola, L.; Nartowski, K. P.; Khimyak, Y. Z.; Round, A. N.; Fábián, L. Mechanistic and Kinetic Insight into Spontaneous Cocrystallization of Isoniazid and Benzoic Acid. *Mol. Pharmaceutics* **2015**, *12*, 2981-2992.
11. Tumanova, N.; Tumanov, N.; Robeyns, K.; Fischer, F.; Fusaro, L.; Morelle, F.; Ban, V.; Hautier, G.; Filinchuk, Y.; Wouters, J.; Leyssens, T.; Emmerling, F. Opening Pandora's Box: Chirality, Polymorphism, and Stoichiometric Diversity in Flurbiprofen/Proline Cocrystals. *Cryst. Growth Des.* **2018**, *18*, 954-961.
12. Ibrahim, A. Y.; Forbes, R. T.; Blagden, N. Spontaneous Crystal Growth of Co-Crystals: The Contirbution of Particles Size Reduction and Convection Mixing of the Co-Formers. *CrystEngComm* **2011**, *13*, 1141-1152.
13. Mandala, V. S.; Loewus, S. J.; Mehta, M. A. Monitoring Cocrystal Formation via In Situ Solid-State NMR. *J. Phys. Chem. Lett.* **2014**, *5*, 3340-3344.
14. Taylor, C. R.; Day, G. M.; Evaluating the Energetic Driving Force for Cocrystal Formation. *Cryst. Growth Des.* **2018**, *18*, 892-904.
15. Ji, C.; Hoffman, M. C.; Mehta, M. A. Catalytic Effect of Solvent Vapors on the Spontaneous Formation of Caffeine-Malonic Acid Cocrystal. *Cryst. Growth Des.* **2017**, *17*, 1456-1459.
16. Friščić, T.; Jones, W. Recent Advances in Understanding the Mechanism of Cocrystal Formation via Grinding. *Cryst. Growth Des.* **2009**, *9*, 1621-1637.
17. Rastogi, R. P.; Bassi, P. S.; Chadha, L. S. Mechanism of the Reaction between Hydrocarbons and Picric Acid in the Solid State. *J. Phys. Chem.* **1963**, *67*, 2569-2573.

18. Friščić, T. Supramolecular Concepts and New Techniques in Mechanochemistry: Cocrystal, Cages, Rotaxanes, Open Metal-Organic Frameworks. *Chem. Soc. Rev.* **2012**, *41*, 3493-3510.
19. Khodaparast, S.; Sharratt, W.; Wang, H.; Robles, E. S. J.; Dalgliesh, R.; Cabral, J. T. Spontaneous Formation of Multilamellar Vesicles from Aqueous Micellar Solutions of Sodium Linea Alkylbenzene Sulfonate (NaLAS). *J. Coll. Interface Sci.* **2019**, *546*, 221-230.
20. Samipillai, M.; Rohani, S. The Role of Higher Coformer Stoichiometry Ratio in Pharmaceutical Cocrystals for Improving Their Solid-State Properties: The Cocrystals of Progesterone and 4-Hydroxybenzoic Acid. *J. Cryst. Growth* **2019**, *507*, 270-282.
21. Nartowski, K. P.; Khimyak, Y. Z.; Berry, D. J. Tuning the Spontaneous Formation Kinetics of Caffeine : Malonic Acid Co-crystals. *CrystEngComm* **2016**, *18*, 2617-2620.
22. Cassidy, A. M. C.; Gardner, C. E.; Jones, W. Following the Surface Response of Caffeine Cocrystals to Controlled Humidity Storage by Atomic Force Microscopy. *Int. J. Pharm*. **2009**, *379*, 59-66.
23. Vigilante, N. J.; Mehta, M. A. A ^{13}C Solid-State NMR Investigation of Four Cocrystals of Caffeine and Theophylline. *Acta Cryst. C* **2017**, *73*, 234-243.
24. Gopalan, S. R.; Kumaradhas, P.; Kulkarni, G. U.; Rao, C. N. R. An Experimental Charge Density Study of Aliphatic Dicarboxylic Acids. *J. Mol. Struct.* **2000**, *521*, 97-106.
25. Goedkoop, J. A.; MacGillavry, C. H. The Crystal Structure of Malonic Acid. *Acta Cryst.* **1957**, *10*, 125-127.
26. Naqvi, A. A.; Bhattacharyya, G. C. Crystal Data for Anhydrous Theophylline. *J. Appl. Cryst.* **1981**, *14*, 464.
27. Miwa, Y.; Mizuno, T.; Tsuchida, K.; Kaga, T.; Iwata, Y. Experimental Charge Density and Electrostatic Potential in Nicotinamide. *Acta Cryst.* **1999**, *55*, 78-84.
28. Ebisuzaki, Y.; Boyle, P. D.; Smith, J. A. Methylxanthines. I. Anhydrous Theophylline. *Acta Cryst.* **1997**, *53*, 777-779.
29. Lehmann, C. W.; Stowasser, F. The Crystal Structure of Anhydrous β-Caffeine as Determined from X-Ray Powder-Diffraction Data. *Chem.—Euro. J.* **2007**, *13*, 2908-2911.
30. Bhattacharya, S.; Saraswatula, V. G.; Saha, B. K. Thermal Expansion in Alkane Diacids—Another Proerty Showing Alternation in an Odd-Even Series. *Cryst. Growth Des.* **2013**, *13*, 3651-3656.
31. Day, G. M.; Trask, A. V.; Motherwell, W. D. S.; Jones, W. Investigating the Latent Polymorphism of Maleic Acid. *Chem. Commun.* **2005**, *1*, 54-56.
32. Brown, C. J. The Crystal Structure of Fumaric Acid. *Acta Cryst.* **1966**, *21*, 1-5.
33. Gopalan, R. S.; Kumaradhas, P.; Kulkarni, G. U.; Rao, C. N. R. An Experimental Charge Density Study of Aliphatic Dicarboxylic Acids. *J. Mol. Struct.* **2000**, *521*, 97-106.
34. Lemmerer, A. Covalent Assistance to Supramolecular Synthesis: Modifying the Drug Functionality of the Antituberculosis API Isoniazid *in situ* during Co-crystallization with GRAS and API Compounds. *CrystEngComm* **2012**, *14*, 2465-2478.
35. Sim, G. A.; Robertson, J. M.; Goodwin, T. H. The Crystal and Molecular Structure of Benzoic Acid. *Acta Cryst.* **1955**, *8*, 157-164.
36. Trask, A. V.; Motherwell, W. D. S.; Jones, W. Pharmaceutical Cocrystallization: Engineering a Remedy for Caffeine Hydration. *Cryst. Growth Des.* **2005**, *5*, 1013-1021.
37. Leyssens, T.; Springuel, G.; Montis, R.; Candoni, N.; Veesler, S. Importance of Solvent Selection for Stoichiometrically Diverse Cocrystal Systems: Caffeine/Maleic Acid 1:1 and 2:1 Cocrystals. *Cryst. Growth Des.* **2012**, *12*, 1520-1530.

38. Trask, A. V.; Motherwell, W. D. S.; Jones, W. Physical Stability Enhancement of Theophylline via Cocrystallization. *Int. J. Pharm*. **2006**, *320*, 114-123.
39. Hathwar, V. R.; Pal, R.; Row, T. N. G. Charge Density Analysis of Crystals of Nicotinamide with Salicylic Acid and Oxalic Acid: An Insight into the Salt to Cocrystal Continuum. *Cryst. Growth Des.* **2010**, *10*, 3306-3310.
40. Karki, S.; Friščić, T.; Jones, W. Control and Interconversion of Cocrystal Stoichiometry in Grinding: Stepwise Mechanism for the Formation of a Hydrogen-Bonded Cocrystal. *CrystEngComm* **2009**, *11*, 470-481.
41. Orola, L.; Veidis, M. V. Nicotinamide Fumaric Acid Supramolecular Cocrystals: Diversity of Stoichiometry. *CrystEngComm*, **2009**, *11*, 415-417.
42. Thompson, L. J.; Voguri, R. S.; Cowell, A.; Male, L.; Tremayne, M. The Cocrystal Nicotinamide-Succinic Acid (2/1). *Acta Cryst.* **2010**, *66*, 421-424.
43. Sarcevica, I.; Orola, L.; Veidis, M. V.; Podjava, A.; Belyakov, S. Crystal and Molecular Structure and Stability of Isoniazid Cocrystals with Selected Carboxylic Acids. *Cryst. Growth Des.* **2013**, *13*, 1082-1090.